NASA CR 72665

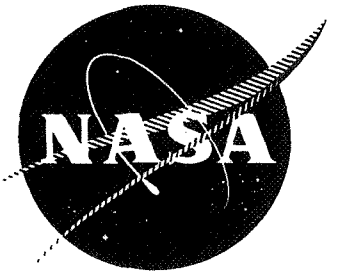

COMPRESSOR END SEAL TEST AND DEVELOPMENT

by

A.N. Pope and C.C. Moore

DESIGN TECHNOLOGY OPERATION

GENERAL ELECTRIC COMPANY

prepared for

NATIONAL AERONAUTICS AND SPACE ADMINISTRATION

NASA-Lewis Research Center

Contract NAS 3-10490

Dennis P. Townsend, Project Manager

Requests for copies of this report should be referred to

National Aeronautics and Space Administration
Office of Scientific and Technical Information
Attention: AFSS-A
Washington, D.C. 20546

NASA CR 72665

FINAL REPORT

COMPRESSOR END SEAL TEST AND DEVELOPMENT

by

A.N. Pope and C.C. Moore

DESIGN TECHNOLOGY OPERATION
GENERAL ELECTRIC COMPANY
Cincinnati, Ohio 45215

prepared for

NATIONAL AERONAUTICS AND SPACE ADMINISTRATION

July 1970

Contract NAS 3-10490

NASA-Lewis Research Center
Cleveland, Ohio
Dennis P. Townsend, Project Manager

FOREWORD

The research described herein which was conducted by the General Electric Aircraft Engine Group, was performed under NASA Contract NAS 3-10490. The work was done under the management of the NASA Program Manager, Mr. D.P. Townsend, of the NASA-Lewis Research Center. Acknowledgment for technical assistance is made to L.P. Ludwig of NASA-Lewis Research Center and to H. Lindeboom of Sealol Corporation.

TABLE OF CONTENTS

LIST OF ILLUSTRATIONS

LIST OF ILLUSTRATIONS (Continued)

LIST OF ILLUSTRATIONS (Continued)

LIST OF ILLUSTRATIONS (Concluded)

ABSTRACT

Two new types of metallic, hydrostatic compressor end seals (22 inches in diameter) were designed, manufactured, and tested up to 600 ft/sec, 1000°F, and 175 psig. A hydrodynamic type was also evaluated. Compared to labyrinth seals, a 20 to 1 reduction in flow was achieved. These seals operated without contact at a film thickness less than 0.001 inch, using hydrostatic air-bearing principles, and are intended for use in aircraft gas turbines and related equipment.

SECTION I

SUMMARY

The program consists of design and/or operation of four seal types. The four seal types were identified as:

1. The -333 seal; an inherently compensated hydrostatic seal.

2. The -131 seal; a hydrostatic step seal.

3. The NASA CD847985 designed seal; a Raleigh step seal.

4. The Flight-Weight Seal; a lightweight hydrostatic step seal.

The -333 seal was statically tested and discarded from the program at an early stage because of the high leak rates inherent in this design. The -131 seal was carried through the entire program and run statically, dynamically up to 4,000 rpm at 70°F, and dynamically up to 6,200 rpm at 750°F. The NASA design seal, CD847985, was tested statically to determine the effectiveness of the hydrostatic liftoff feature and was returned for rework of the seal face vent to prevent opening at operating pressure levels. Due to damage received during modification, further testing was not possible. The flight-weight seal design was run statically, dynamically to 4,186 rpm and 70°F, and dynamically to 1,826 rpm, 1010°F, and 168 psig.

The program came close to the goal of 20-1 reduction in flow rate through a compressor discharge seal. During the last flight-weight buildup, a flow rate equivalent to a 0.0013-inch height gap in a labyrinth seal was obtained. This flow rate can be compared to a 3.5-lb/sec leakage at 750°F which was experienced on a labyrinth seal of the same diameter operating at clearances in older models of the J79 engine, or an equivalent gap height of 0.0246 inch. The demonstrated improvement was therefore 19 to 1.

The following table summarizes the total dynamic testing done during the program:

Type	Max. Speed (RPM)	Max. Temp (°F)	Max. Press. (PSIG)	Hours
-131	4000	70°	175	8.33
Flight-Weight	4185	70°	175	3.61
-131	6200	750°	170	6.04
Flight-Weight	1820	1010°	168	0.16

SECTION II

INTRODUCTION

This program is concerned with reducing the parasitic leakage from compressor end seals in aircraft gas turbine engines. In the past, the problem of compressor discharge seal leakage has been solved using labyrinth seal technology. This type of seal has been improved through the use of special tooth designs, selected rubbing materials, and close control of stator and rotor thermal, inertial, and pressure deflections to permit operation with minimum clearance. At this time, use of the best technology allows 1% of total engine weight flow for compressor discharge seal parasitic leakage, and any further gain appears marginal by labyrinth seal.

Recently, the results of design analysis and development testing of high-speed face seals which operate on air-bearing principles, show promise of reducing compressor discharge seal leakage flows by a factor of as much as 20 to 1. The potential performance improvement offered by four air-bearing-type seals is investigated. In addition, a new flight-weight design is developed and tested at considerations up to 40,000 fpm, 1000-1200°F, and 175 psig.

SECTION III

TASK I - TEST RIG MODIFICATIONS

A. Bypass Lines

Figure 1 is a photograph of the test rig before modification to include bypass lines which permitted hot air to be admitted into the upper and lower sections of the disk, bypassing the seal, and allowing the rig to come to temperature more rapidly. There are four two-inch lines on top of the disk to exhaust seal leakage from the top seal, and four two-inch lines on the bottom of the rig to exhaust seal leakage from the bottom seal/bearing. These flows are combined into a larger four-inch line and exhausted up a stack. The hot-air inlet enters the bolted two-inch flange to the left of the test rig; a similar opening exists 180° away. The modification consisted of installing two one-inch valves on either line and directing hot gases into the top and bottom of the test rig, using one of the two-inch exhaust lines as an entrance port. Later in the program, multiple one-inch lines were introduced around the circumference of the seal manifold to permit a more uniform distribution of air inlet temperature. This was accomplished by drilling and tapping the two-inch wall and installing these lines. These modifications were successful, and temperatures over 1000°F, without the use of insulation on the test rig, were obtained.

B. The Original Hydrostatic Bottom Bearing

Figure 2 shows the test rig partially disassembled with the two two-inch inlet lines at 3 o'clock and 9 o'clock in the manifold. The original inherently-compensated air bearing (which served as a bottom bearing for the test rig) is shown with 200 0.04-inch diameter air inlets. This scheme was modified later in the program to permit the use of a floating seal/bearing which was less sensitive to temperature gradients in the base. The rotating disk is also shown in Figure 2. This disk was made from AISI 4140 steel for the 750°F hot testing and from A286 for the testing above 1000°F. Figure 3 shows the next level of assembly of the test rig, before installation of the top plate and air turbine drive.

The air turbine drive is an 8-inch air turbine which can produce 25 horsepower at the test speed of 7,200 rpm with 200 psig air inlet. This is about the friction power consumed by the rotating disk and seal shear areas in 750°F air at 7,200 rpm. The assembly in Figure 3 shows the seal housing and -131 seal in a retracted position, held by spring loads. The application of about 10 psig air pressure caused the seal to seat, depending upon the number of springs used.

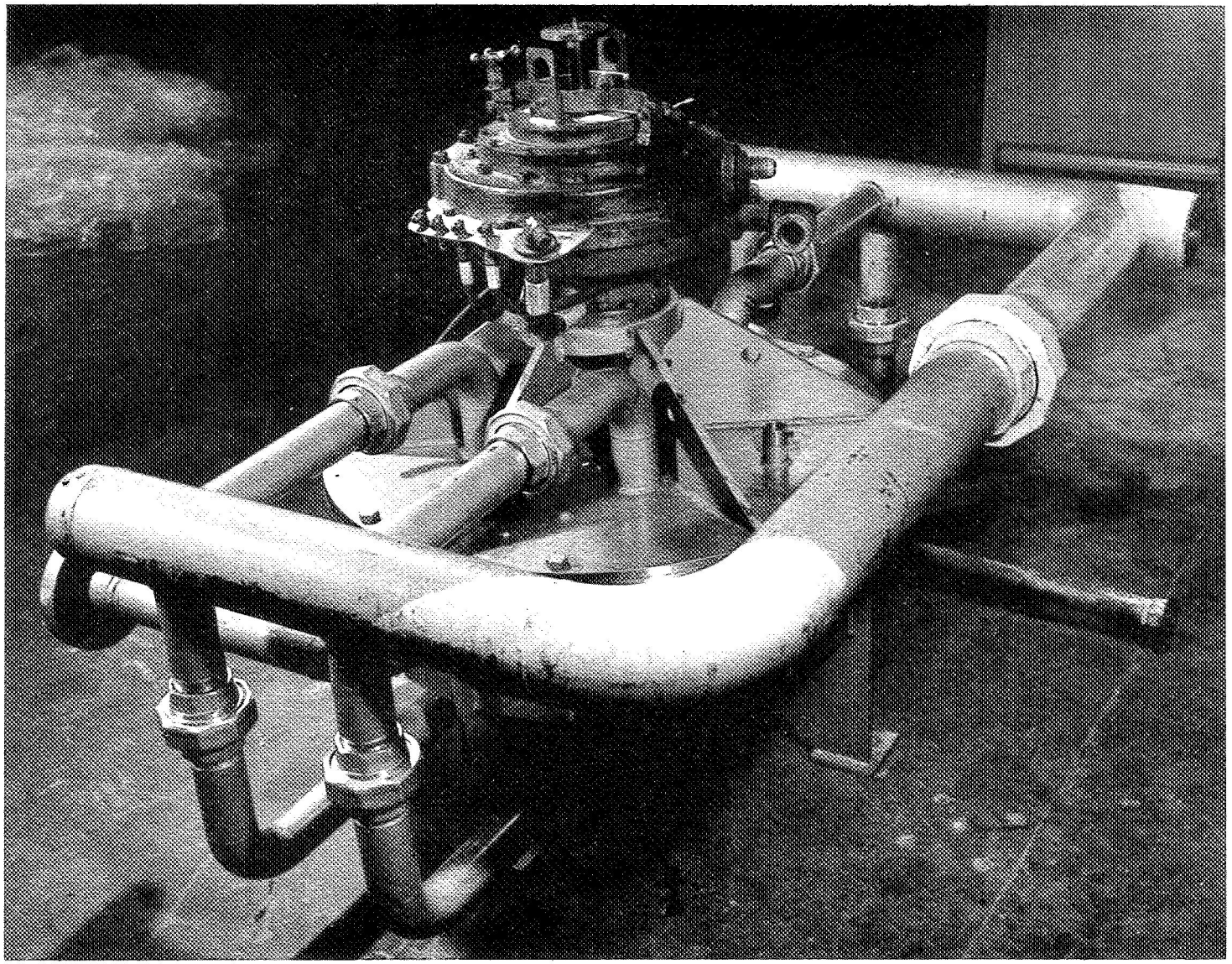

Figure 1. Dynamic Test Rig and Air Turbine Drive

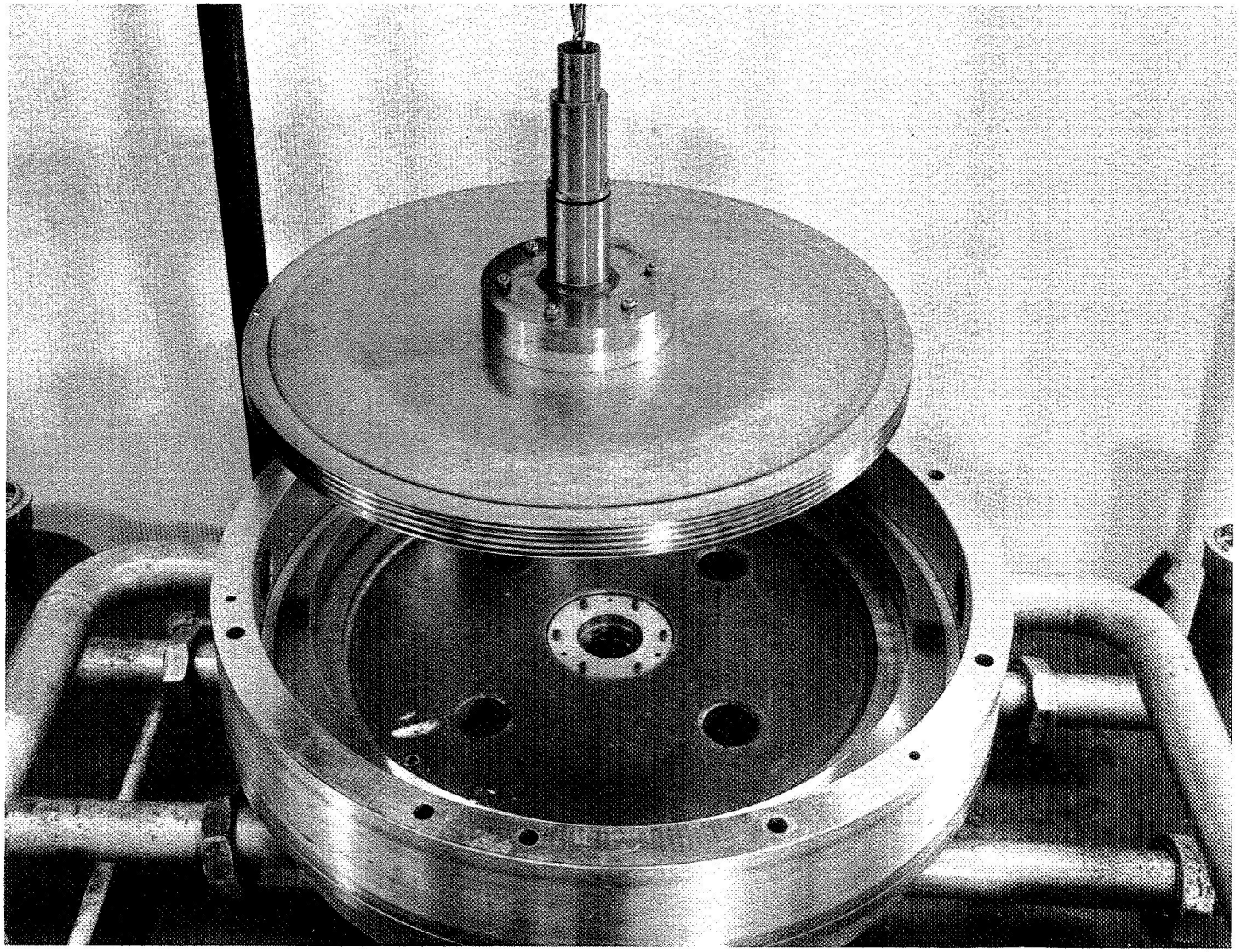

Figure 2. Test Rig and Air-Bearing Disk (C66102544)

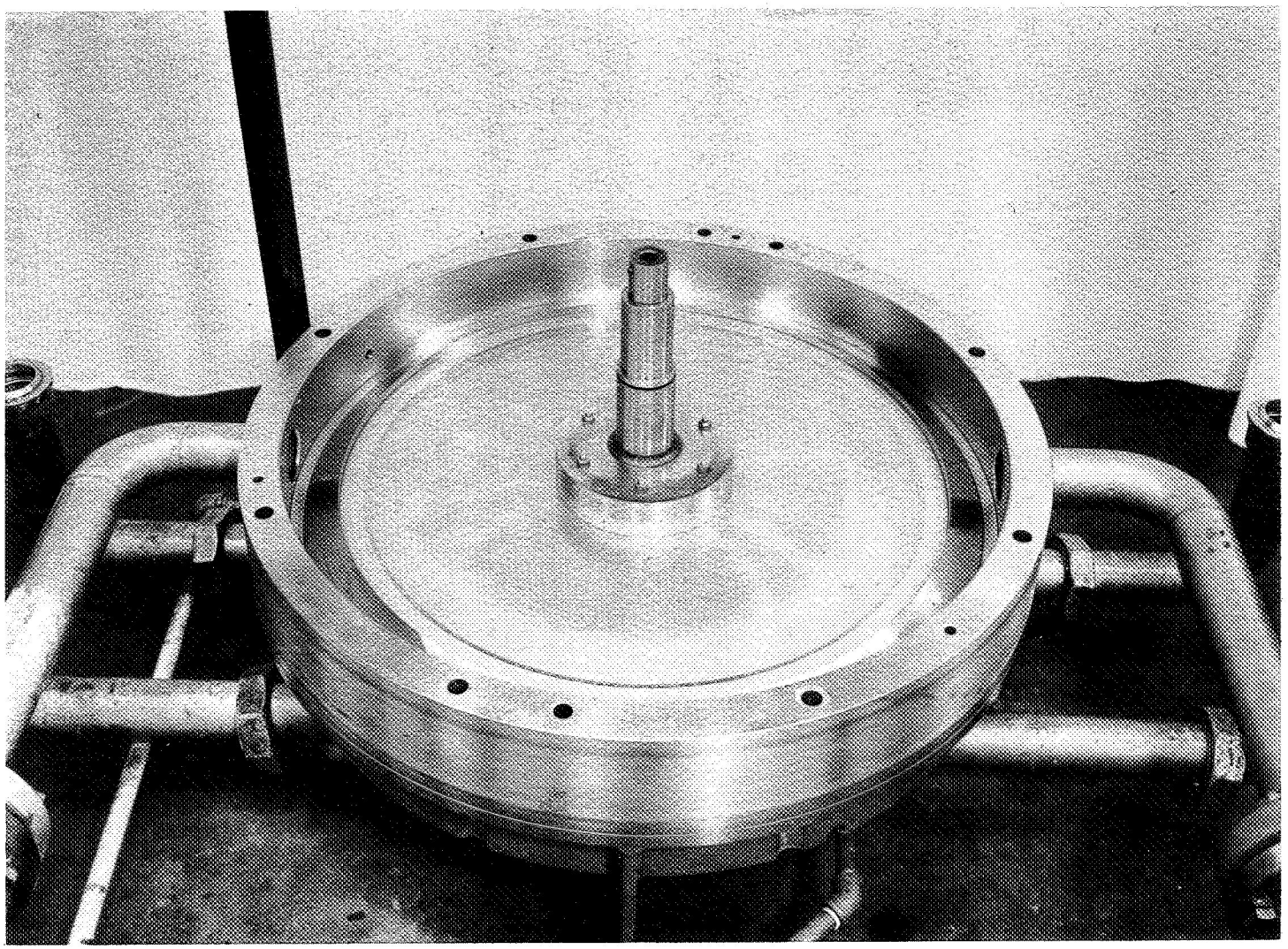

Figure 3. -131 Seal and Seal Housing Installation (C66102545)

C. The -333 Seal Assembly

The test rig assembly representative of most testing of this seal is shown in Figure 4. Modifications were made for each seal, and these are described further in the text. This section shows the shaft which was radially and axially located by two ball bearings (Item 5) and the rotating disk (Item 8). High pressure hot air is supplied through A_1 to pressurize the circumferential manifold area. The seal (Item 13) shown in this assembly drawing was not used in the program, but similar details of test seals will be shown in a further section. The bottom support bearing shown at A_6 as an inherently-compensated bearing was later replaced with a floating step bearing which freed that surface from thermal deflections imposed by the rest of the test rig. Exhaust air left the system through A_5 and A_{11}. Oil was supplied to the 206 size ball bearings through orifices indicated as Item 14.

D. The -131 Seal Assembly

The -131 assembly is shown in Figure 5 using a solid 4140 disk. In this assembly, the bottom bearing had been replaced by a hydrostatic step bearing similar in design to the seal being tested. Leakage in the system occurred through the two faces adjacent to the disk and through two piston rings. This assembly was run statically and dynamically from 70°F to 750°F and at a maximum speed of 6,200 rpm. Details of the seal design and testing appear in later sections.

E. The NASA CD847985 Seal Assembly

The assembly of the NASA design Raleigh step seal is shown in Figure 6. P_H is the pressure supplied to a manifold connected to multiple tubes, which supplied the seal face with an inherently-compensated hydrostatic liftoff assist at disk speeds too low to support the seal hydrodynamically. Testing of this seal progressed only through the static stage due to difficulties resulting from rework of the seal face vent grooves and face plating which destroyed the geometry of the bearing. Details of this testing and the design appear later in the report.

F. The Flight-Weight Seal Assembly

Figure 7 shows the final assembly of the flight-weight seal. This seal was similar to the -131 seal except that much lighter sections were employed to reduce the weight of the seal. In addition, a pressure-balanced race (Item 9) was installed to simulate one which could be used in actual engine design. The support system is similar to that of the assembly shown in Figure 5. The bottom support was a stepped-face air bearing similar to the seal being tested, so that the pressure loads on the disk in an axial direction were essentially zero and the assembly weight is carried on a spring mount (Item 16). Details of the design and testing of this assembly are given further in the text.

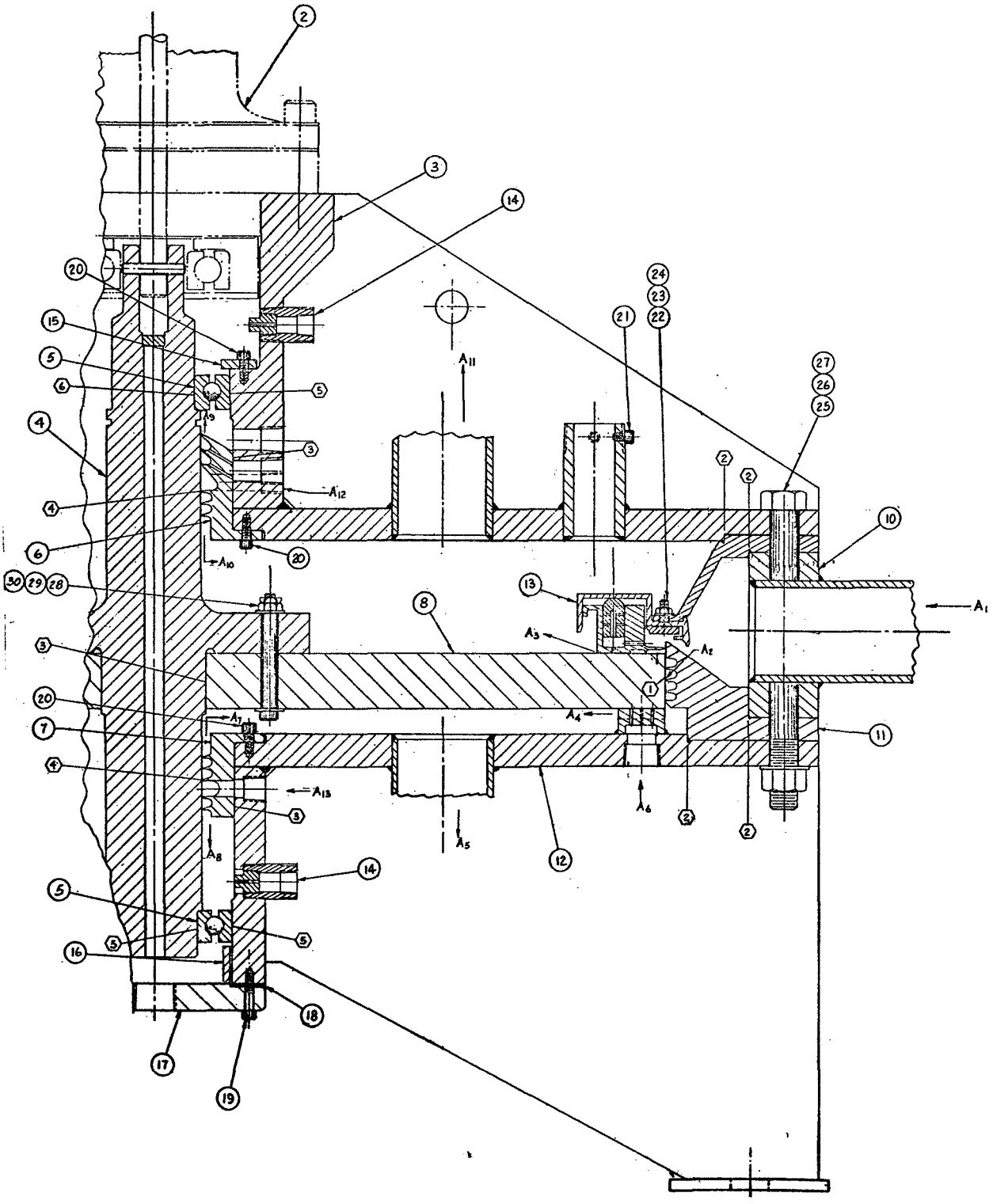

Figure 4. Dynamic Test Rig Assembly

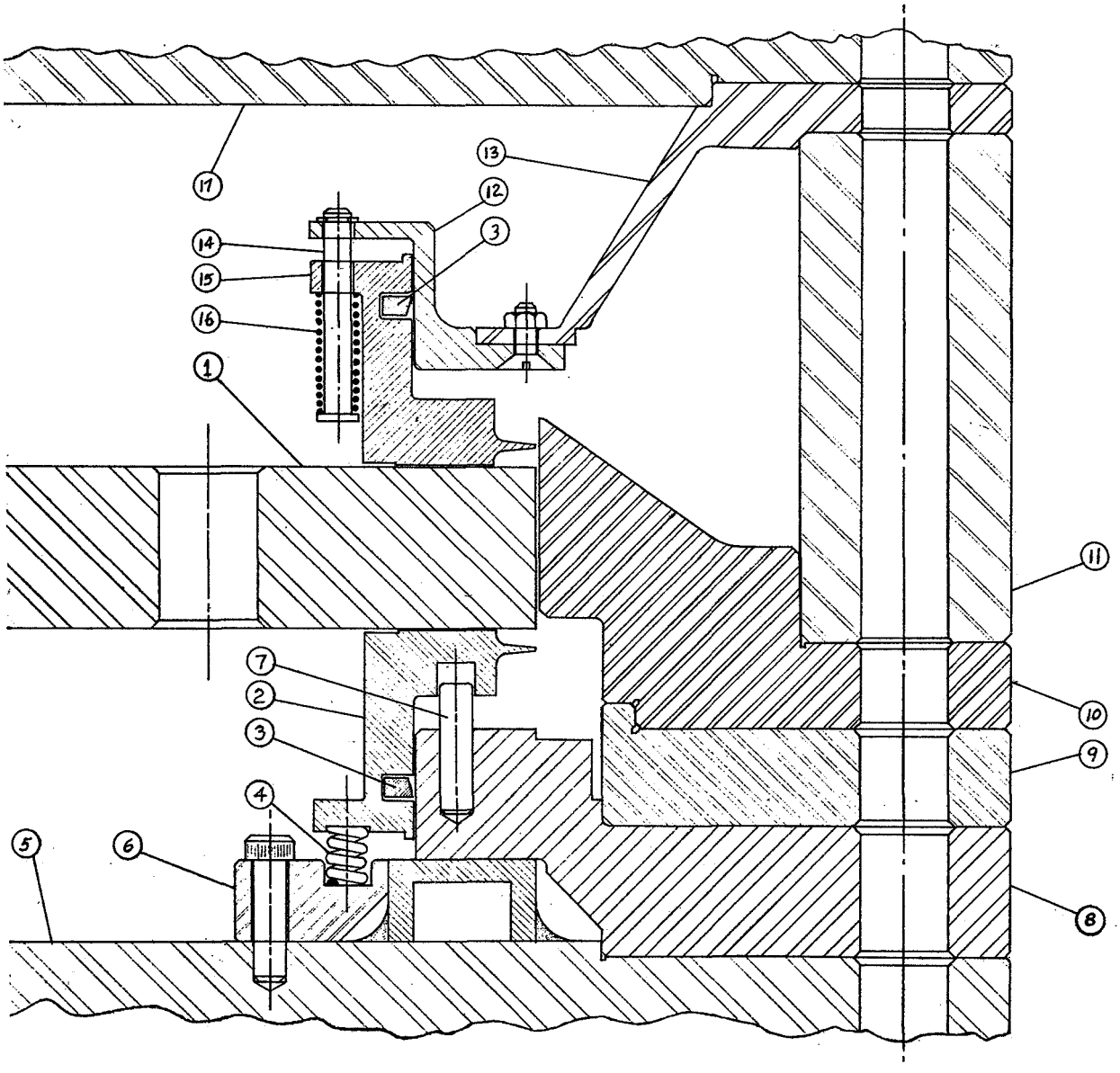

Figure 5. Dual -131 Seal Assembly

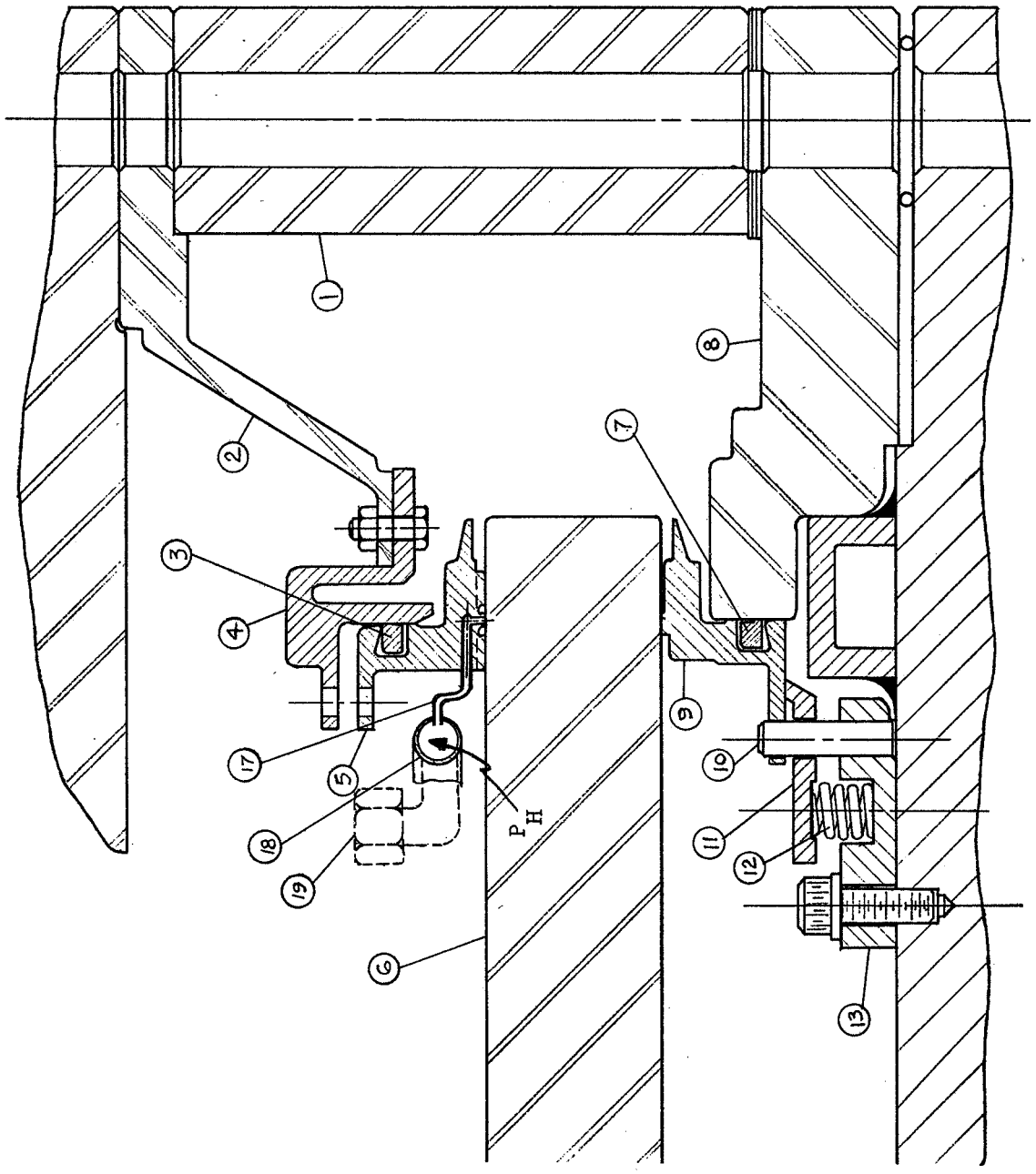

Figure 6. NASA CD847985 Seal Assembly

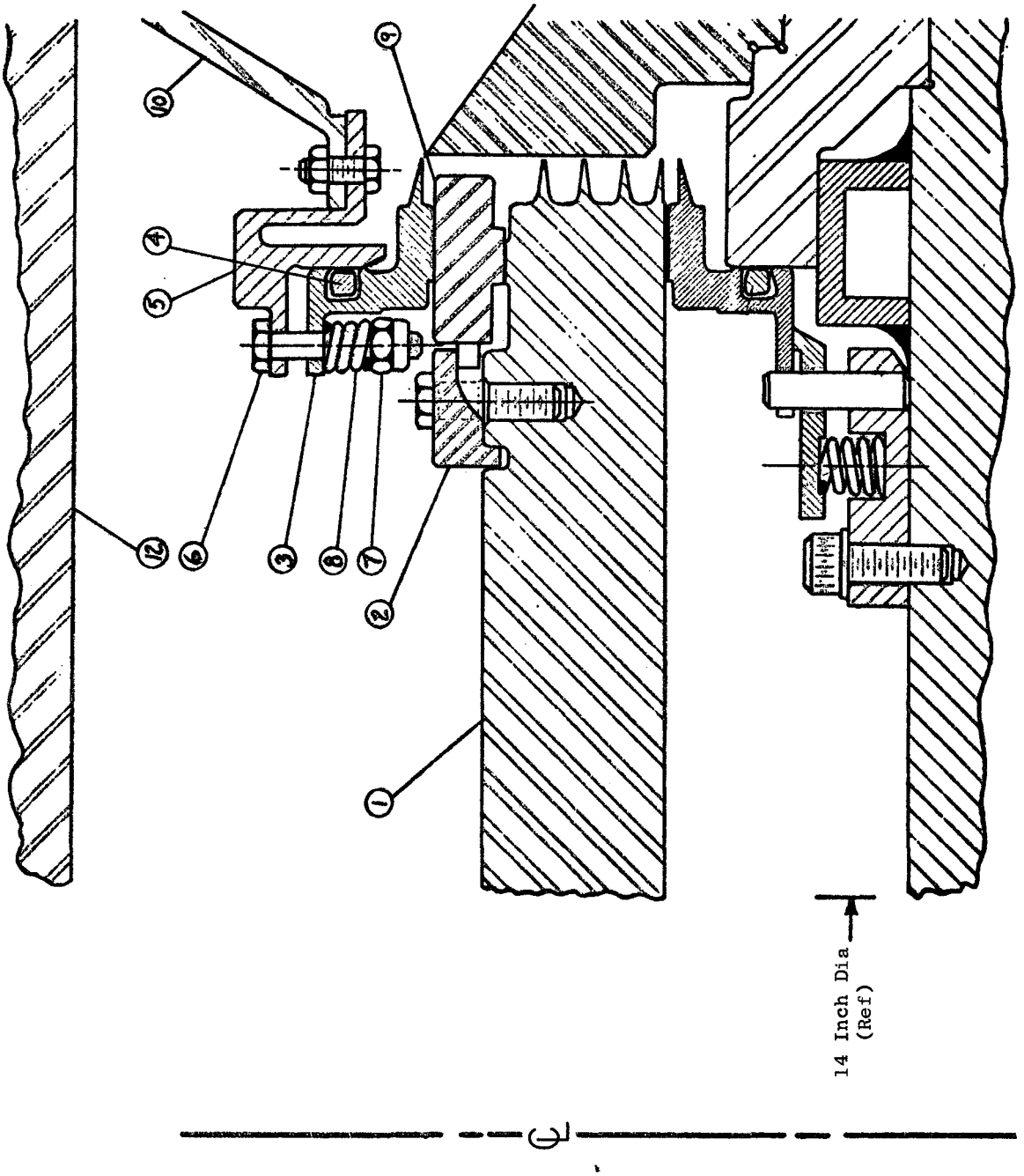

Figure 7. Dual Flight-Weight Seal Assembly

SECTION IV

TASK II - SEAL DESIGN AND DEVELOPMENT

A. -333 Seal

Figure 8 is a photograph of the -333 seal body, piston ring, and housing. Also shown in the photograph is the smaller sectioned -131 piston ring for comparison. The photograph shows clearly the seal face including 200 0.040-inch diameter inherent-compensation orifices and 100 0.250-inch diameter pressure relief holes between the inherently-compensated bearing face and the single-tooth primary seal. A section through this seal is shown in Figure 9.

Figure 9 shows the component parts of the seal assembly, namely: (1) the seal body, (2) the seal retraction springs, (3) the secondary piston ring seal, (4) the double air bearing, and (5) the primary seal tooth. The secondary piston ring seal (3) seals the manifold air from leakage around the seal body and is held in position by the smaller coil springs. The location of this piston ring seal on the housing was undesirable (because, as the axial stackup clearance varied from build-up to buildup, the radial inward force on the seal body about its center of gravity changed). In later designs, the secondary piston ring was placed in a groove on the body of the seal so that no change in radially inward pressure force could be experienced as a function of axial position. The secondary piston ring seal was held circumferentially against the seal body by means of a spring. The primary seal tooth blocked flow from the high pressure manifold and was positioned away from the rotating disk by means of a double orifice air bearing which operated on an inherent compensation principle. Air at high pressures is admitted to these orifices radially inward from the high pressure area, while air which leaks through the primary seal tooth is relieved through quarter-inch holes through the seal body into the low pressure area.

The design of the air bearing support was made possible by an empirically derived relationship between film thickness and load which is shown in Figure 10. The curves of film thickness versus load at various supply pressures, 50 to 200 psi, were obtained experimentally after constructing a model of the thrust face and running tests statically while measuring load and film thickness. Experience has shown that this curve is virtually the same when relative motion occurs between the disk and bearing surface; that is, there is no appreciable hydrodynamic action exerted on the face because of the non-converging surfaces. After this curve was obtained, it was then possible to size the secondary piston ring seal diameter. This diameter determined the resulting axial force which seated the seal body against the disk. Shown on Figure 10 are operating lines for a secondary piston ring seal net area of 10 and 15 square inches. As would be expected, a higher piston area causes operation

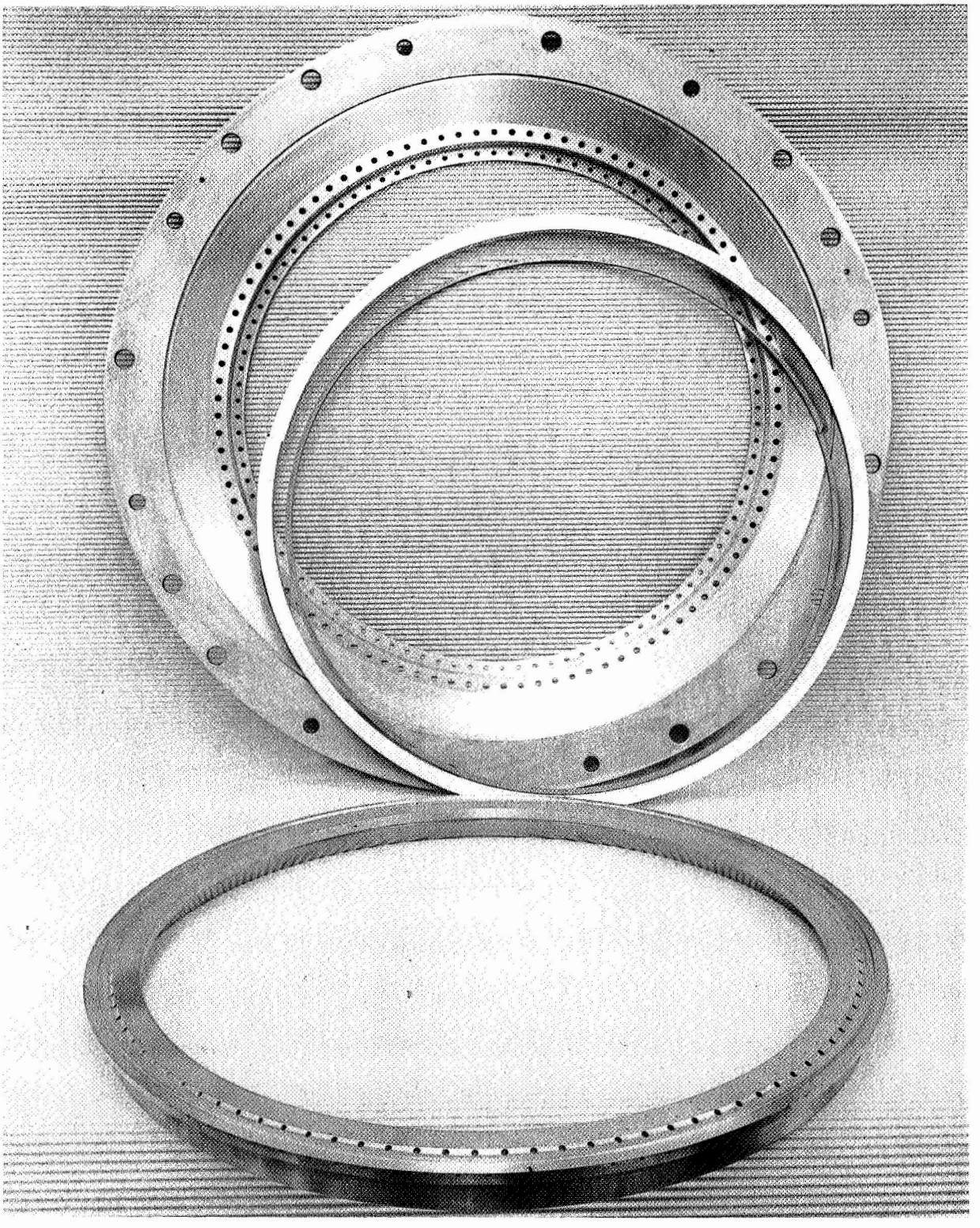

Figure 8. -333 Seal Assembly (C67120542)

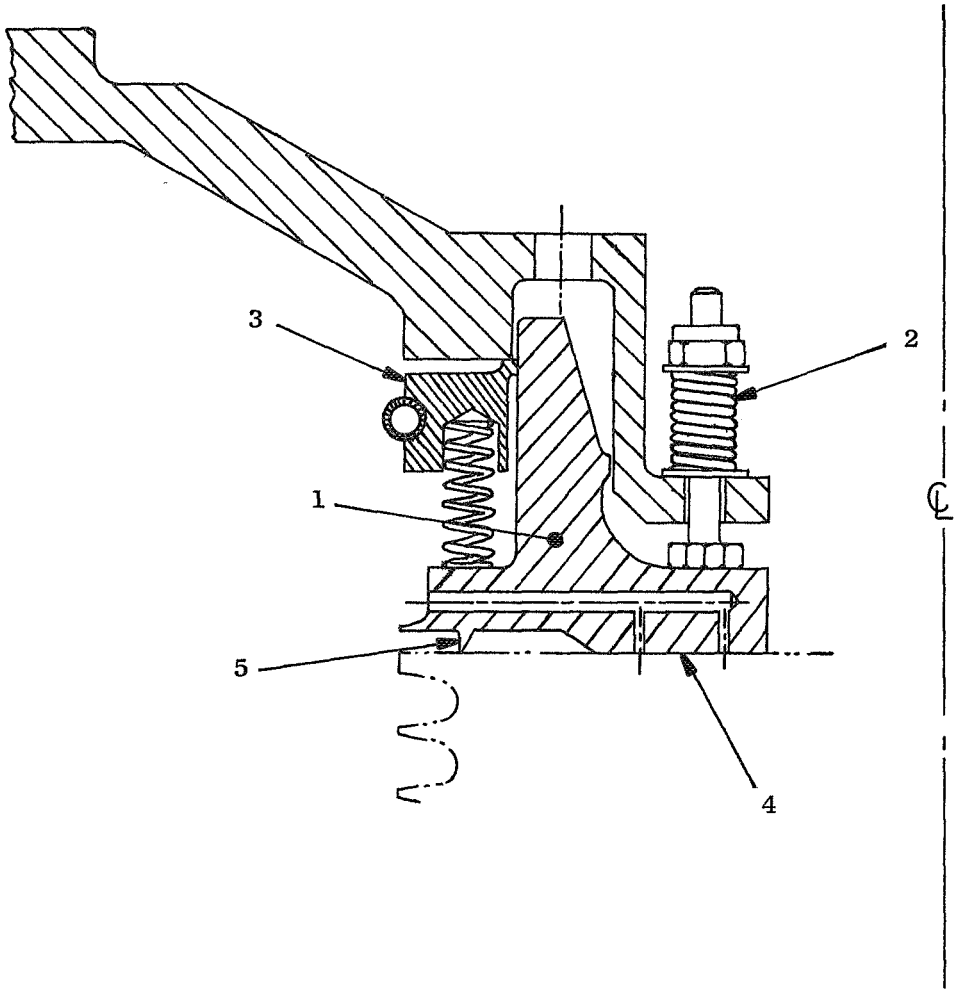

Figure 9. -333 Seal Section

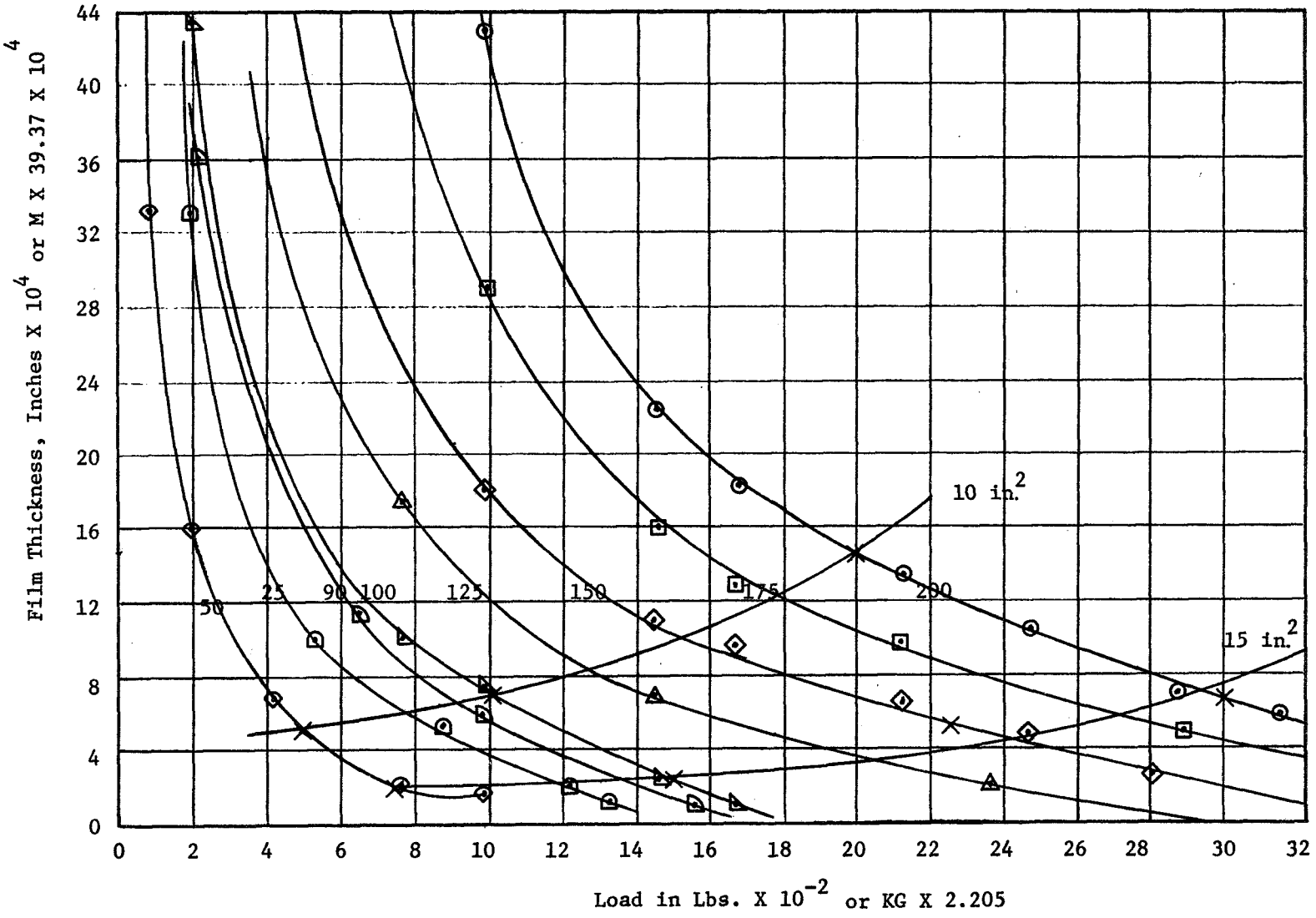

Figure 10. Film Thickness Vs. Load for -333 Seal

at a lower film thickness. The final selection of 10 square inches for the net bias area was based on the desire to operate at a film thickness of about 0.001 inch. Operation at this film thickness gives more margin for 1 per rev excursion of the disk than does, for example, a film thickness of 0.005 inch. Using stiffness values of the air bearing obtained by measuring the slope of film thickness versus load in Figure 10, it was estimated that 1 per rev following of the seal body to the rotating disk would take place.

Figure 11 shows a force balance about the center of gravity of the seal body. The seal body section center of gravity was located in such a way as to present a zero summation of moments about the section. The radially-inward force, F_1, could be varied by the location of a secondary piston ring seal. The axial seating force, F_2, could be varied by changing the secondary sealing dam diameter. The inherently-compensated air bearing reaction, F_3, could not be varied once the design had been selected. This design was accomplished by trial and error, so that the section of the seal body remained undeflected at the highest condition of pressure. Because F_3 does not vary linearly with pressure, and F_1 and F_2 do, there was some slight deflection of the section at lower pressure levels. It was assumed that the vent area would be at ambient. In practice, this pressure rise caused section tilt, and the bleed holes were enlarged to reduce this effect. These results are given in the experimental section.

B. -131 Hydrostatic Seal

The general theoritical operation of the -131 stepped face hydrostatic seal assembly, as shown on Figure 5, is as follows:

Pressurized air is introduced through radial holes in the air inlet manifold (Item 11) into an annulus around the outside diameter of the hydrostatic seal rings (Items 2 and 15). Air escapes from this annulus by passing through two piston rings (Item 3) and through the interfaces between Items 1 and 2, and 1 and 15. The escaping air enters the areas between Items 1 and 17, and Items 1 and 5, which are vented to atmospheric pressure.

In the unpressurized state, the top seal (Item 15) is lifted off the disk (Item 1) by a force generated with coil springs (Item 16). As inlet pressure is increased, a pressure drop is generated by the restriction between the labyrinth tooth at the outside diameter of the seal face (Item 15) and the seal guide (Item 10). When the pressure force on the back surface of the seal face exceeds the retracting coil spring force, the seal face slides downward, approaching the surface of the disk. As the seal face approaches the disk, its interface clearance replaces the labyrinth tooth as the controlling air flow restriction, and the pressure drop across the labyrinth tooth becomes inconsequential.

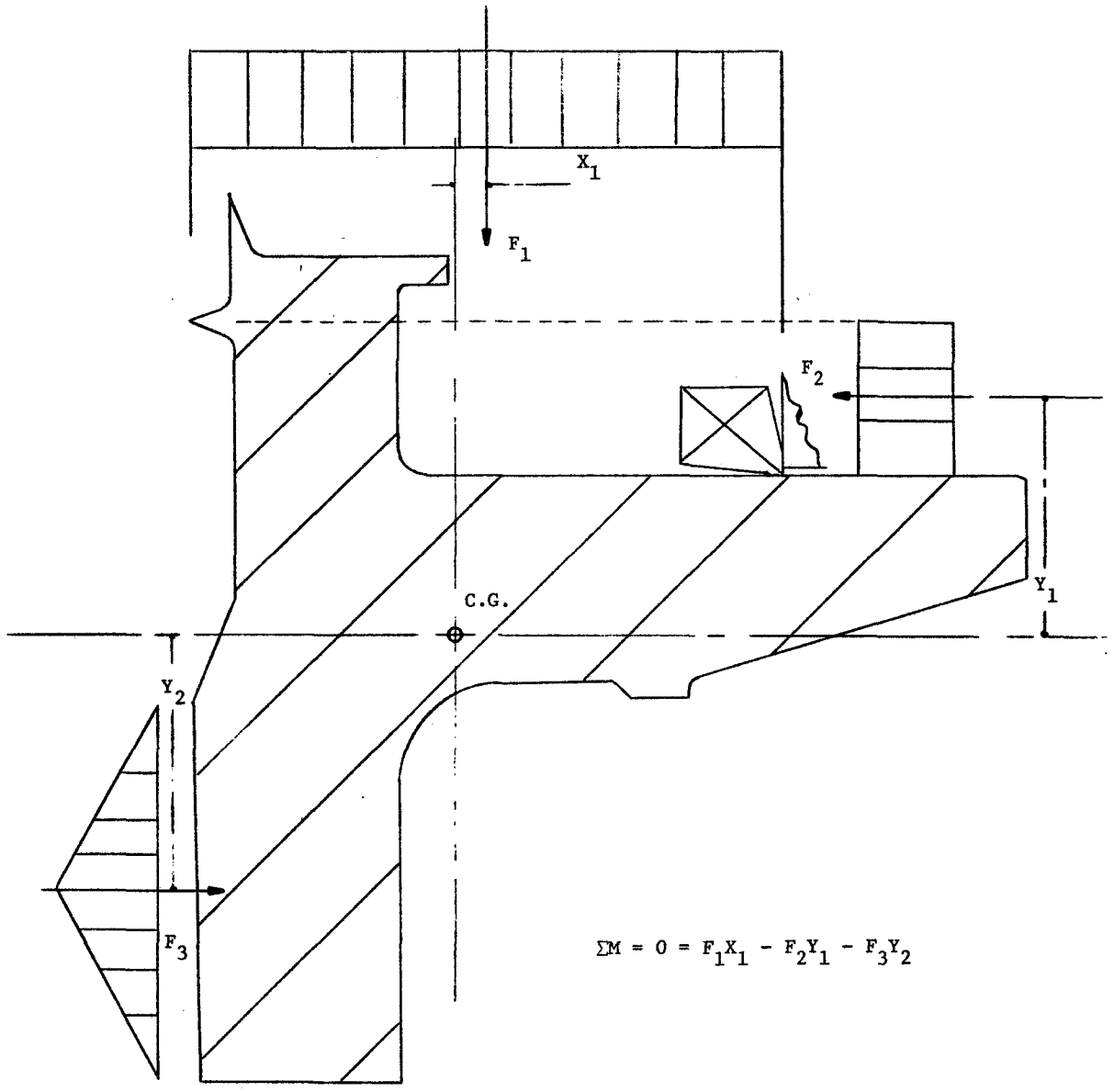

Figure 11. Pressure Balance on -333 Seal

The pressure level at which the seal approaches the disk varies with the applied spring force, and is governed by the stiffness requirement of the interface air film which increases as pressure increases.

The pressure acting on the area of the back surface of the seal face, bounded by the diameter on which the piston ring seats (balance diameter) and the outside diameter of the seal face, generates a downward (seating) force on the seal body. Pressure force acting on the seal face, in the area bounded by the seal face inside and outside diameters, generates an upward (unseating) force.

As air moves through the restriction between the seal face and the disk, its static pressure decreases so that the average static pressure in the interface is lower than the uniform pressure acting against the back surface of the seal face; however, the interface surface area is made larger than the back surface so that, at some interface clearance dimension, the seating and unseating pressure forces (pressure x area) reach equilibrium.

The bottom seal (Item 2) has the same geometry as the top seal (Item 15) and is pressurized from the same source. Except for the retraction due to spring force, as described previously, equilibrium of pressure forces is established in the same manner as the top seal. The interface clearance (air film thickness) will be slightly smaller in magnitude, however, because it supports the static weight of the parts above it [i.e., Items 1, 3, and 15, plus the weight of the center shaft, Figure 4 (Item 4), and the shaft bearings, Figure 4 (Item 5), 2 places].

Once equilibrium is established, a servo, generated by a step on the seal face, provides resistance to any change in interface air film thickness. The magnitude of force required to change the air film thickness by a given distance from equilibrium may be defined as the "stiffness" of the air film. The following sketch shows the pressure distribution for equilibrium and for displacement from equilibrium for the stepped face hydrostatic seal with compressible flow:

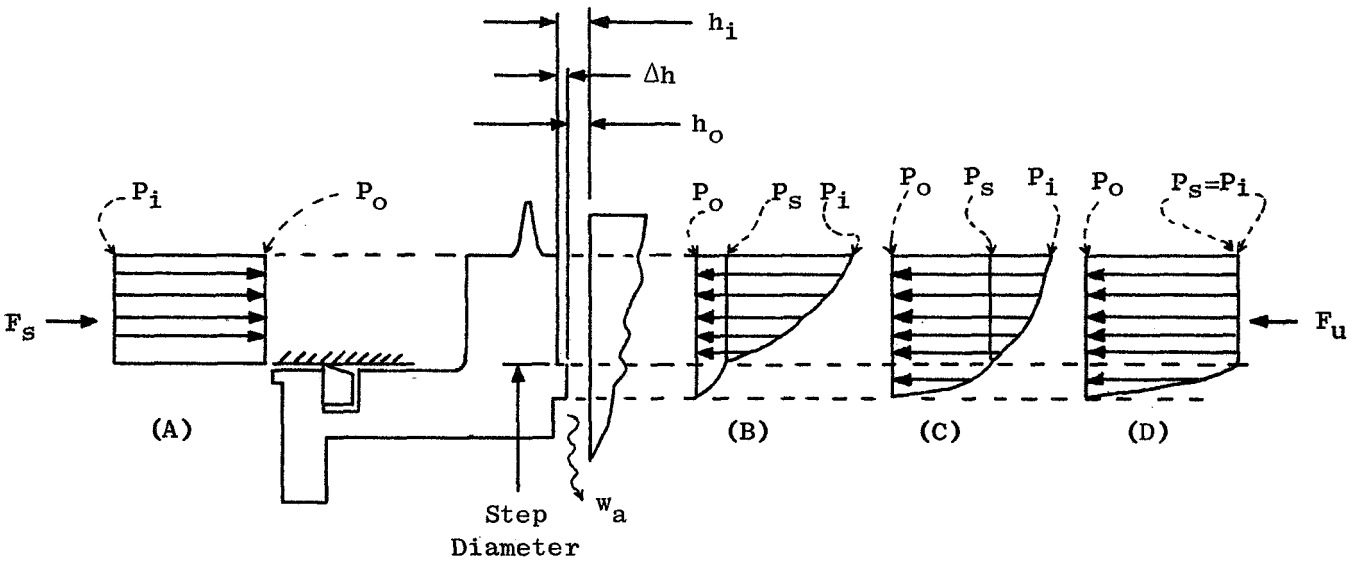

For a given inlet pressure and seal geometry, the force to seat, F_s, is constant and is represented by the area inside the force diagram at (A). The force to unseat the seal is represented by the area inside the force diagrams at (B), (C), and (D).

Let:

w_a = weight flow rate

h_o = air film thickness at exit

Δh = step height

h_i = inlet film thickness = $h_o + \Delta h$

P_i = inlet (upstream) pressure

P_s = pressure at the step diameter

P_o = exit (downstream) pressure

Also, let the areas inside the curves at (A) and (C) be equal, so that F_s and F_u are at equilibrium.

If h_o is decreased from eqiulibrium, the following changes are effected:

(a) P_s increases and approaches P_i as h_o approaches 0

(b) w_a decreases and approaches 0 as h_o approaches 0

(c) F_u increases, as represented by the area inside the force diagram at (D), and a net force ($F_u > F_s$) is generated to return the seal to equilibrium.

Increasing h_i effects the following:

(a) P_s decreases

(b) w_a increases

(c) F_u decreases, as represented by the area inside the force diagram at (B), and a new force ($F_s > F_u$) is generated to return the seal to equilibrium.

The above described force changes, effected by changes in operating clearance, comprise the servo for the stepped face hydrostatic seal.

The force curves for the hydrostatic seal were calculated based on the following equations for laminar, isothermal, compressible flow:

$$q = \frac{h^3 \pi D}{24\ u\ L} \left(\frac{P_i^2 - P_o^2}{P} \right) \left(\frac{T}{T_i} \right) \qquad \text{Eq (1)}$$

h = clearance between parallel plates

D = mean diameter of seal face

u = absolute viscosity

L = length of flowpath

P_i = absolute pressure at inlet

P_o = absolute pressure at outlet

P = absolute pressure, standard atmosphere

T = absolute temperature, standard atmosphere

T_i = absolute temperature at inlet

q = standard volume flow rate

For flow through the inlet flowpath:

$$q_i = \frac{h_i^3 \pi D_i}{24 u L_i} \left(\frac{P_i^2 - P_s^2}{P} \right) \left(\frac{T}{T_i} \right) \qquad \text{Eq (2)}$$

For flow through the outlet opening:

$$q_o = \frac{h_o^3 \pi D_o}{24 u L_o} \left(\frac{P_s^2 - P_o^2}{P} \right) \left(\frac{T}{T_1} \right) \qquad \text{Eq (3)}$$

For continuity of flow:

$$q_i = q_o \qquad \text{Eq (4)}$$

Substituting Eqs (2) and (3) in Eq (4), cancelling like terms, substituting $(h_o + \Delta h)$ for h_i, and rearranging, gives the following:

$$\frac{h_o^3}{(h_o + \Delta h)^3} = \left(\frac{D_i}{D_o} \right) \left(\frac{L_o}{L_i} \right) \left(\frac{P_i^2 - P_s^2}{P_s^2 - P_o^2} \right) \qquad \text{Eq (5)}$$

Knowing inlet conditions, exit conditions, and seal geometry, h_o can be calculated by substituting various values of P_s in Eq (5), with $P_i > P_s > P_o$.

Using various values of P_s, the interface forces, F_u, can be calculated using the following equations:

$$F_u = (P_s - P_o)(A_i + A_o \lambda o) + (P_i - P_s) Ai \lambda i \qquad \text{Eq (6)}$$

where:

A_i = face area of inlet flowpath

A_o = face area of outlet flowpath

λ = gas compressibility factor based on pressure ratio, as follows:

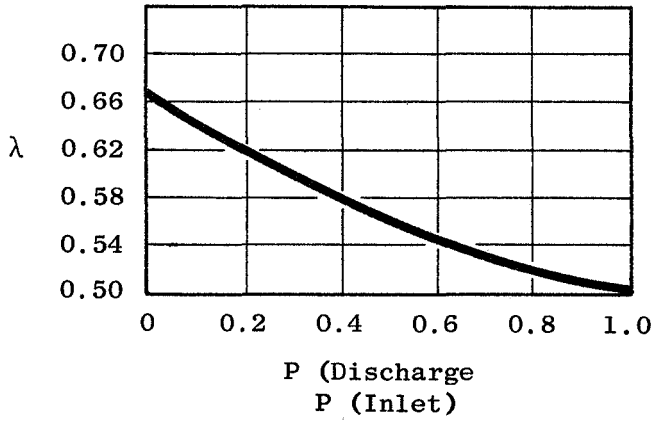

The seating forces, F_s, are as follows:

$$F_s = (P_i - P_o)\, A_s \qquad \text{Eq (7)}$$

where A_s = seating area

Finding the net force ΔF, as follows:

$$\Delta F = F_u - F_s \qquad \text{Eq (8)}$$

and plotting these values against h_o as calculated using Eq (5) gives the force curve for the seal, with stiffness (k), defined as:

$$k = \frac{\Delta F}{\Delta h_o}$$

The force curves for the -131 seal are shown on Figure 12. The geometry assumed was the following:

h = 0.0009 inch

L_i = 0.600 inch

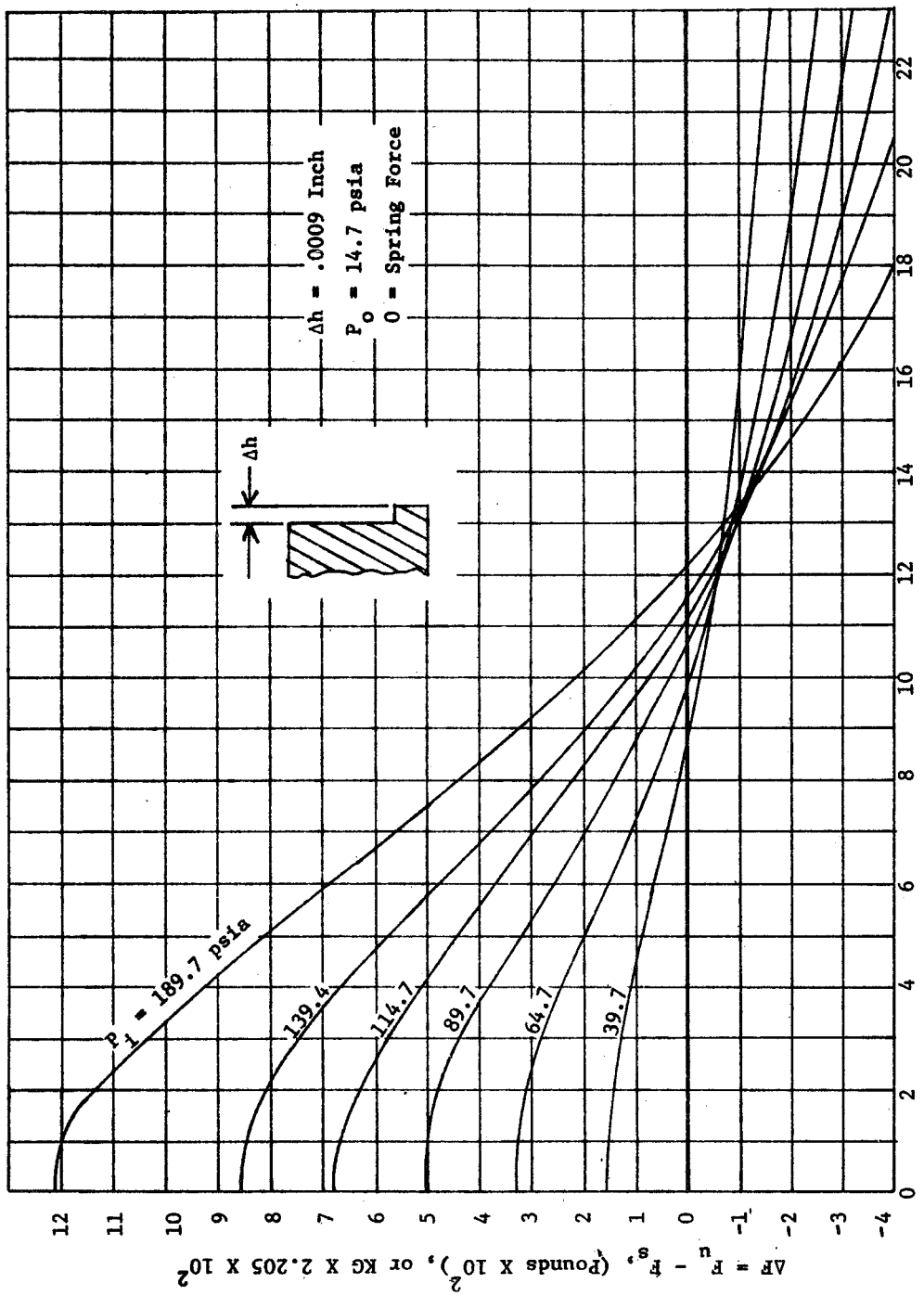

Figure 12. -131 Seal h_o ΔF for Stepped Face

L_o = 0.155 inch

D_i = 22.800 inches

D_o = 22.045 inches

For all calculations, P_o is assumed to be 14.7 psia and T_i is 520°R. In addition, the balance diameter (piston ring seat) and the seal face are assumed to be concentric.

Calculated leakage rates for the stepped face are shown on Figure 13. These leakage rates are based on the following equation for sonic flow at minimum area, since the values calculated using the laminar flow equation resulted in leakage rates which gave Reynolds Numbers in the turbulent flow region:

$$q_o = 42\ P_s\ D_i\ h_o$$

where:

q_o = volume flow rate, scfm

P_s = pressure at inlet to step, psia

D_i = mean step diameter, inches

h_o = film thickness at step, inches

In the course of the test program, the seal face was modified by lapping a taper on the face in place of the step; and, since some of the testing included in this report was done with a tapered face, the leakage rates and servo forces were calculated. The results are shown on Figures 14 and 15. All dimensions were the same as for the stepped face, with the exception of the geometry at Δh. Δh was assumed to be formed by a taper of constant slope with the large opening at the inlet (OD). The taper angle, θ, was 1.33 milli-radians, as shown on the following sketch:

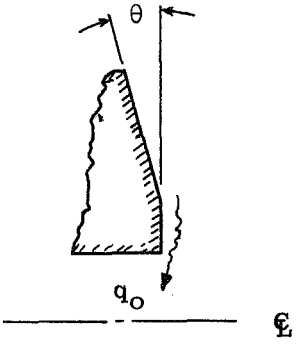

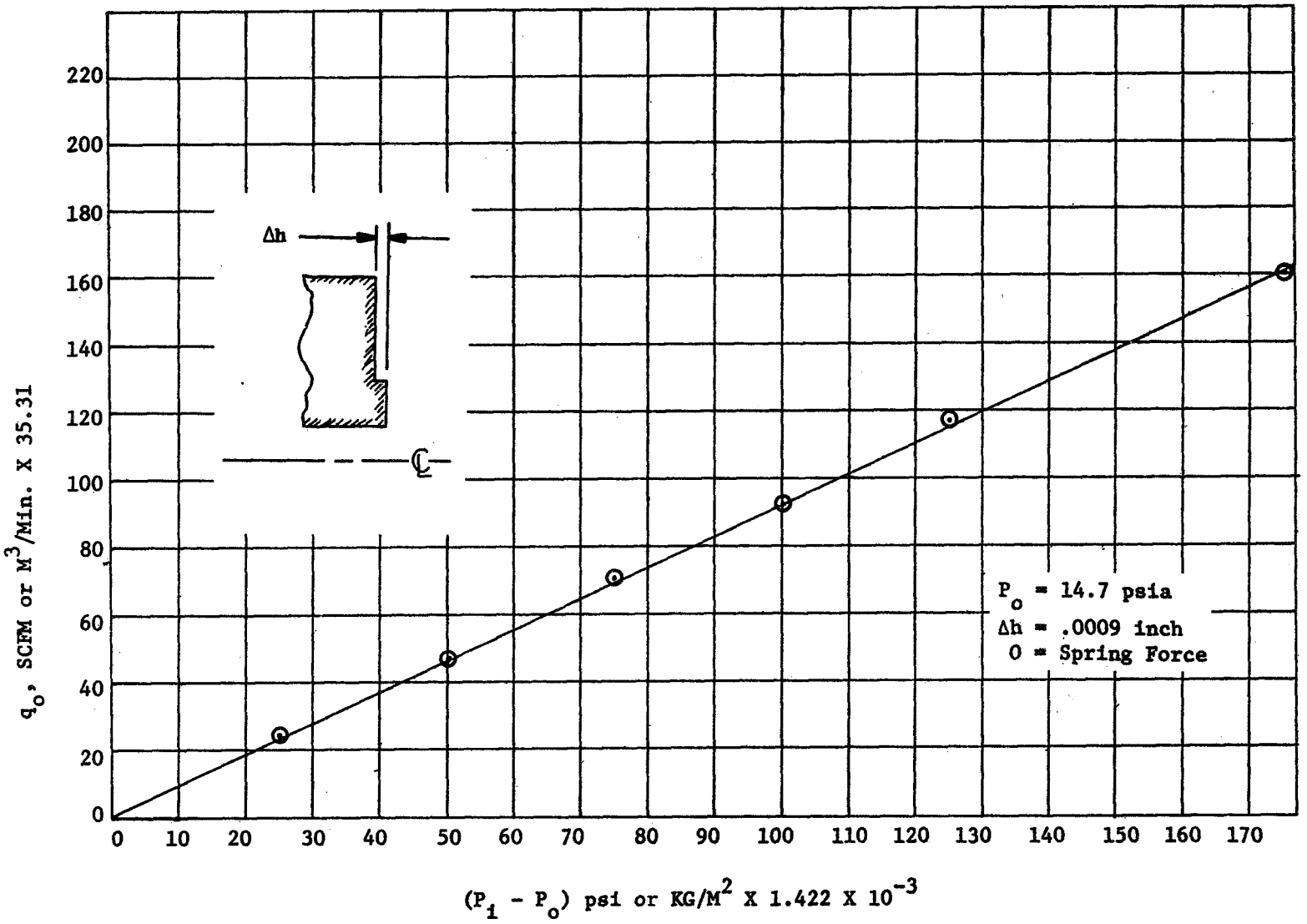

Figure 13. -131 Face Leakage Vs. Seal ΔP (Stepped Face)

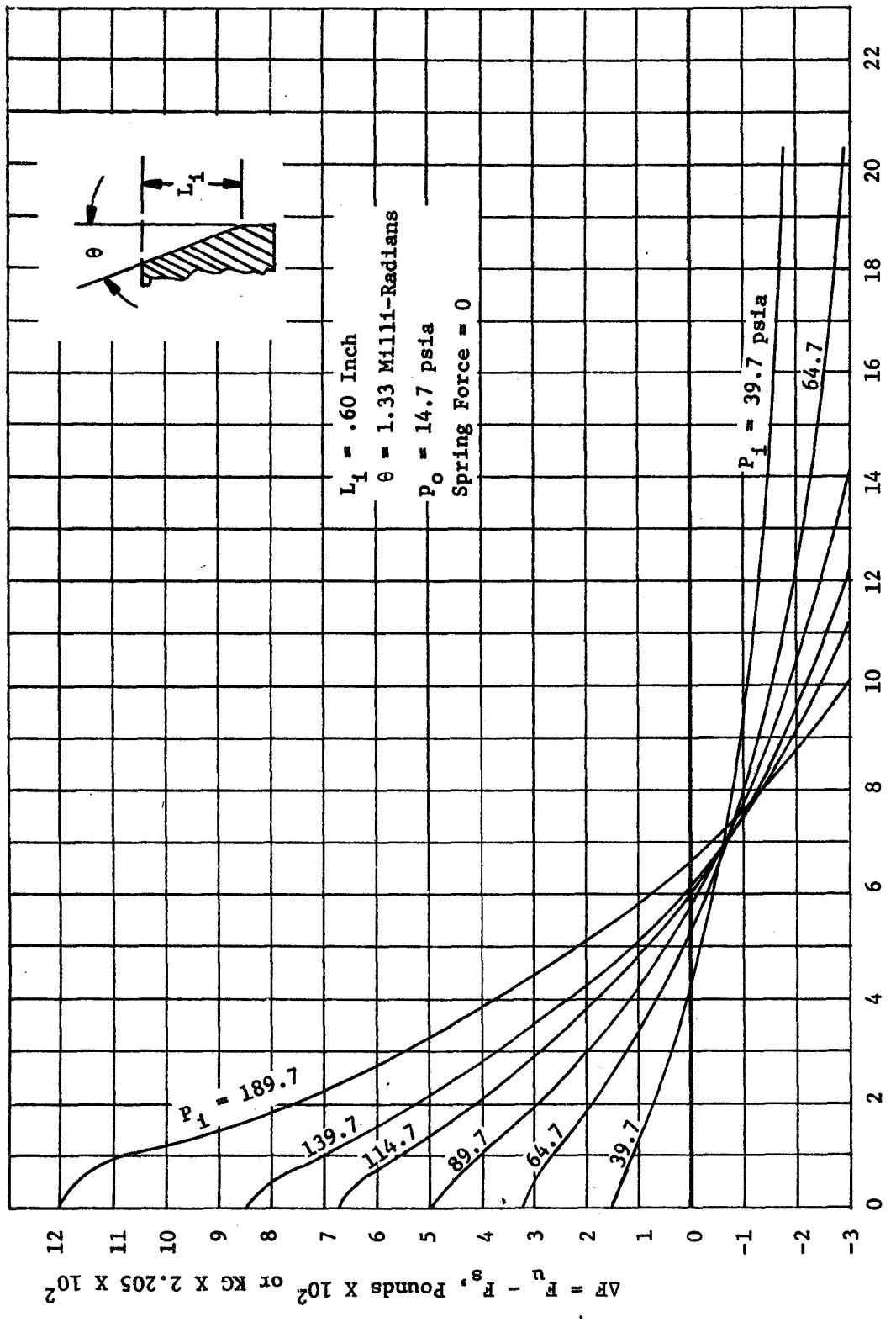

Figure 14. -131 Seal h_o Vs. ΔF for Tapered Face

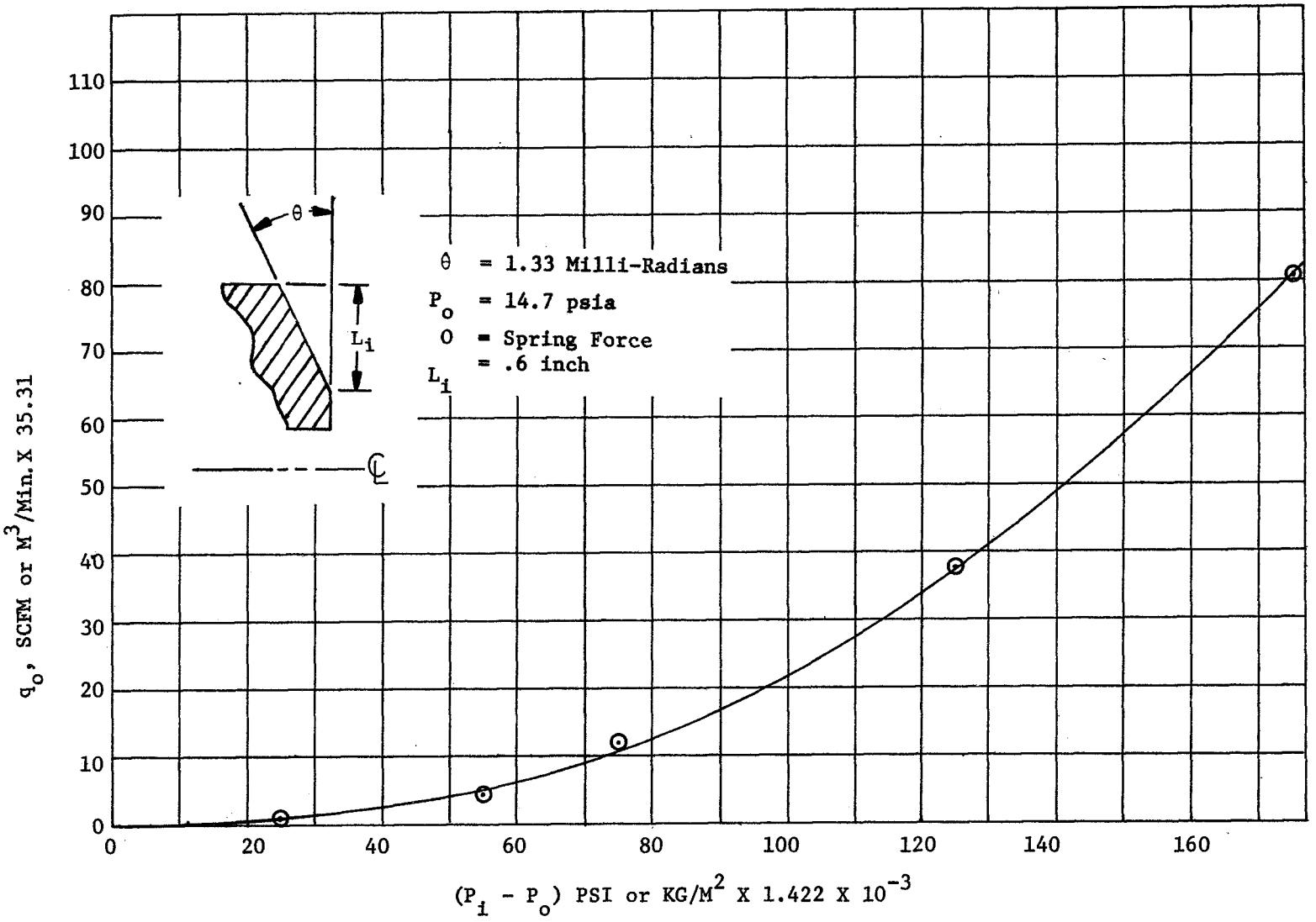

Figure 15. -131 Face Leakage Vs. Seal ΔP (Tapered Face)

The mechanical design considerations for this seal would be similar to that described for the flight-weight seal presented in Section VA.

C. CD487985 Design

The third seal used in the program was designed at the NASA-Lewis Flight Propulsion Laboratory facility by L. Ludwig and D. Townsend. A drawing of this seal is shown in Figure 16. This design was conceived to incorporate a Raleigh step face which would act as a lift-off device by means of hydrodynamic action. The balance sealing dam and piston ring groove were designed so that this configuration could be used in the same testing set up as employed by the flight-weight seal design which will be discussed later. The seal was manufactured of 310 stainless steel material, and a chrome plate was applied to the seal face at a later date to improve its touchdown capability. In addition, an inherently-compensated hydrostatic lift-off system was incorporated as shown in Figure 17 to permit the seal to be lifted off during startup. Details of the testing of the seal appear further in the text.

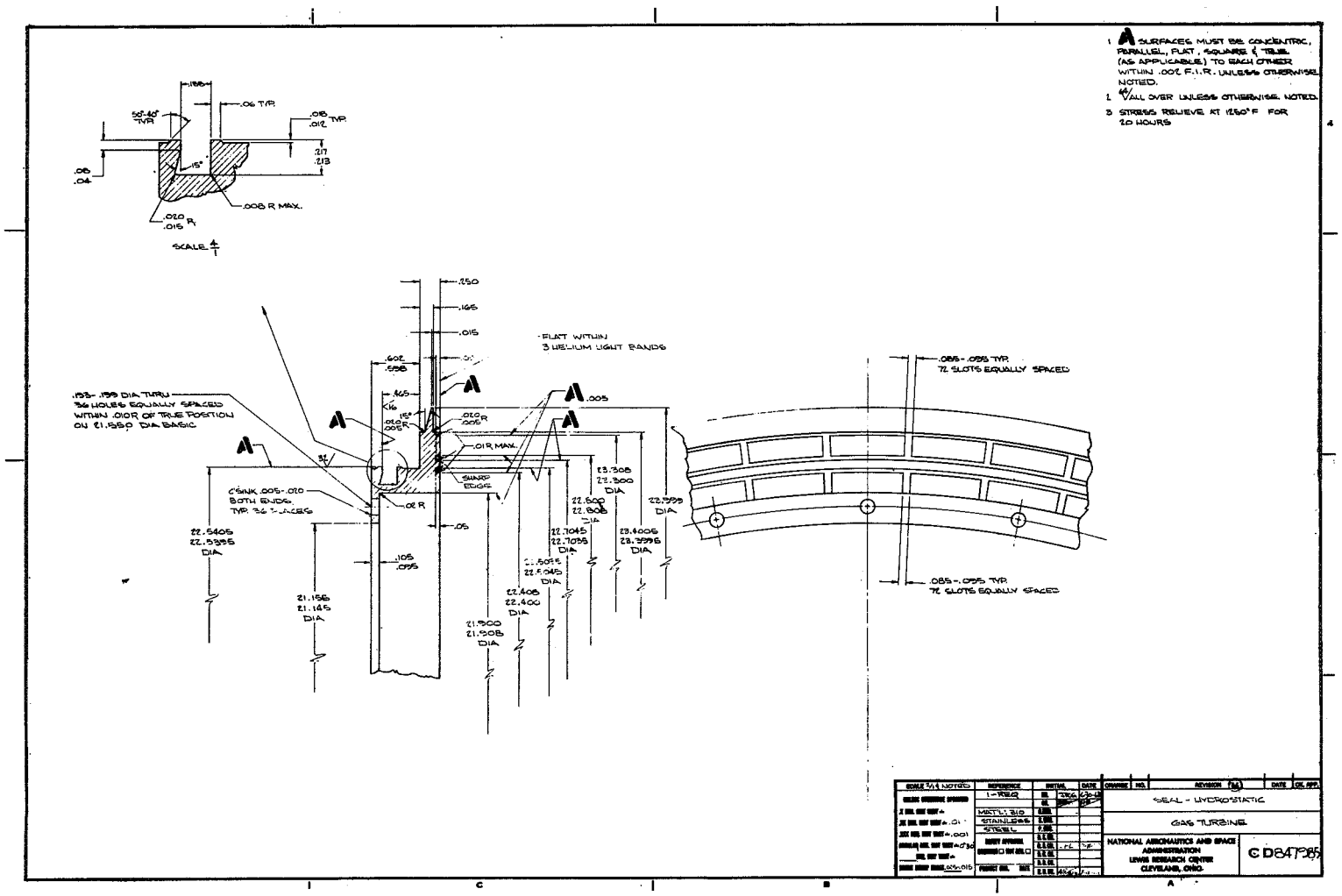

Figure 16. CD847985 Seal

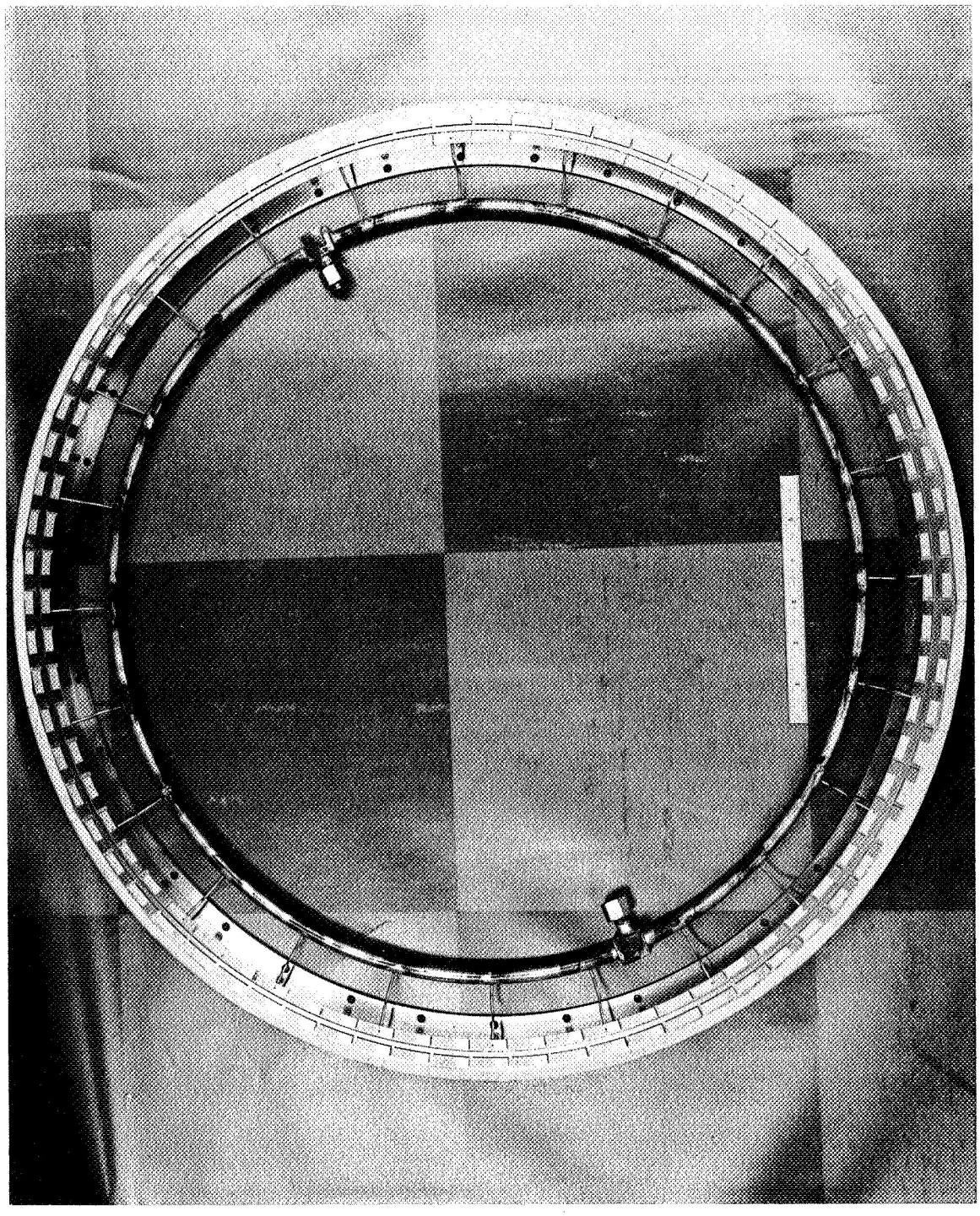

Figure 17. NASA CD847985 Hydrodynamic Face Seal

SECTION V

TASK III - EXPERIMENTAL EVALUATION

A. Room Temperature Static Tests

1. -333 Static Tests

Static testing of the -333 seal was done by modifying the test rig shown in Figure 4. This modification consisted of fastening the disk (Item 8) to the bottom air bearing by means of silicone cement, to prevent flowout of this area. The -333 seal was assembled in the housing piece (Item 9); and, with the upper plate (Item 3) removed, this assembly was bolted together and manifold pressure supplied through A-1. In addition, a special top cover was placed over the seal housing so that the flow collected from the seal face and piston ring could be measured and compared to the flow supplied to the machine. The flow to the test rig was measured in an ASME orifice, where the inlet conditions were 293 psig, 80°F. The orifice flow is based on an ASME calculation of an area provided by a 1.0335-inch diameter orifice. The ΔP across this orifice was measured by a manometer, and these values are not given in the test data shown in Figure 18. The flowout of the test rig (which was collected by a top plate) was measured in a rotometer. The pressure to the rotometer is called P_3. P_1 is the pressure at the inlet of the manifold of the test rig, and P_2 is the pressure on the downstream side of the primary tooth of the seal body as shown on Figure 18.

Film thickness of the static test was measured in two places, noted as No. 1 and No. 2, which were 180° apart on the seal circumference. In addition, the tilt of the seal face was measured by means of a third dial indicator at an arm of 1.5 inches from the face of the seal section. This latter measurement was made to confirm that the seal section was being tilted by a pressure build up at the discharge of the primary tooth, P_2. The analysis of pressure balance of the section had assumed that this pressure was negligible; however, the static tests showed that the quarter-inch outlet holes evacuating A (shown in Figure 18) were inadequate and should be enlarged to prevent unfavorable section tilt.

Results of the flow versus pressure are shown in Figure 19. The flow reported here includes the leakage through the primary sealing tooth, the secondary piston ring seal, and the inherently-compensated air-bearing face. Flange leakage is also included and can be estimated by comparing the orifice measured flow versus the rotometer flow. This difference is quite small, indicating that flange leakage in the test rig was small. The flow measured here (400 at 120 psig) was greatly in excess of that calculated, 195 scfm. The reason for this was that the piston ring flow was quite high due to nonconformity of the piston

P_1-P_3 (psig)	$\Delta P=P_2-P_3$ (In. H_2O)	Orifice Dia. (In.)	Orifice Flow, Calc. (SCFM)	Rotometer		Film Thickness		
				Flow, Ind. %	Flow, Act. (SCFM)	No. 1 (In.)	No. 2 (In.)	Tilt Extension (In.)
25	3.6	1.0335	123.4	70	123.2	0.00120	0.00134	0.00155
50	5.9	(293 psig)	158.5	70	157.5	0.00109	0.00122	0.00115
75	10.3	---	209.5	78	205.0	0.00111	0.00123	0.00102
100	17.7	(80°F)	274.0	88	266.0	0.00119	0.00128	0.00090
125	27.8	---	344.0	98	326.0	0.00124	0.00134	0.00091
150	45.6	---	439.0	---	---	0.00132	0.00141	0.00094
175	70.5	---	545.0	---	---	0.00148	0.00128	0.00050

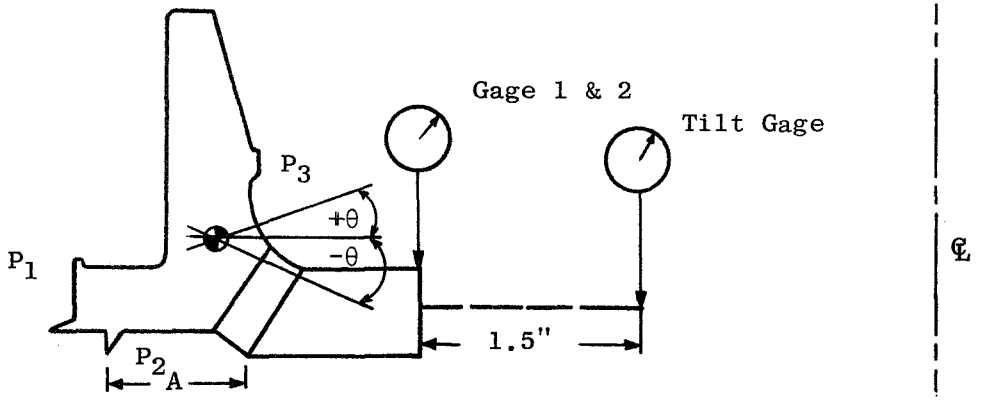

Figure 18. Static Test Data for -333 Seal

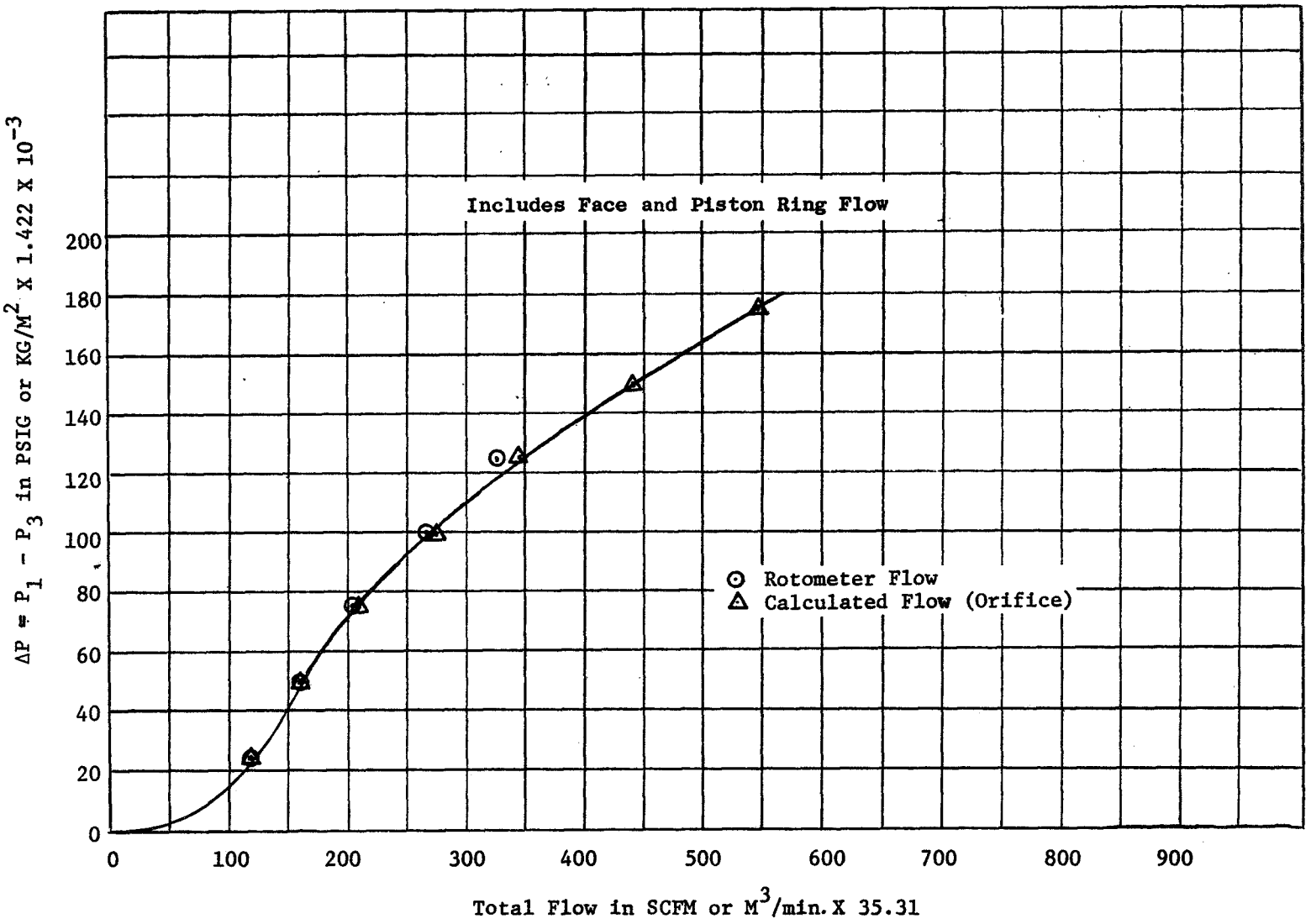

Figure 19. Measured Flow for -333 Seal Vs. Supply Pressure

ring to the face and bore. Although this could not be measured as a separate item, this conclusion is justified based on observable gap in the fit of the piston ring. The piston ring section was so massive, compared to the pressure deflection forces, that conformity could not be achieved. We were able in the later -131 and Flight-Weight designs to reduce the section size of this ring, so that piston ring leakage became a negligible item, although a great deal of hand lapping of all parts was necessary to achieve this result. Figure 20 shows a plot of pressure versus film thickness and extension tilt. Agreement of film thickness with design can be determined by comparing this curve with the design curve shown in Figure 10. With the ten-square-inch bias area for which the seal had been designed, a film thickness of 0.0012 inch would be expected at 175 psi. A film thickness of 0.0014 inch was actually attained. Agreement at lower pressure levels was not as good, and, at 100 psi, a film thickness of about 0.0012 inch was observed compared with a calculated film thickness of 0.0007 inch. An examination of the tilt extension showed clearly that at high pressure levels the pressure at the discharge of the primary seal tooth, P_2, was tilting the section to a high degree. This condition could be relieved by enlarging the inlet holes.

2. -131 Seal Static Tests

Inspection at initial buildup showed damage to the chrome carbide plating on the bottom air-bearing surface (Figure 4, Item 12); repair attempts (by hand lapping) were unsuccessful. The piece was returned to the vendor for rework (stripping of existing plating, replating with chrome carbide, and regrinding).

All parts were received and assembled, and static testing commenced. Measured -131 seal leakage was 160 scfm at 166 psig air pressure and room temperature, with the piston ring accounting for 7 scfm (see Figures 21 and 22). Air film thickness at this condition was 0.0012 inch on the -131 seal as measured with a one ten-thousandths-inch dial indicator, with the base mounted on the air bearing disk and the dial point on the tail section of the seal.

A static leakage in another buildup for the total system, top seal, and piston ring, plus bottom support air bearing, is shown on Figure 23. Leakage at 165 psig and room temperature inlet air was approximately 230 scfm. Due to face lapping and other factors, leakage varied between buildups.

Because of the large disk surface area on the low pressure side of the seals, a small disk ΔP would generate a large force which must be supported by the hydrostatic air film. The disk ΔP, required to cause touchdown on the bottom support bearing due to this force, was measured.

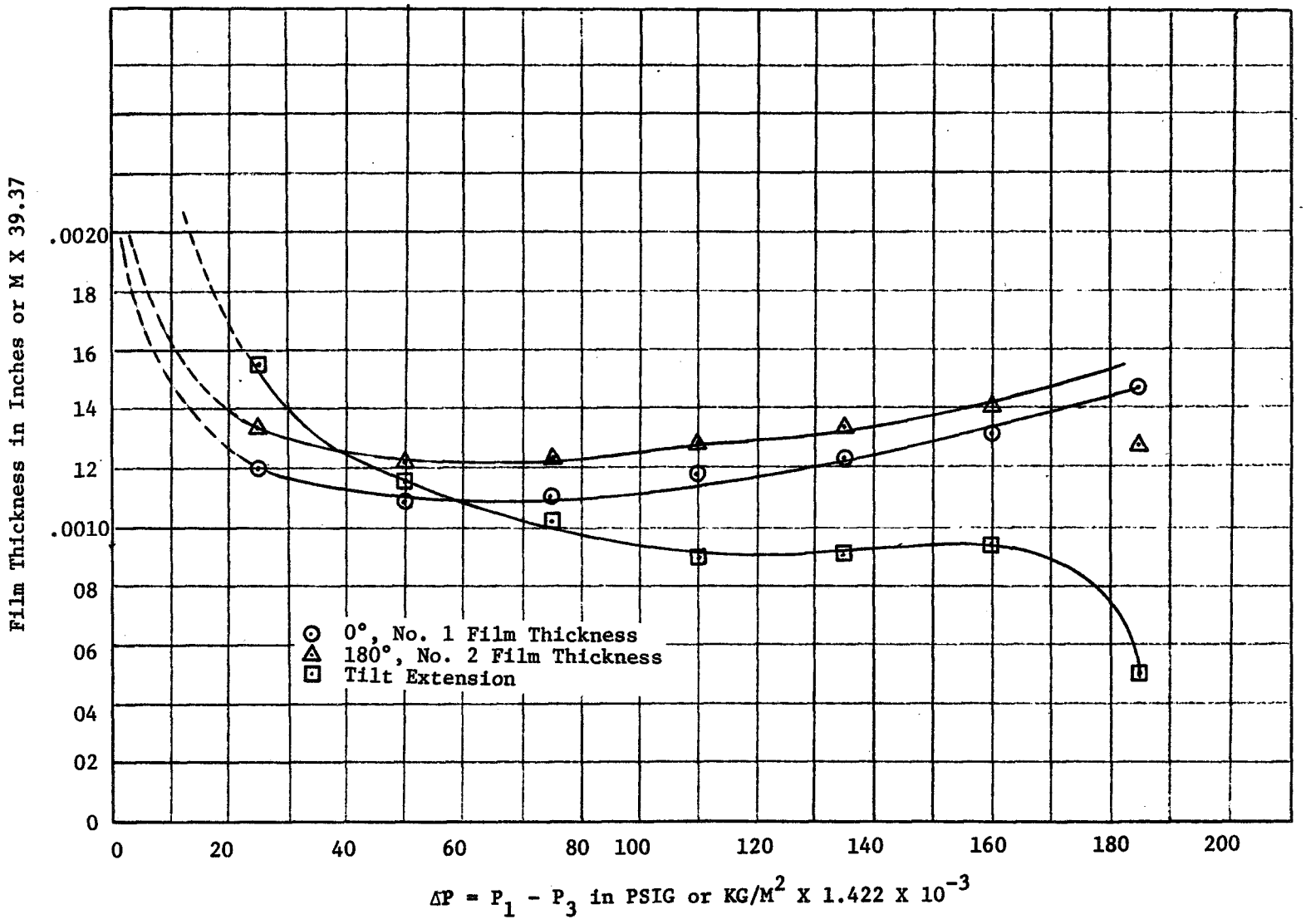

Figure 20. Film Thickness and Tilt Extension Vs. Pressure for -333 Seal

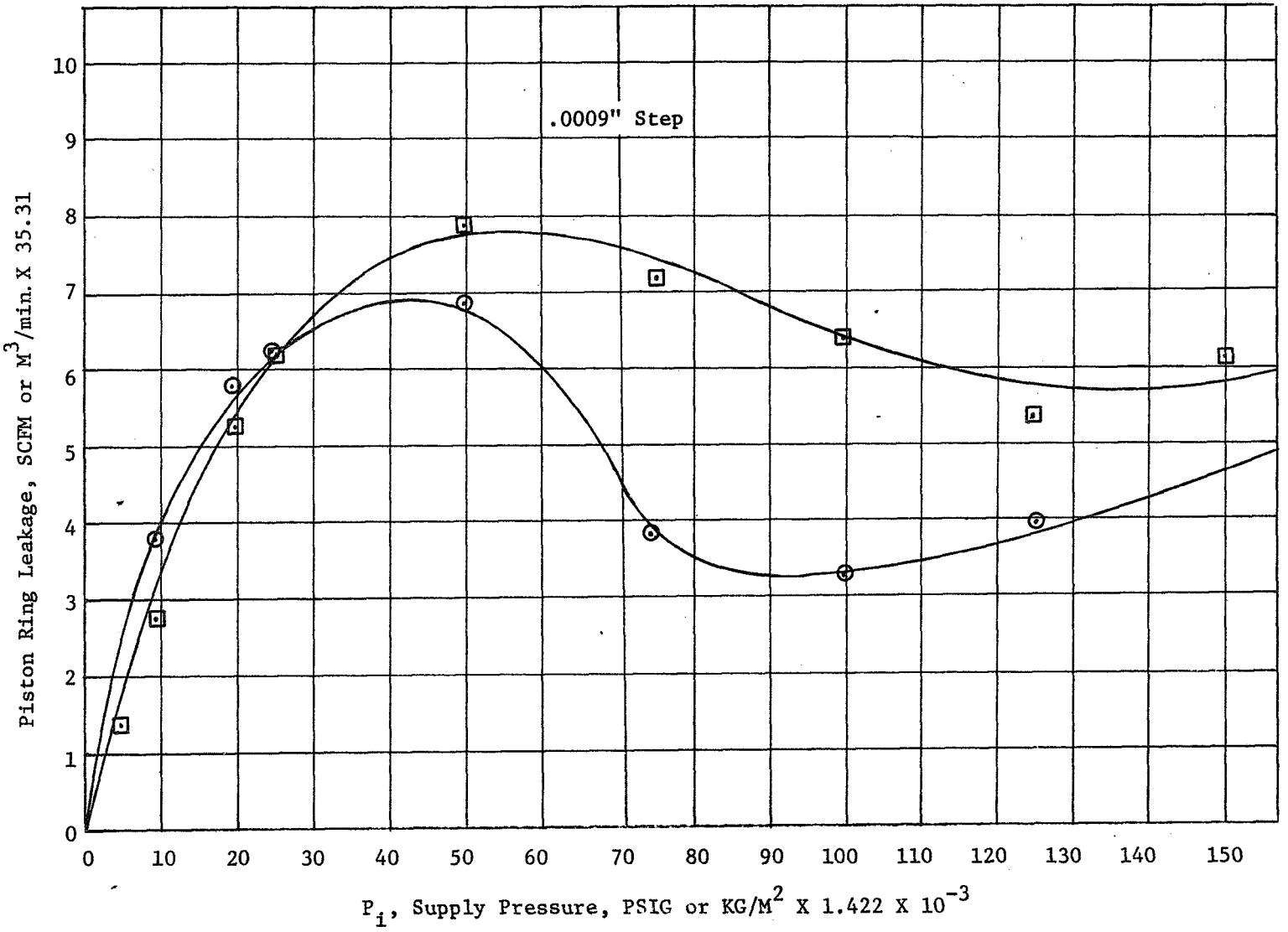

Figure 21. Piston Ring Leakage Vs. Supply Pressure for -131 Step Seal

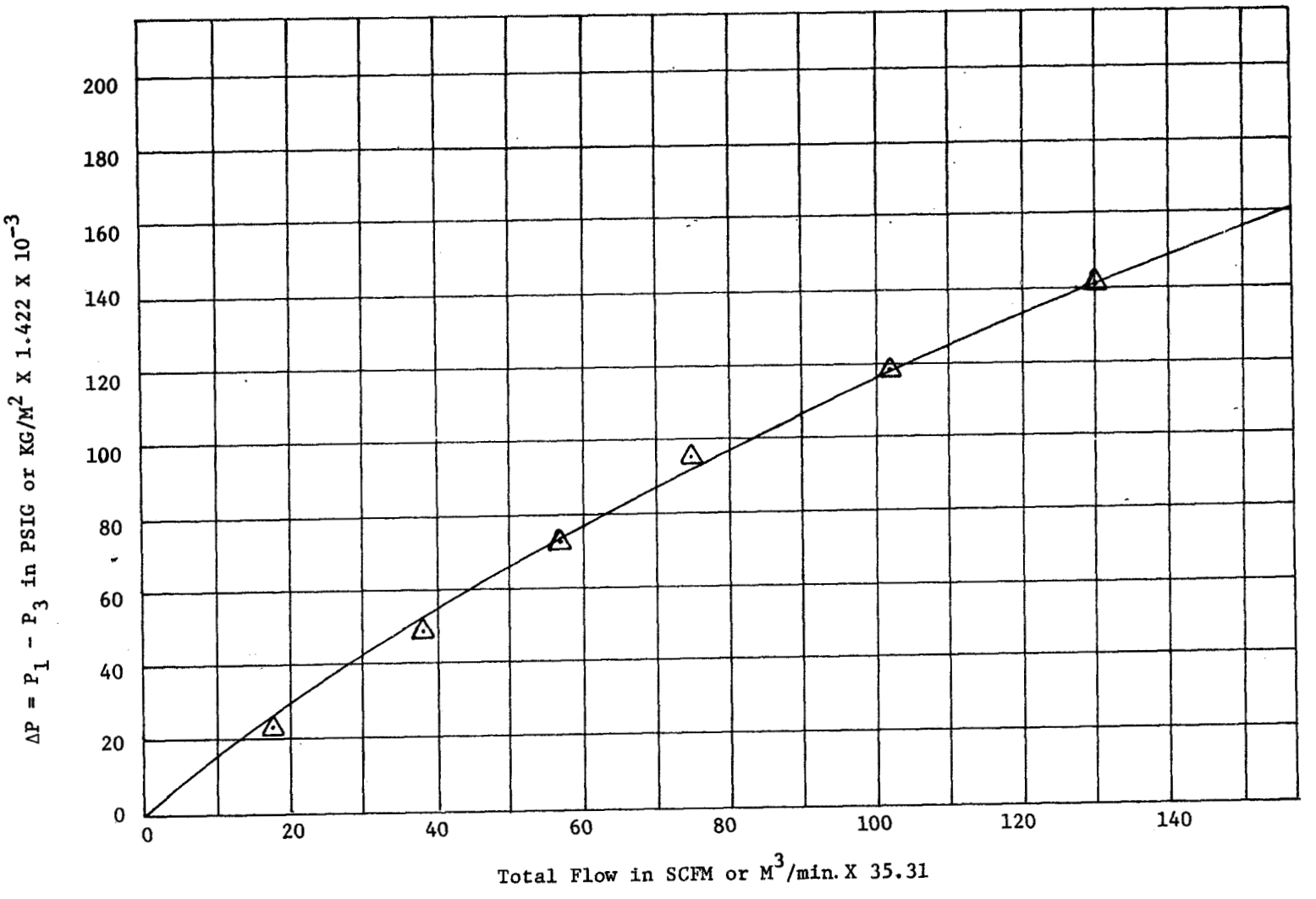

Figure 22. Measured Face and Piston Rig Flow for -131 Seal Vs. Supply Pressure

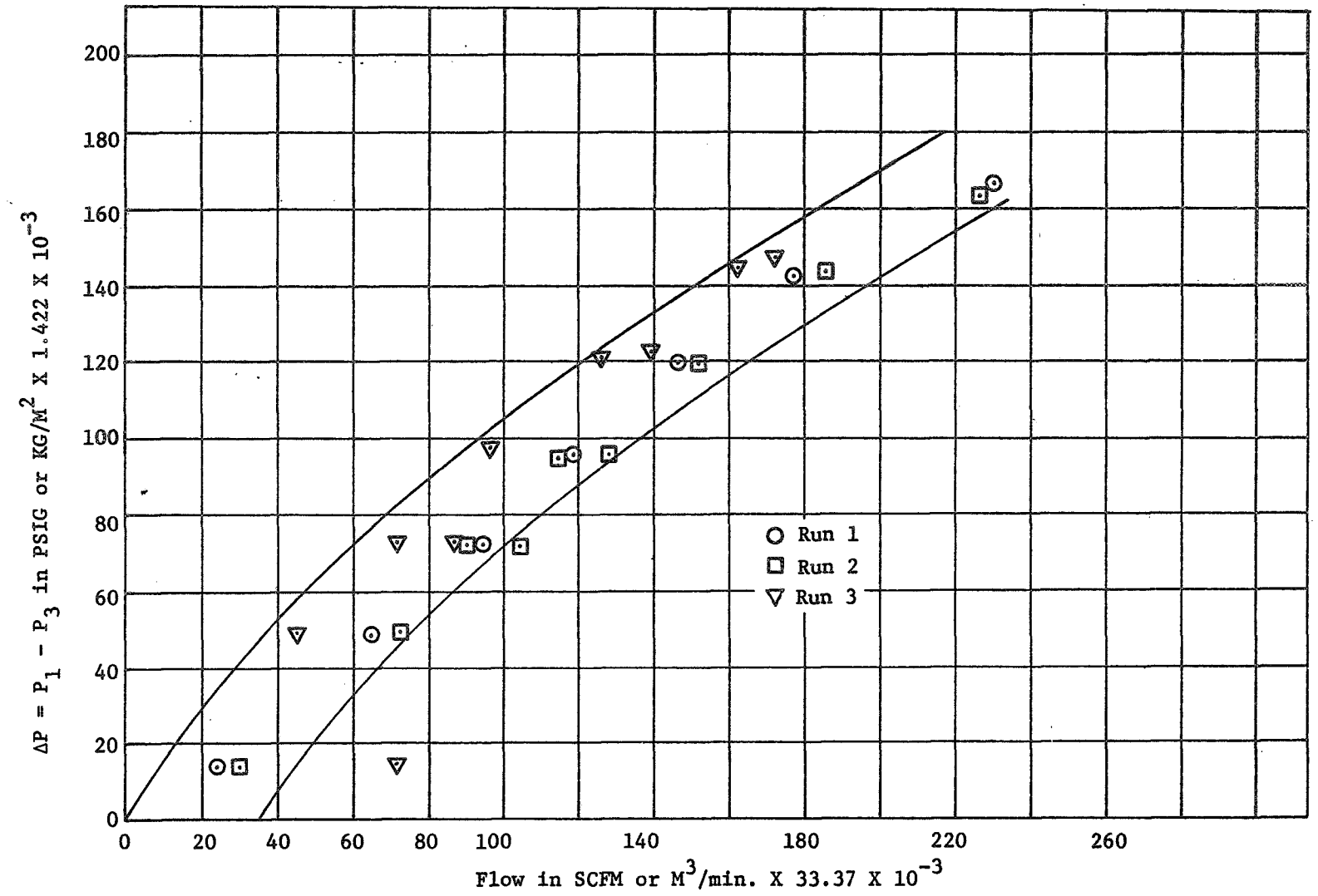

Figure 23. Bottom Bearing, Flange, Face, and Piston Ring Leakage, -131 Static Check

Results are shown on Figure 24. The theoretical touchdown line is also shown on this curve. The difference between calculated and measured values is assumed to be caused by geometric discrepancies and distortion of parts.

Bently probes were installed to measure air film thickness. Results are shown on Figure 25.

3. CD847985 Static Tests

Inspection of the CD847985 hydrodynamic seal (See Figure 16), as received from NASA, revealed the following design problems:

a. No provision was made to hold the sealing dam on the seal face concentric to the secondary balance diameter. Since the clearance between the seal and the balance diameter was 0.012 inch radially (nominal) per print, a nonuniform seating force equivalent to ± 1.2 pounds per inch at 100 psi would be imposed on the seal at the most eccentric position.

b. No provision was made to prevent the unplated seal face from rubbing the rotating race at speeds too low to provide hydrodynamic lift.

A meeting was held with NASA representatives during which it was resolved that NASA would rework the seal to provide a manifold and face orifice system. This rework would allow hydrostatic liftoff capability at rotational speeds too low to provide sufficient hydrodynamic lift. The rework was completed (See Figure 17), and static testing was begun.

Tests were completed to determine liftoff parameters of the hydrostatic manifold and orifices system. Those parameters measured were the following:

a. Air flow versus film thickness (Figure 26)

b. Film thickness versus supply pressure (Figure 27)

c. Supply pressure versus airflow (Figure 28)

Liftoff pressure versus supported load can also be estimated by extrapolating the curves on Figure 27 to zero film thickness. This extrapolation will show that liftoff will occur when manifold inlet pressure (in psig) is approximately equal to the total supported load (in pounds, force).

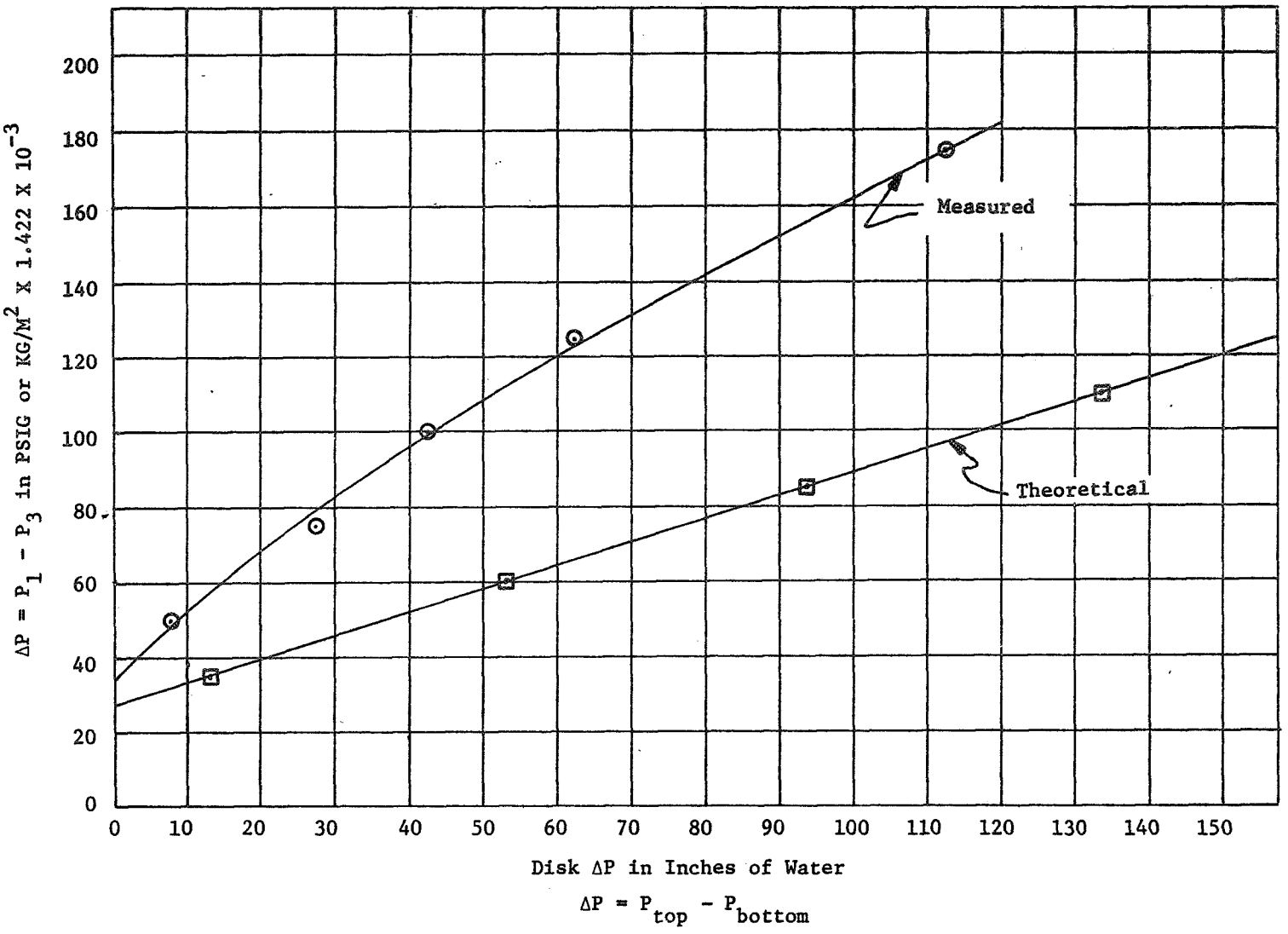

Figure 24. Disk Pressure Difference for Lower Bearing Touchdown, -131 Seal

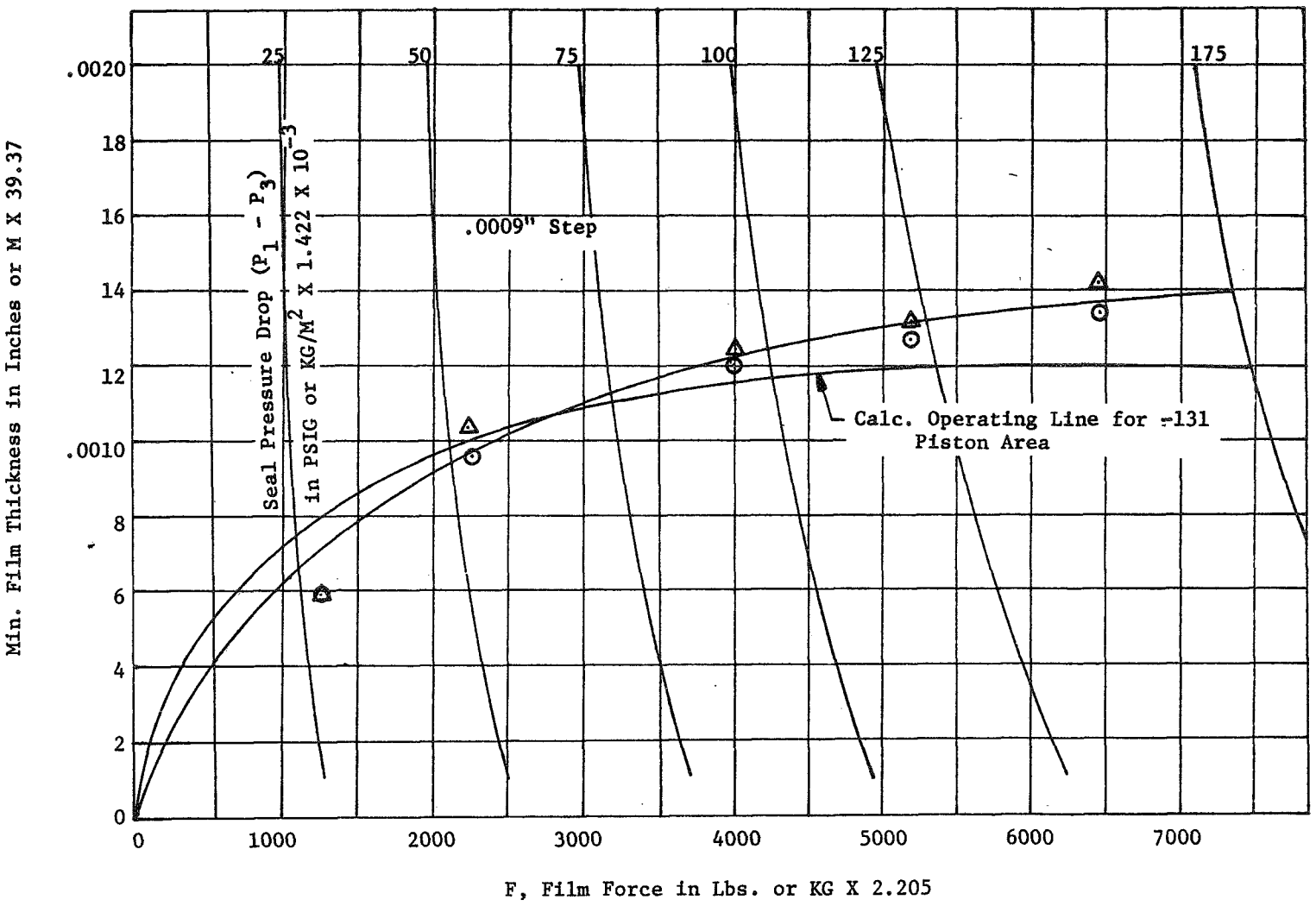

Figure 25. Film Thickness Vs. Film Force for Various Supply Pressures, -131 Seal

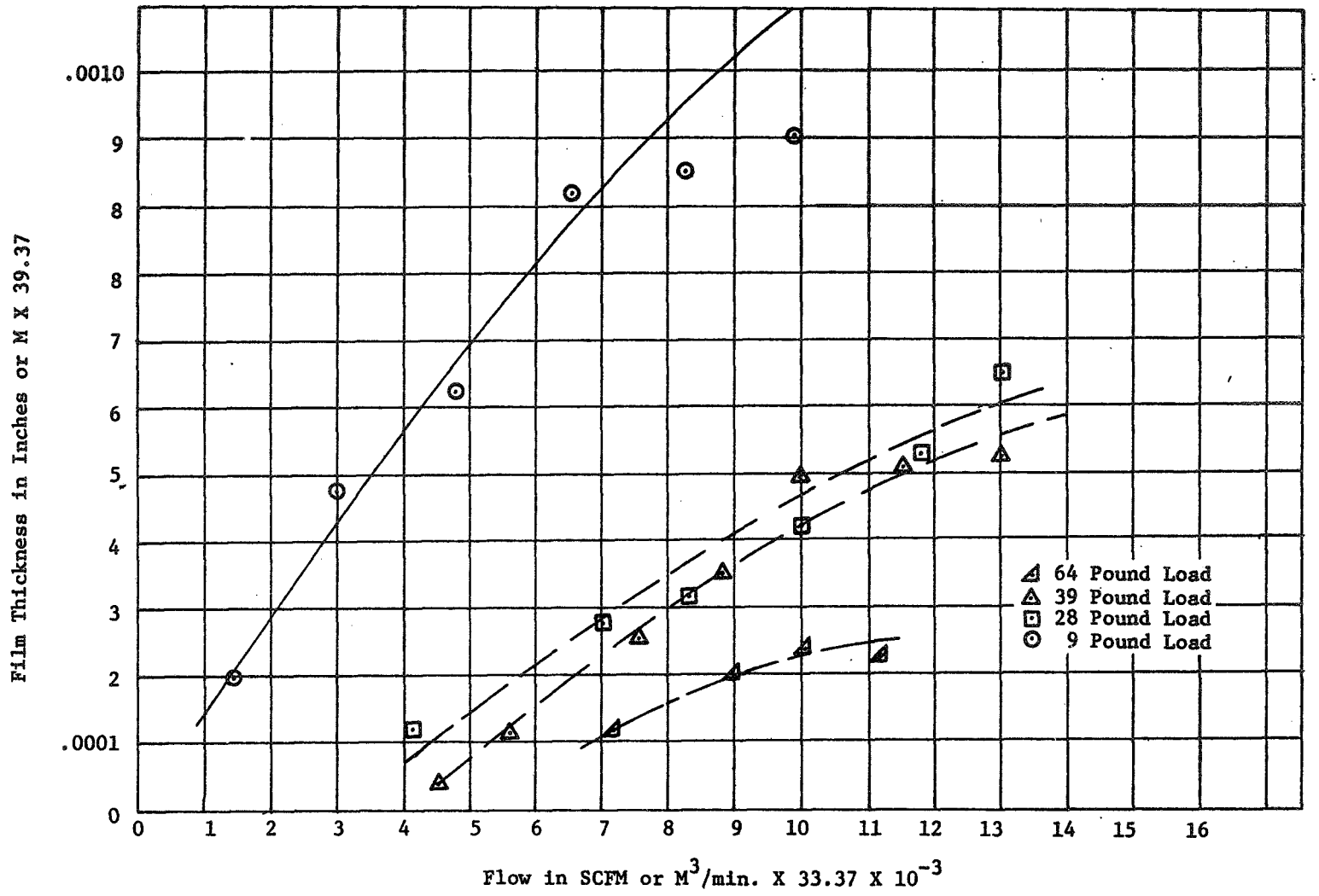

Figure 26. Air Film Thickness Vs. Hydrostatic Flow, CD847985 Seal

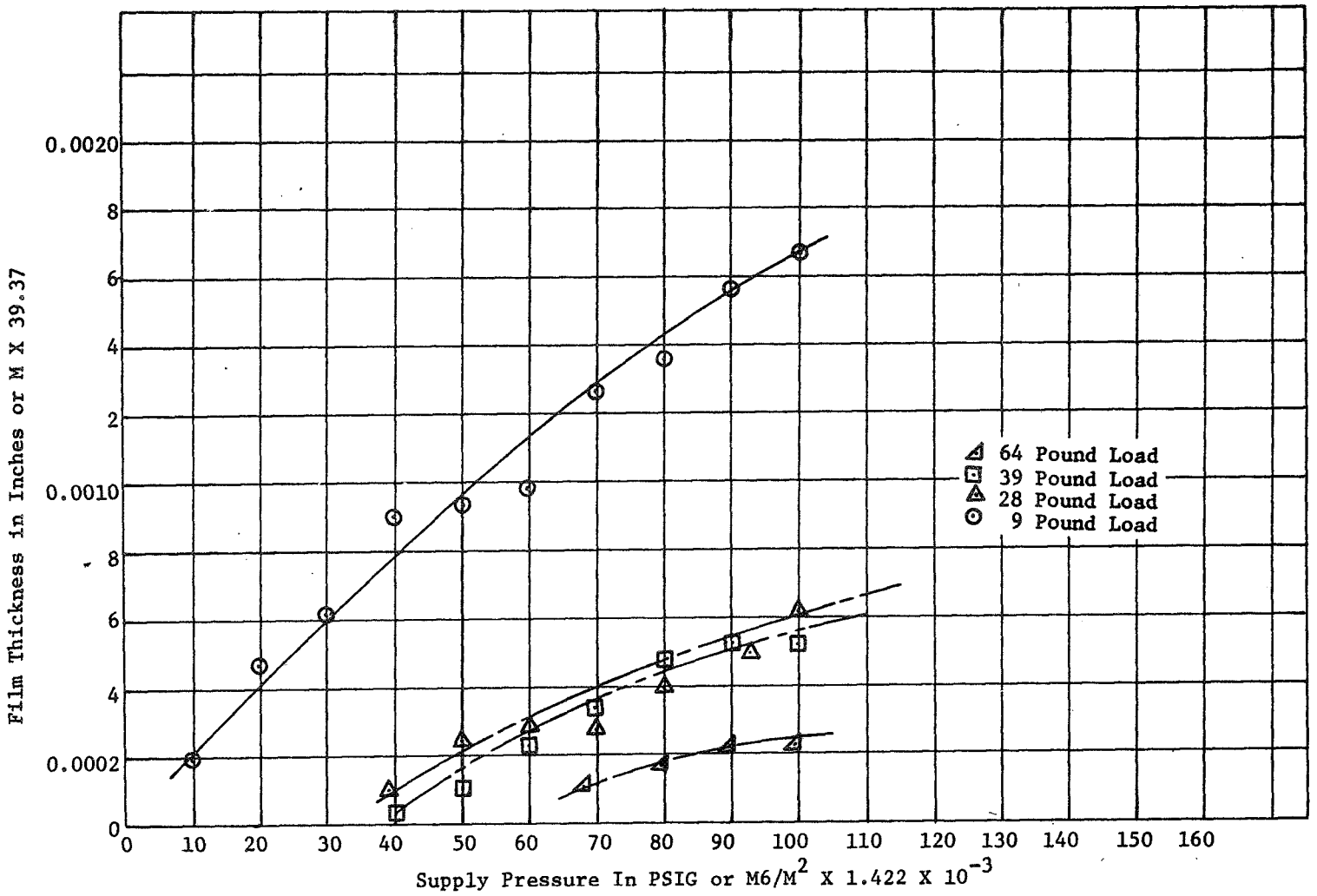

Figure 27. Air Film Thickness Vs. Hydrostatic Supply Pressure, CD847985 Seal

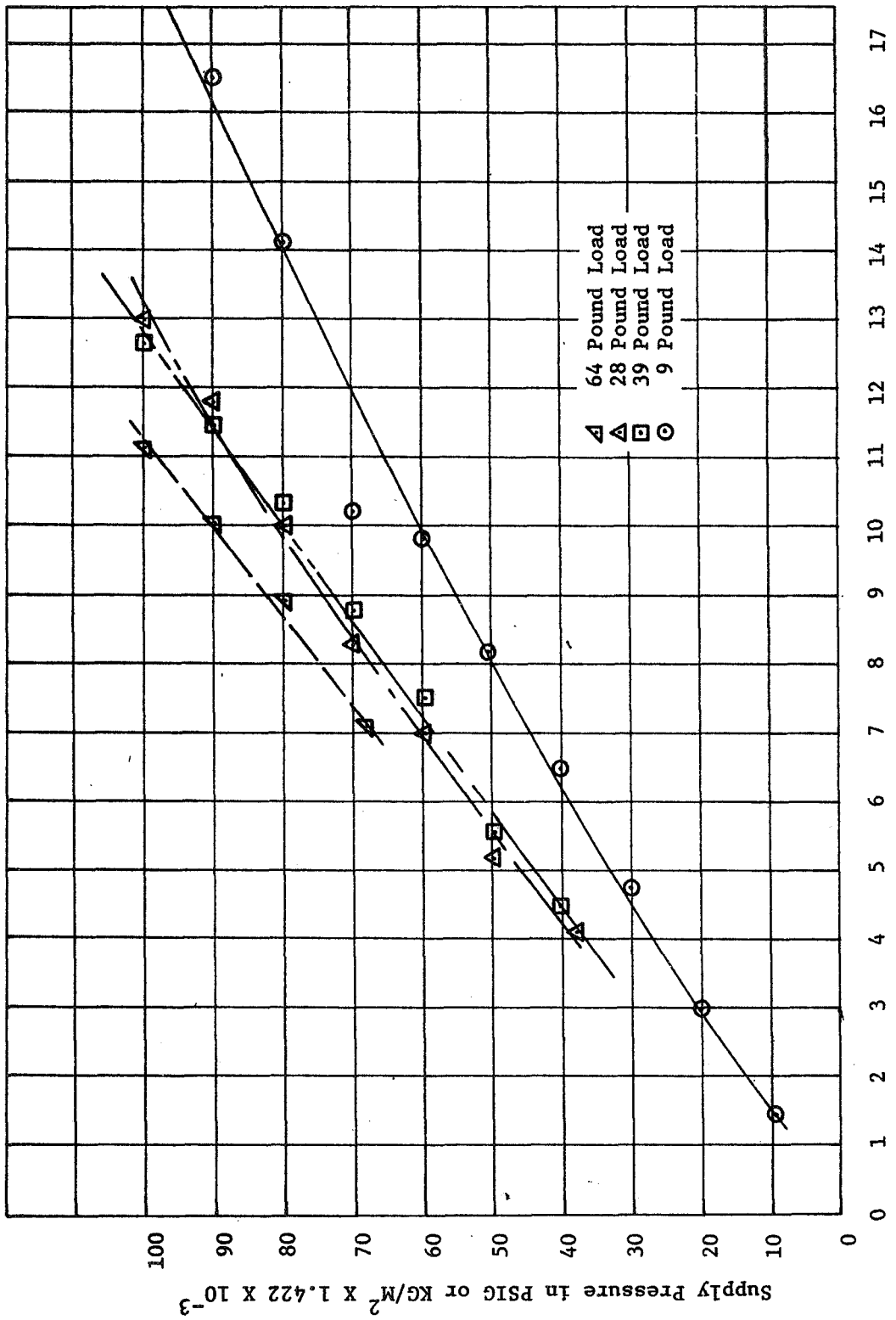

Figure 28. Hydrostatic Supply Pressure Vs. Flow, CD847985 Seal

The above tests were conducted by placing the seal face down on a 24- x 24-inch flat granite plate, pressurizing the seal while applying a static downward force, and measuring airflow rate and film thickness. Airflow was measured through a rotometer. Film thickness was measured with a one ten-thousandths dial indicator, and readings were taken at circumferential locations 180° apart and averaged.

The seal was then assembled in the dynamic test rig (See Figure 6) to conduct additional static tests; however, the seal diameter was 0.006 - 0.008 inch oversized at the piston ring slot and would not slide freely in the seal balance piston diameter (which was 0.024 inch out of round). In addition, the piston ring was bound in the ring groove on the tail section of the seal because the groove width was undersized. To fix these problems, the balance piston diameter was machined round, and a piston ring which was undersize in the axial dimension was installed. The oversized seal tail section was not reworked, since this discrepancy would serve to reduce the allowable eccentricity between the sealing dam and the balance piston diameter from ± 0.012 inch per print, to 0.008 inch.

The seal was reassembled in the test rig and was hydrostatically pressurized. Floating occurred to the extent that the disk could be rotated by hand with some effort, but was not free floating. The seal was inspected after teardown and face scoring had occurred. Close inspection of the seal face under a microscope revealed the presence of hundreds of various size burrs in the face grooving. Some of these burrs were loose enough to be lifted out on a pencil point. It is likely that these burrs were the cause of the face scoring and disk handing. To fix this problem, all face grooves and channels were deburred by hand.

The rig was then reassembled for static tests. Seal inlet pressure was gradually increased until, at approximately 129 psig, the seal face blew open (off the race). An air line was then installed between the hydrostatic manifold and the seal inlet pressurizing cavity. The inlet cavity was then pressurized and it was determined that the seal blew open at a lower pressure, approximately 65 psig.

These results implied that face air leakage was being restricted in the downstream face grooves and vents, with the resulting pressure rise causing a force unbalance on the seal and driving the seal face open.

Additional tests were conducted to determine the increase in seal face leakage due to hydrostatic lift pressures. The results were included in Monthly Progress Report No. 27. In general, the results were the following:

(a) At all constant inlet pressures up to and including 100 psig, the seal lifted off when hydrostatic pressure was between 8 and 12 psig. Figure 29 shows leakage rates versus varying hydrostatic pressures with inlet pressure constant at 100 psig. The change in slope on the curve occurs at liftoff. Similar curves were generated for constant inlet pressures of 25, 50, and 75 psig and are included in Monthly Progress Report No. 27.

The following data points at which seal blowoff occurred were also recorded:

Pressure (psig)		
Inlet	Hydrostatic	Remarks
100	30	No rig vibration
75	50	No rig vibration
137	0	Rig vibration
125	25	Rig vibration
65	63	Rig vibration

The above results were discussed with the NASA Program Manager and a recommendation was made that the vent groove area on the low pressure side of the face sealing dam be increased. The seal was then returned to NASA for modification.

The following rework was done by NASA:

(a) The vent groove on the low pressure side of the face sealing dam was increased by widening the slot widths.

(b) The sharp corners on the inlet side of the low pressure vent grooves were changed to radii.

(c) The seal face was chromium plated.

The part was returned to General Electric Company, where inspection revealed the following:

(a) The seal face was saddled 0.007 inch

(b) The hydrostatic manifold was removed from the seal. Some of the small diameter feeder tubes were bent beyond repair.

(c) The diameter of the tail section of the seal at the piston ring groove was 0.043 inch out of round.

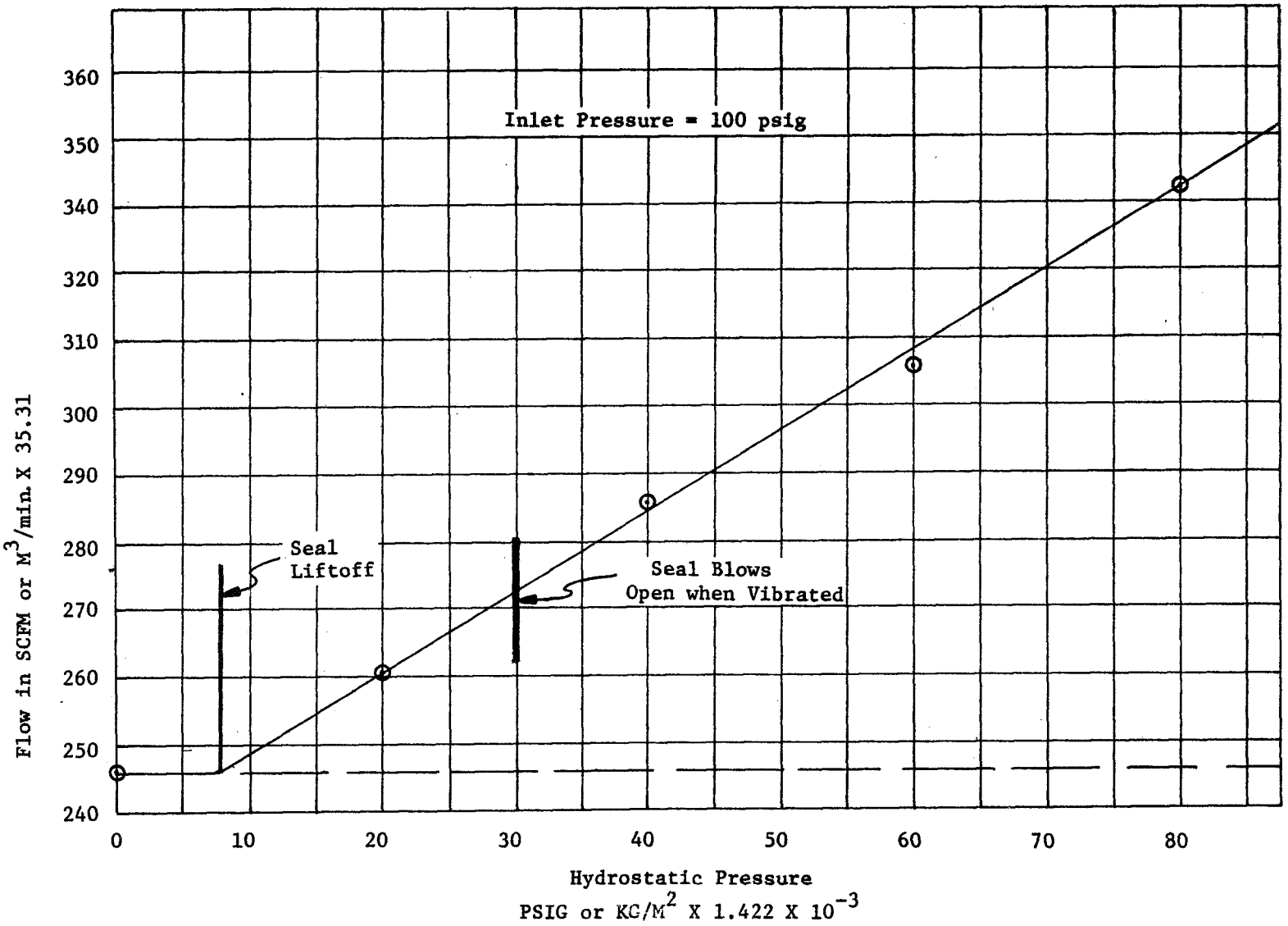

Figure 29. System Leakage Vs. Hydrostatic Pressure, CD847985 Seal

Possible cause for the above distortions are the following:

(a) Plating stresses

(b) Grinding stresses

(c) Fixture clamping during rework

Because of this seal distortion, all further testing on this phase of the program was terminated.

B. Room Temperature Dynamic Tests

1. -131 Seal Room Temperature Dynamic Tests

On the first buildup for room temperature dynamic testing, gasket compression in the rig flange stackups caused misalignment of the test rig and seal hanging. A new (thinner) gasket material was acquired, and the rig was reassembled for dynamic testing. A dynamic test was conducted after this modification with the following results:

First Room Temperature Dynamic Tests, -131 Seal						
Run	Speed (rpm)	Man. Press. (psig)	Disk ΔP ("H_2O)	Film Thick. (mils)	Orifice (psig)	Flow (scfm)
1	1000	174	10	2.2	292	---
2	2000	175	12.5	1.96	---	---
3	3000	175	11.5	1.72	---	---
4	4000	175	7	1.96	---	---
5	1000	125	9.5	2.1	---	161
6	2000	125	11	1.9	---	146
7	3000	125	12	1.96 (± .0001")	---	131

A successful run was completed at 4000 rpm, 175 psig inlet pressure, and room temperature. While attempting to run a 125-psig ΔP condition, a seal rub occurred in the speed range between 3000 to 4000 rpm, causing plating damage to the top seal, top and bottom surfaces of the bearing disk, and the bottom stepped-face air bearing (See Figures 30 through 35). The exact cause for the rub is not known; however, observations during test indicated that the cause was a sudden increase in ΔP across the air bearing disk, overloading the capacity of the bottom bearing hydrostatic air film.

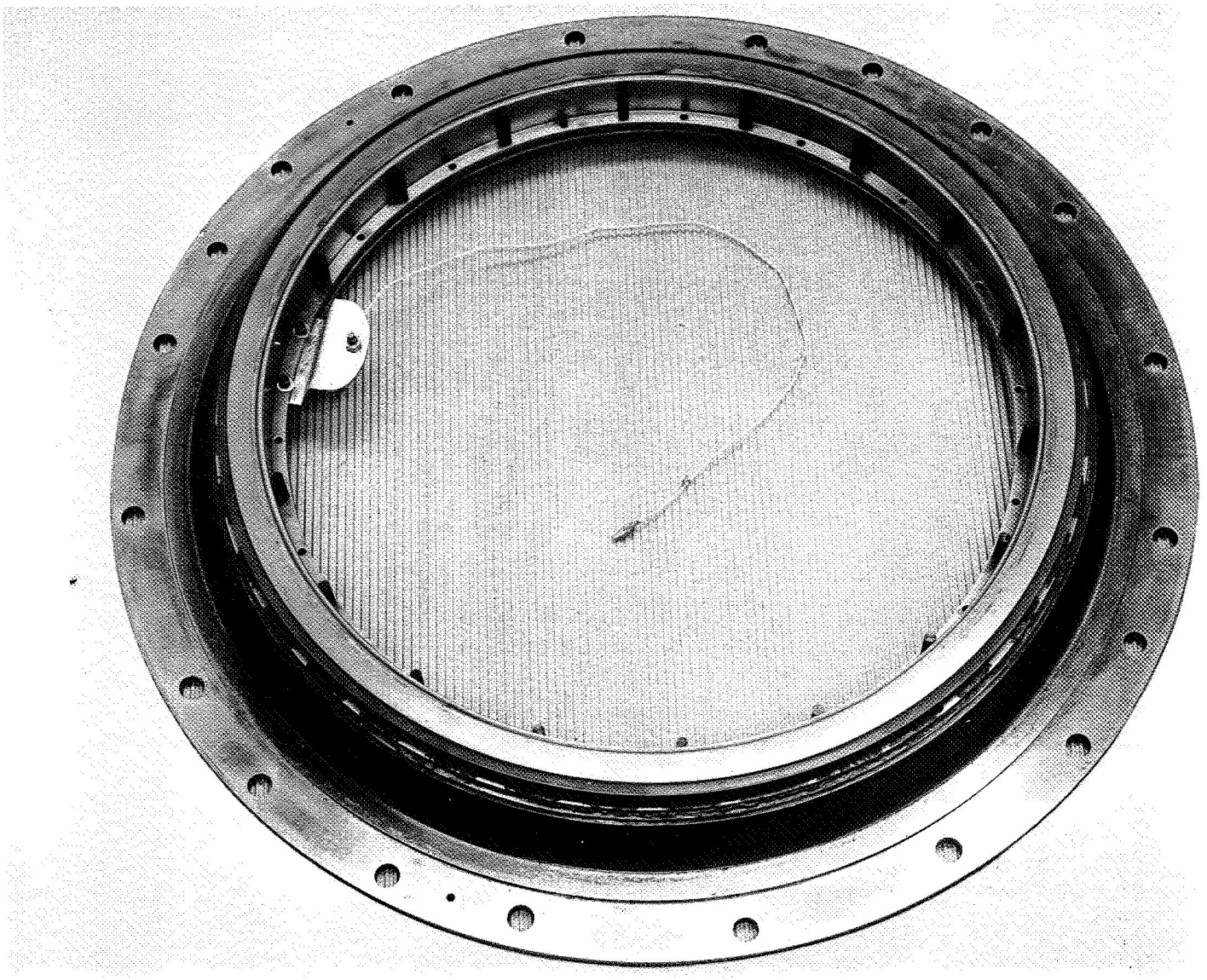

Figure 30. -131 Seal Assembly Showing Plating Damage on Seal Face (C680313109)

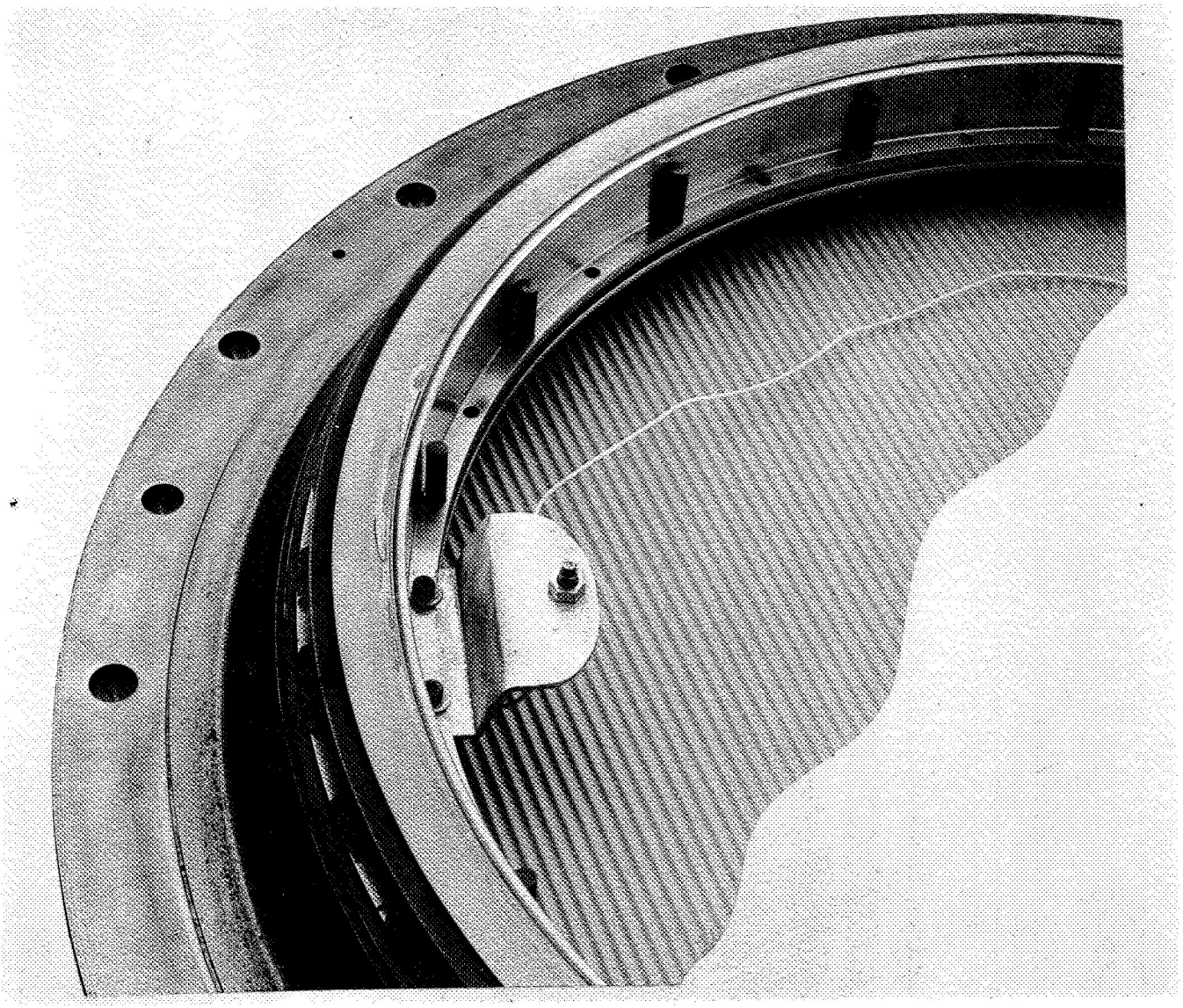

Figure 31. -131 Seal Face Plating Damage After Dynamic Test (C 680313110)

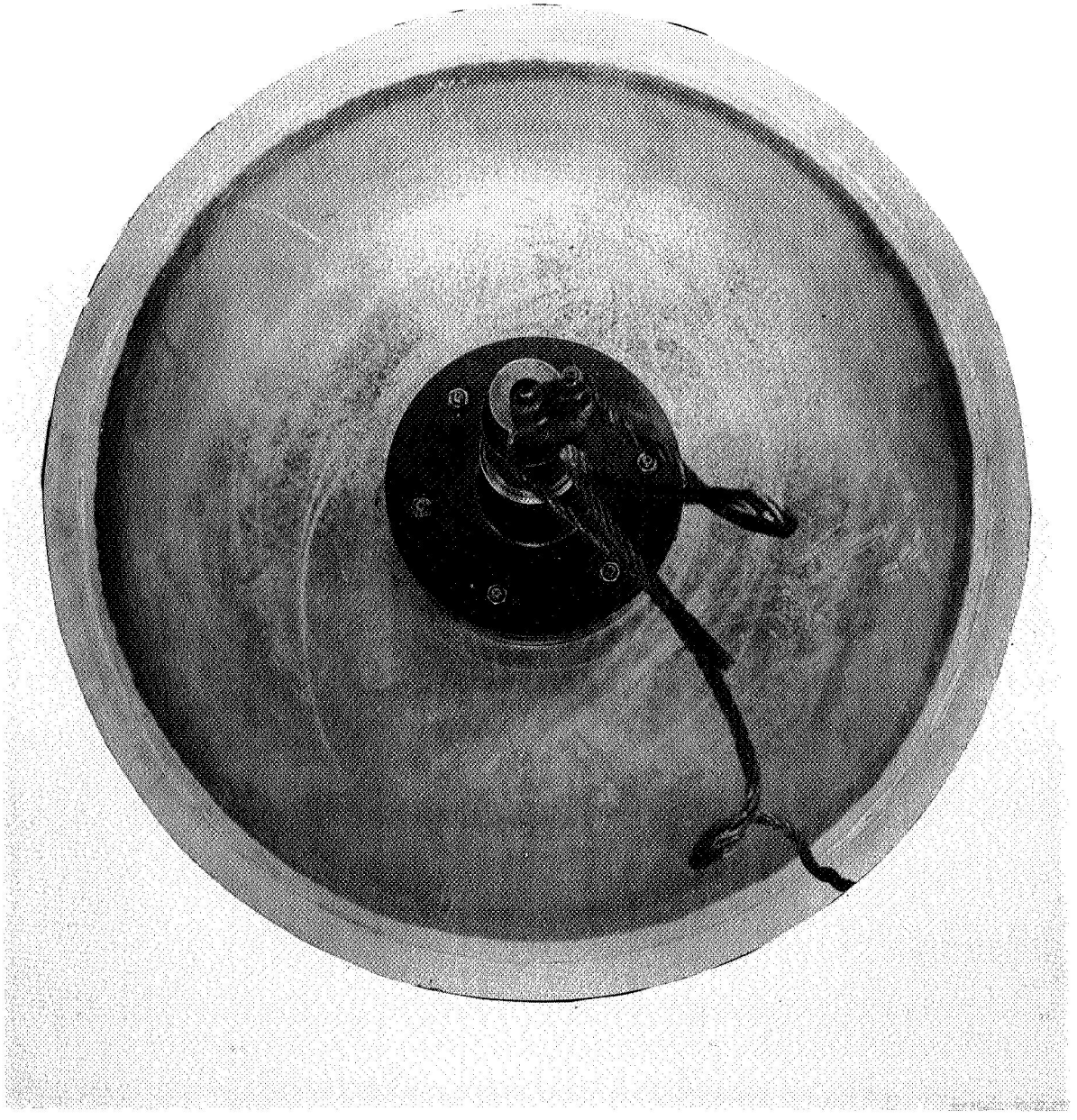

Figure 32. Plating Damage on Air-Bearing Disc Top Face (C680313111)

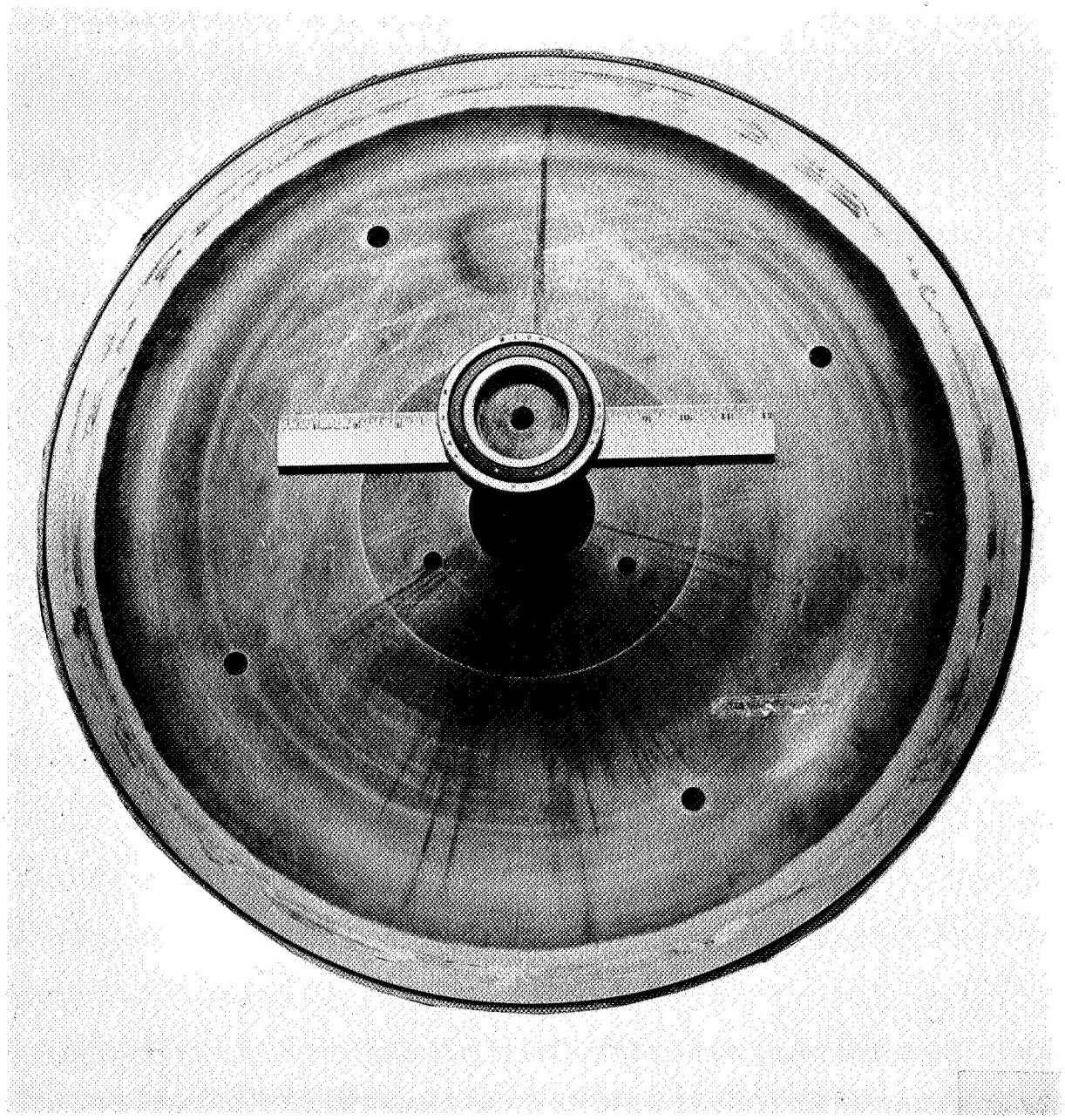

Figure 33. Plating Damage on Air-Bearing Disk Bottom Face (C680313107)

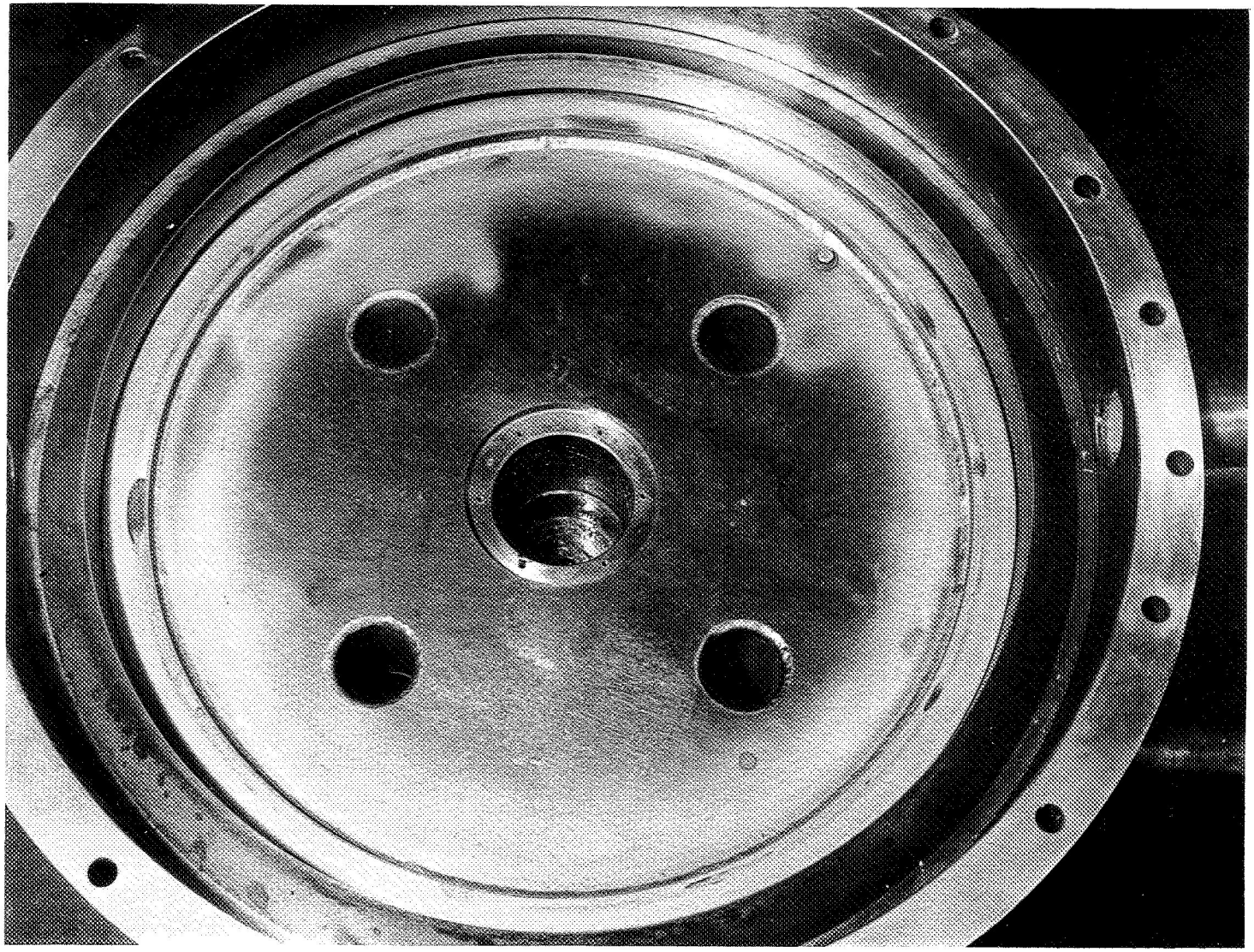

Figure 34. Face Plating Damage - Test Rig Air-Bearing

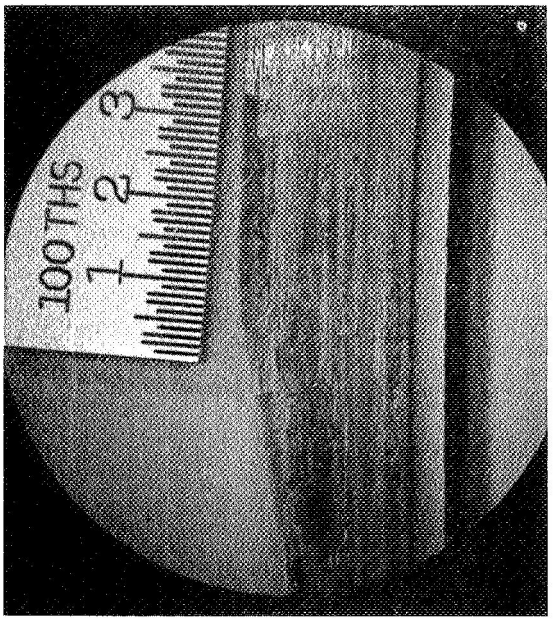

-131 Seal

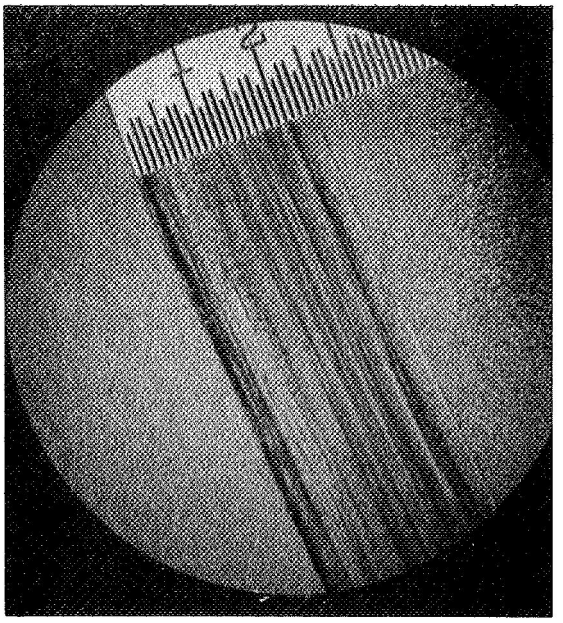

Upper Disk

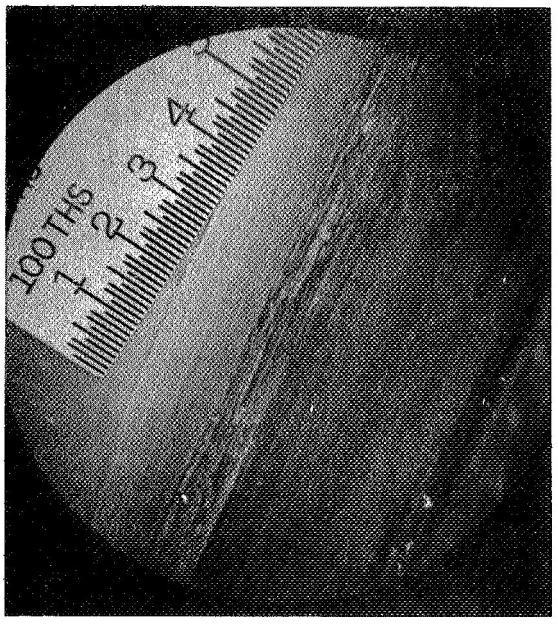

Bottom Step-Bearing

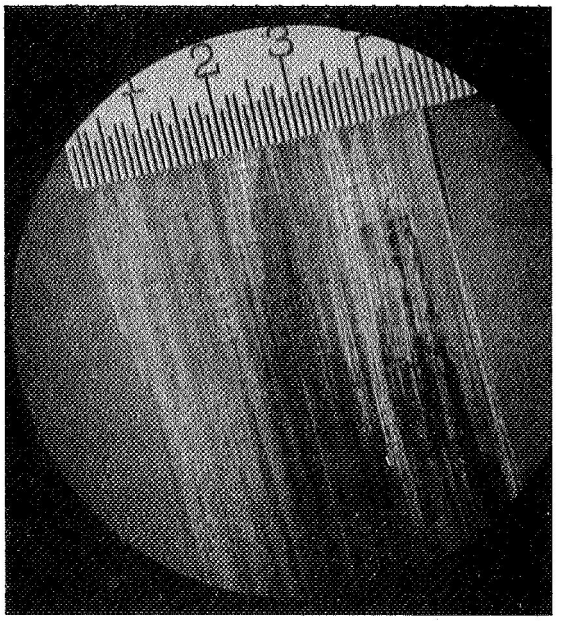

Lower Disk

Figure 35. -131 Seal and Tester Damage

All parts were repaired and reassembled for dynamic testing. Static testing showed total system leakage of 520 scfm at 175 psig, with high piston ring leakage. The rig was disassembled, lap rings were made, and the seal was relapped with a converging taper (See Figure 36). Lapping on the bottom air bearing proved too time consuming, and a new flanged-type bottom air bearing was made. Because of time and expense, the bearing face was not plated.

It was also found that the piston ring groove in the -131 seal was not deep enough to preclude bottoming and subsequent hanging of the piston ring between the I.D. of the groove and the balance piston diameter, so the groove was deepened.

Many subsequent builds were made, but clamping distortions repeatedly caused disk hangup. Finally, the bottom flanged air bearing was laid on a bed of wet ceramic cement which was allowed to harden before tightening the flange bolts. This, and selective torquing of the flange bolts, improved the situation. It was found that by "tuning" the flange bolts, the theoretical lift-off pressure of 22/24 psig could be achieved (see Figure 24).

Five subsequent runs were made with no rubs occurring on the first four, as shown below:

Second Room Temperature Dynamic Tests -131 Seal

Date (May, 1968)	RPM	Seal ΔP, (PSI)	Total[1] q, (SCFM)	Film Thickness (h_o, Inches)	
				Top	Bottom
13	0 - 1680	150	228	0.0010	0.0018
14	0 - 2100	155 - 160	178 - 194	0.0008	0.0010 - 0.0012
20	0 - 2000	170	458 - 486	0.0012	0.0017
20	0 - 2250	170 - 190	---[2]	---	---
20	0 - 2400	155 - 170	---[3]	---	---

(1) Bottom bearing, -131 seal face and piston ring, flange, and other parasitic leakages

(2) Measured total pressures on disk only

(3) Witnessed by NASA representatives

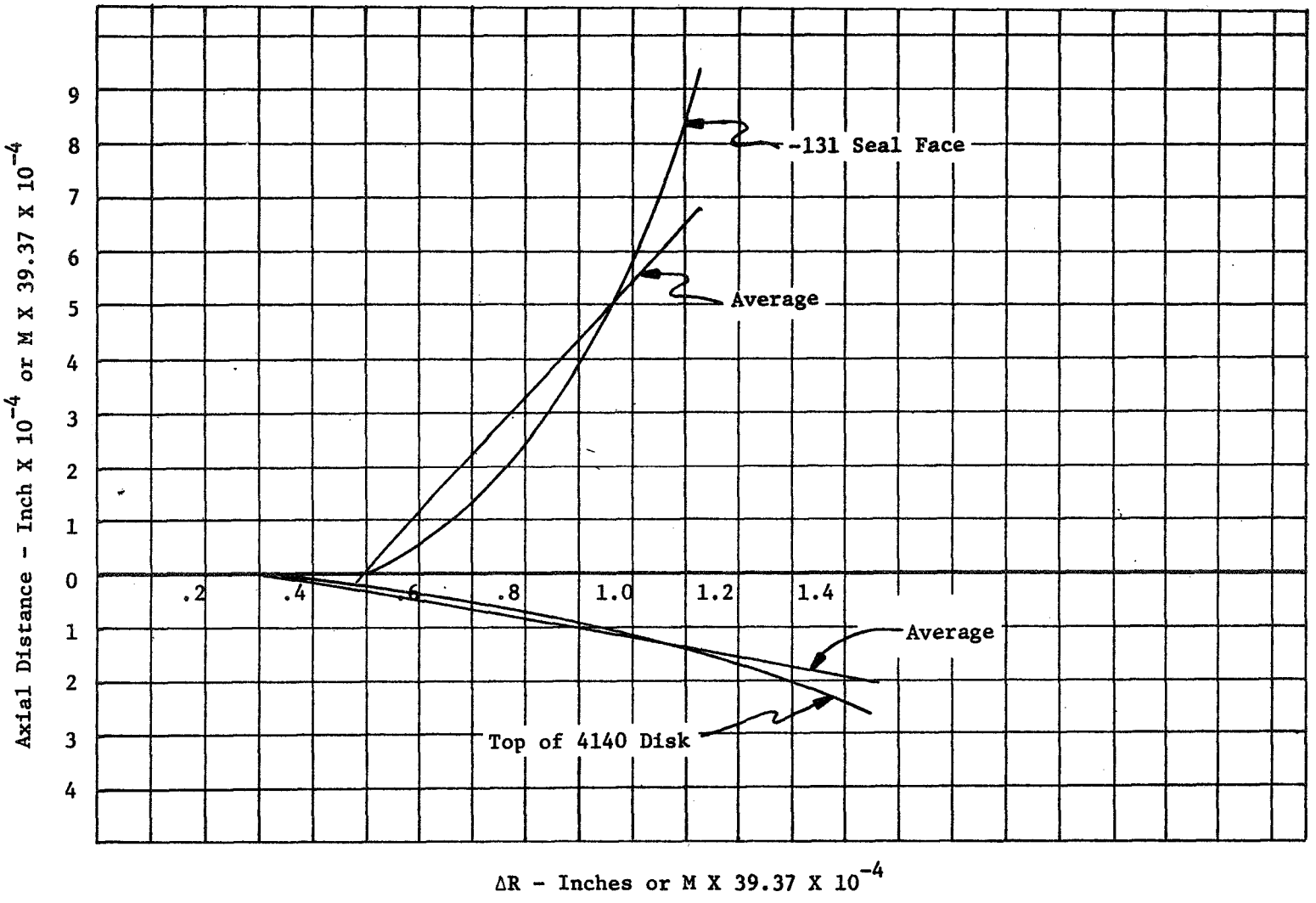

Figure 36. Measured Operating Flowpath, -131 Seal

During this test a rub occurred on the bottom air bearing while operating near 2400 rpm, 170 psig, and room temperature. The test seal did not rub. Rig vibration was high during this test, suggesting the probability that G-forces in conjunction with disk pressure forces exceeded the load capacity of the bottom air bearing, resulting in a rub.

To relieve the force problem due to pressure drop across the air bearing disk, twenty-four three-quarter-inch-diameter holes were drilled through the disk (see Figure 37). The bottom air bearing was repaired, but subsequent buildups were plagued by out-of-flatness from clamping distortions.

A dynamic test was successfully conducted during the week of July 8, 1968, at 3700 rpm, 175 psig, and room temperature, as a check-out run prior to hot testing. Static and dynamic leakage rates are shown on Figure 38 and 39. No problems were experienced. The reduction in leakage with increasing disk speed is attributed to piston ring seating due to rotational vibration. No change in face leakage was normally experienced with speed.

C. Hot Dynamic Testing

1. -131 Seal

The rig was disassembled to remove the Bentley Probes prior to hot testing. Subsequent attempts for hot dynamic testing were aborted when scale dislodged itself from the JP-4-fueled air heater and became ingested in the seal and air bearing.

The system was cleaned and several additional attempts were made to run hot. Distortion of the bottom air bearing, due to thermals in the clamping stack, damage to the ceramic cement bed under the bottom air bearing flange, and additional particles of dislodged dirt from the air heater system caused the disk to hang shortly after firing the air heater.

At this point, the separable, flanged, bottom air bearing was discarded and the air bearing which is integral with the rig base was lapped with a 0.0015-inch taper. The rig was reassembled, and the disk floated freely at room temperature; however, air heater scale and thermal distortions continued to plague the program.

A hot air filter was purchased and installed. The rig was reworked to provide nine circumferentially located air inlet lines in place of the one existing inlet, to reduce local hot spots. Thermocouples were installed to measure air and metal temperature distribution. (See Figures 40, 41, and 42). Since the metal temperature distribution of the rig bed

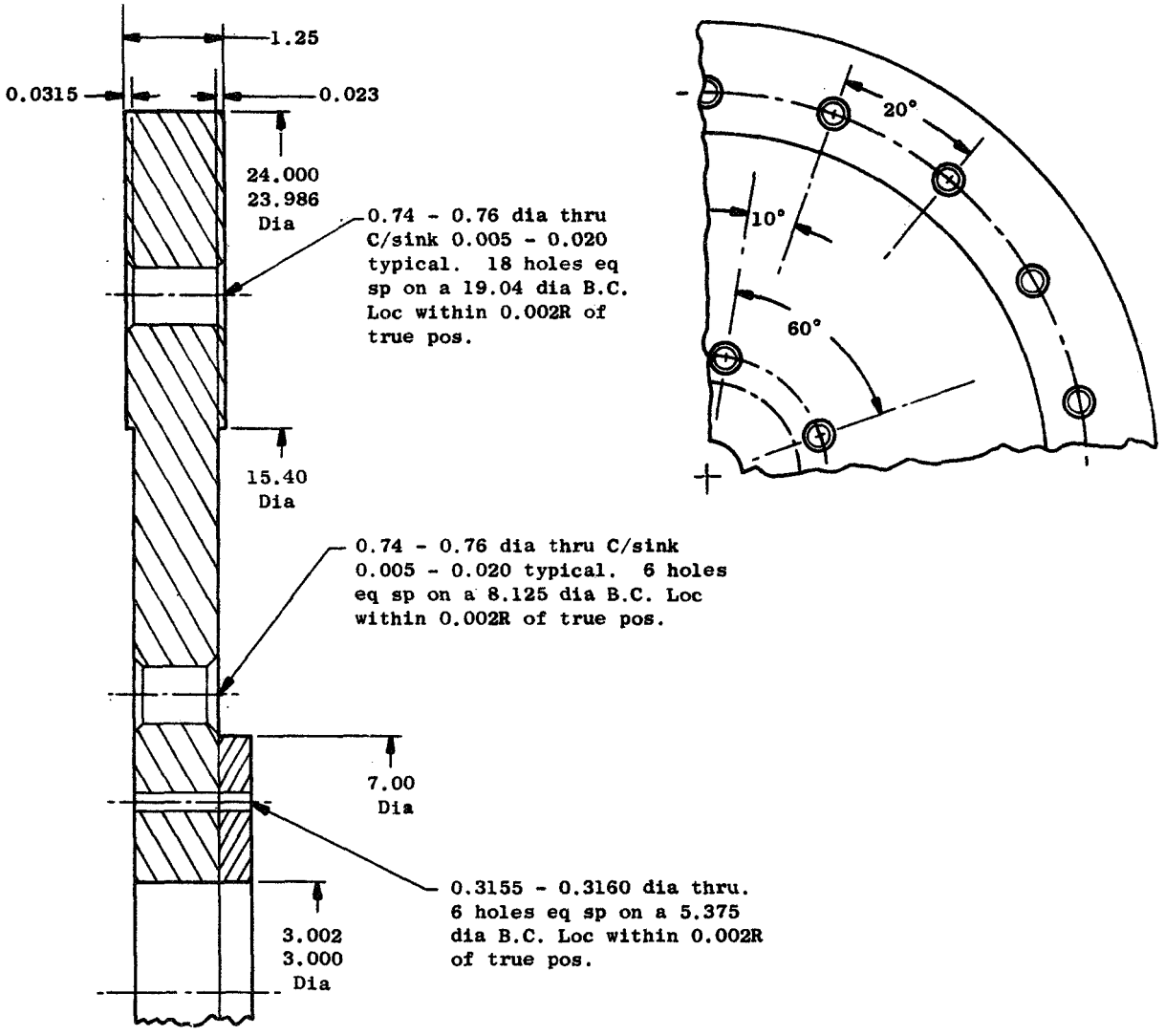

Figure 37. Vent Hole Modification for Disk

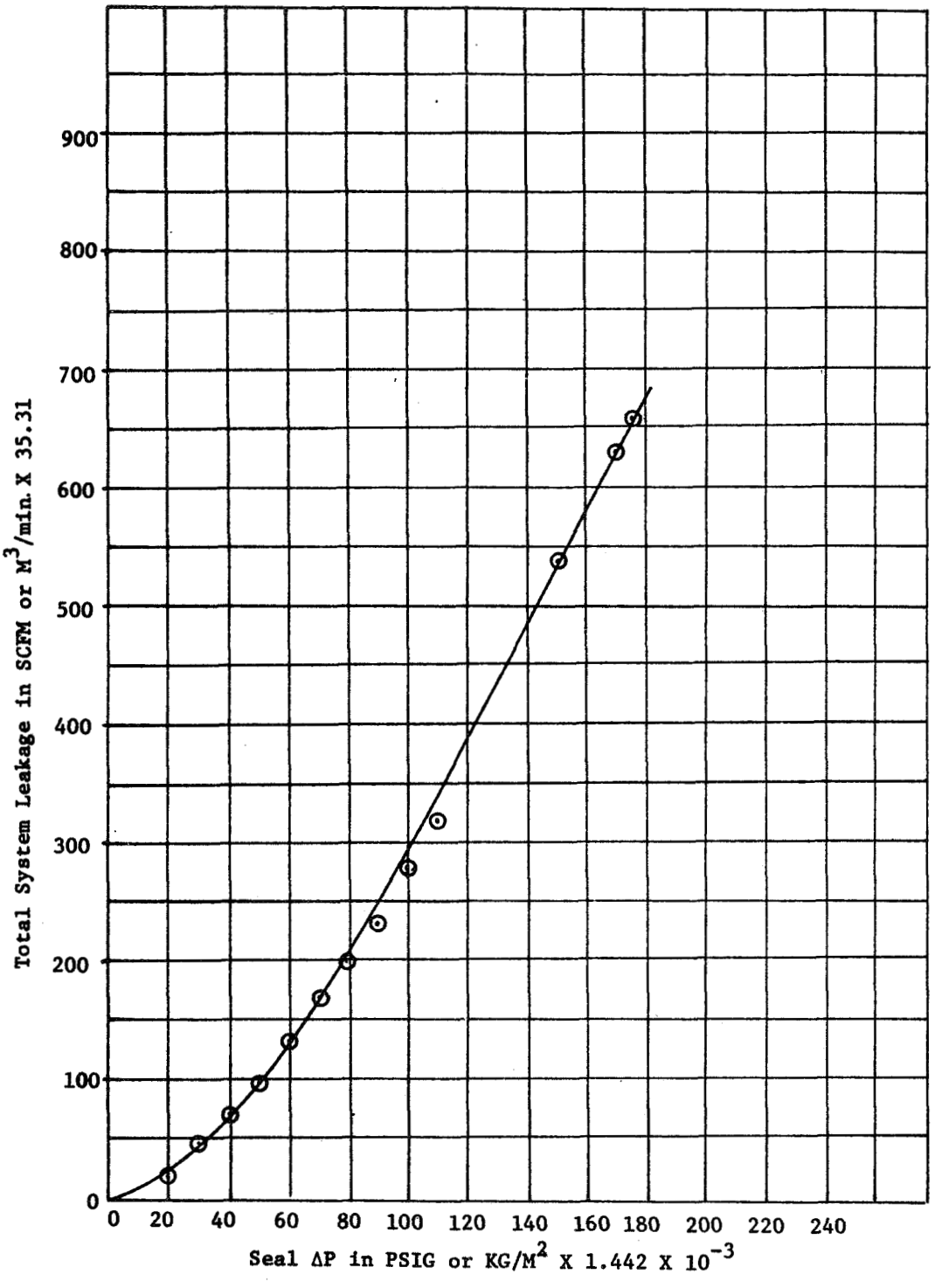

Figure 38. Total Air Leakage Vs. Inlet Pressure for -131 Seal

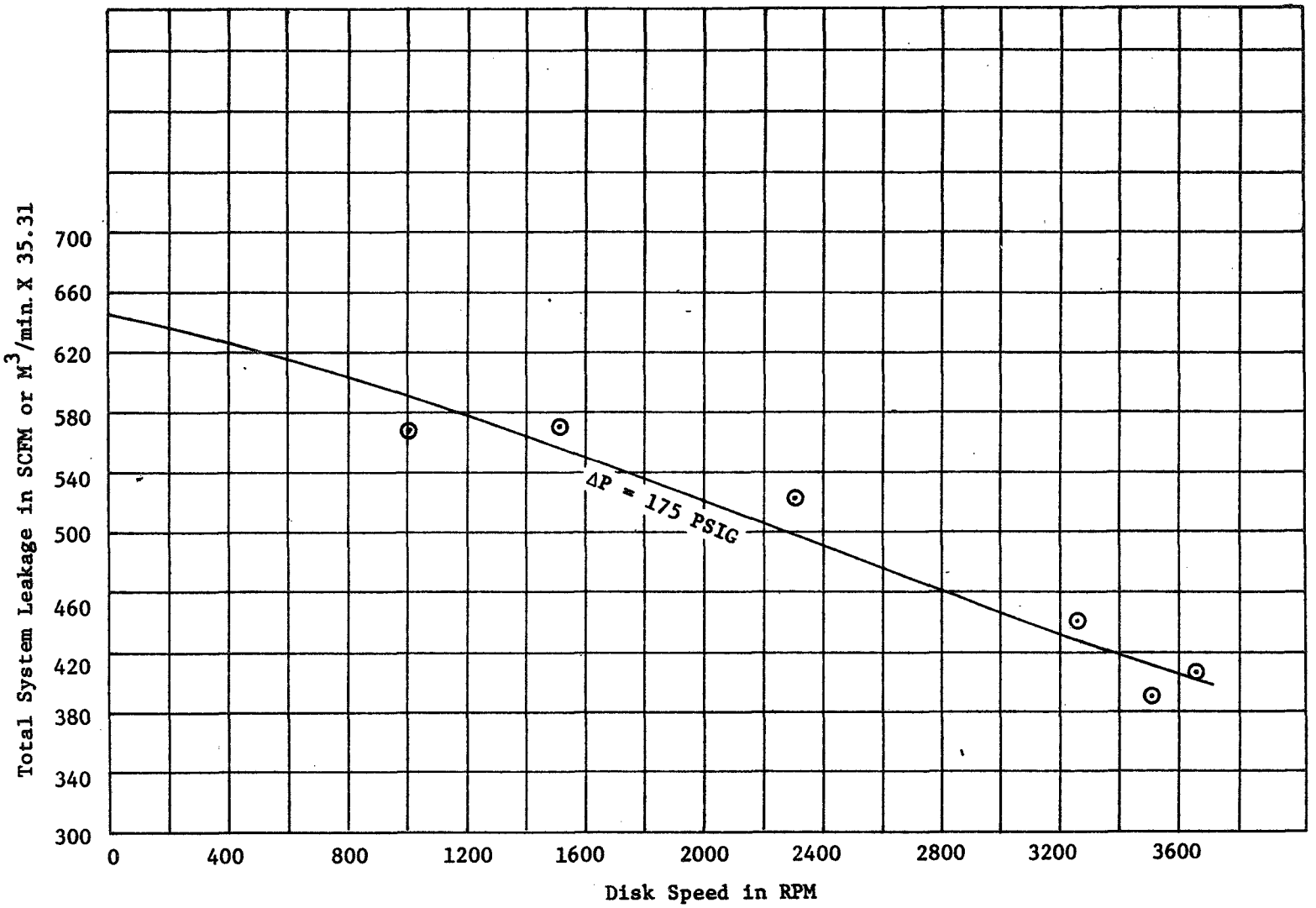

Figure 39. Total Air Leakage Vs. Disk Speed for -131 Seal

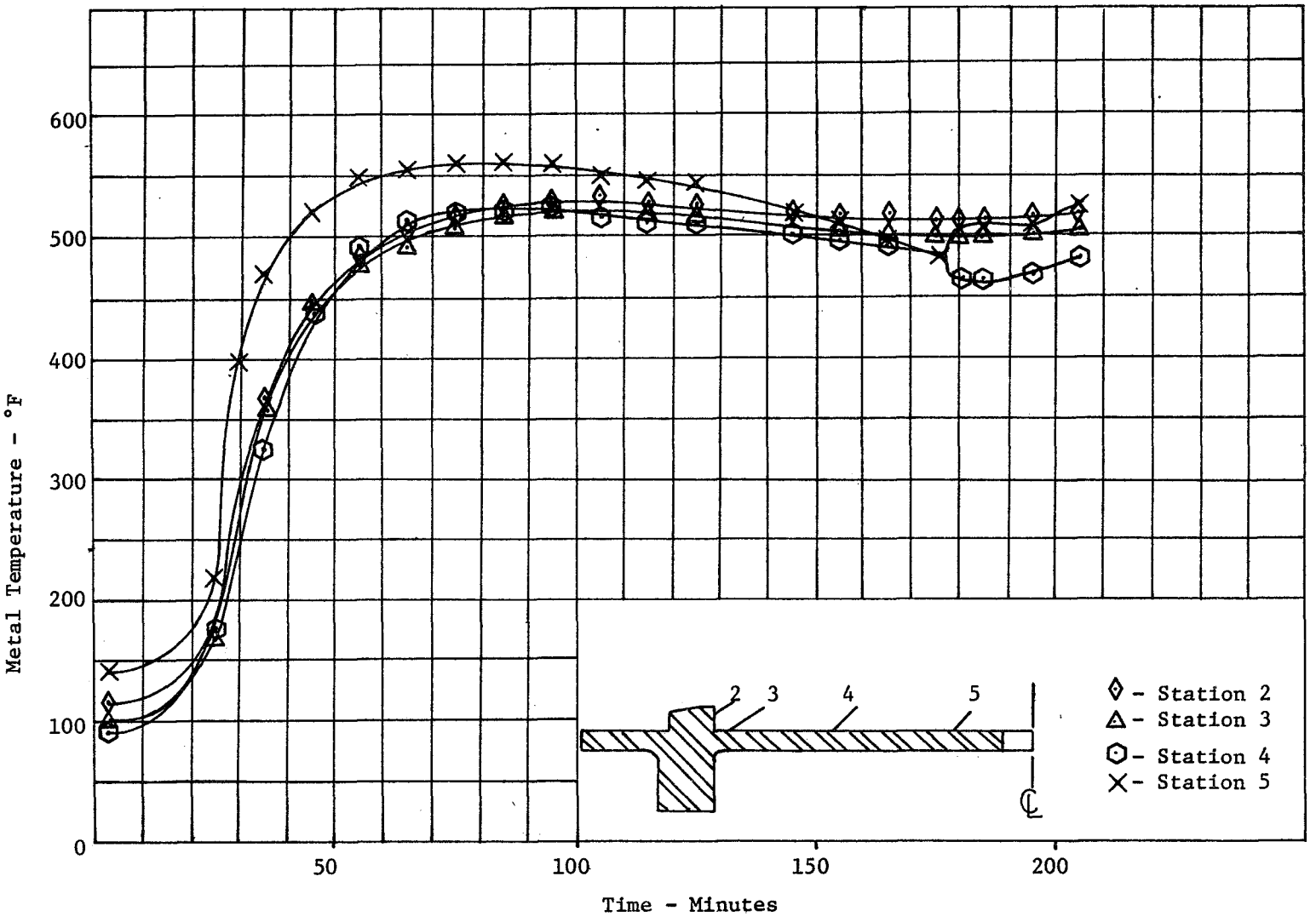

Figure 40. Transient Base Temperature

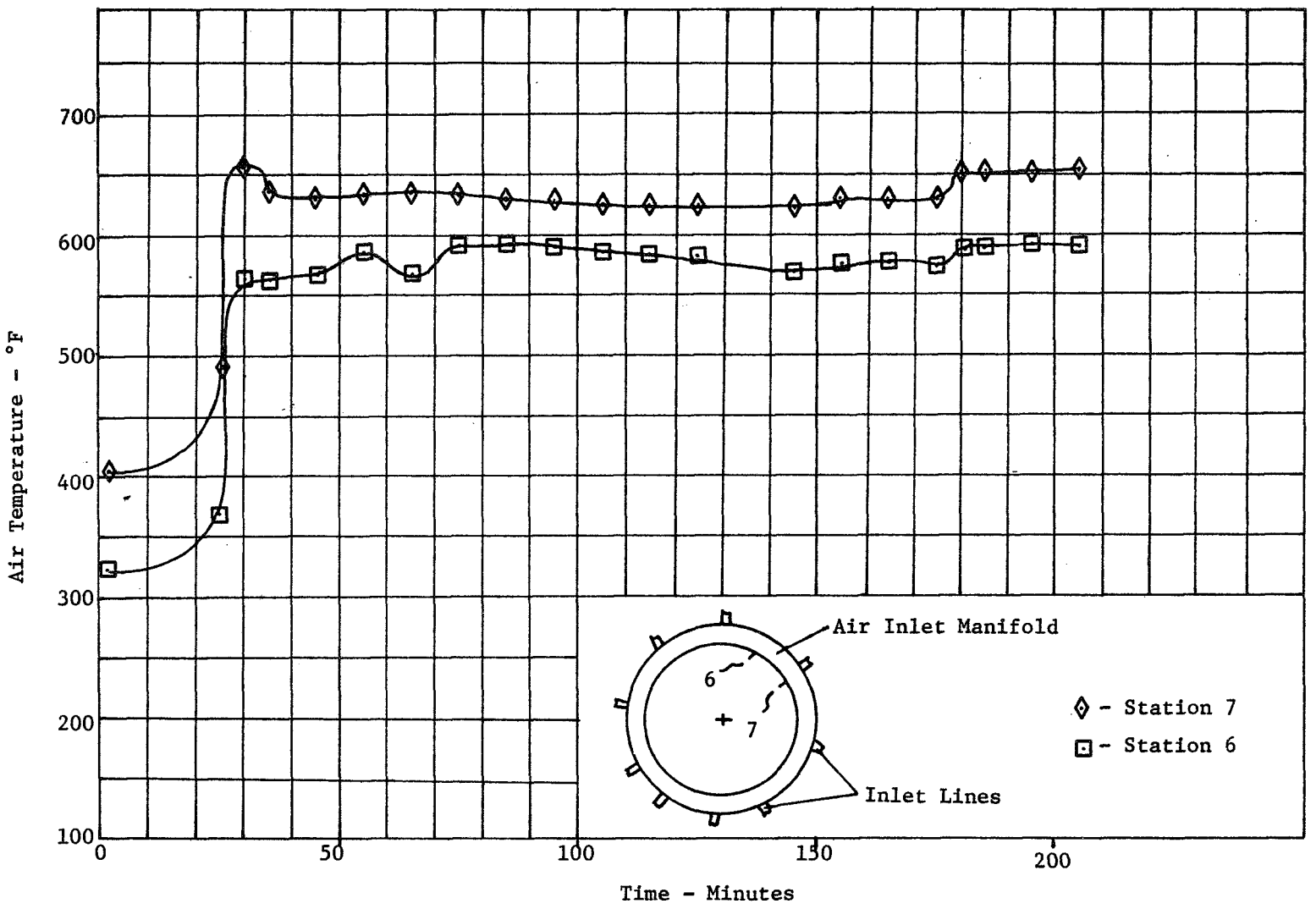

Figure 41. Transient Air Manifold Temperature

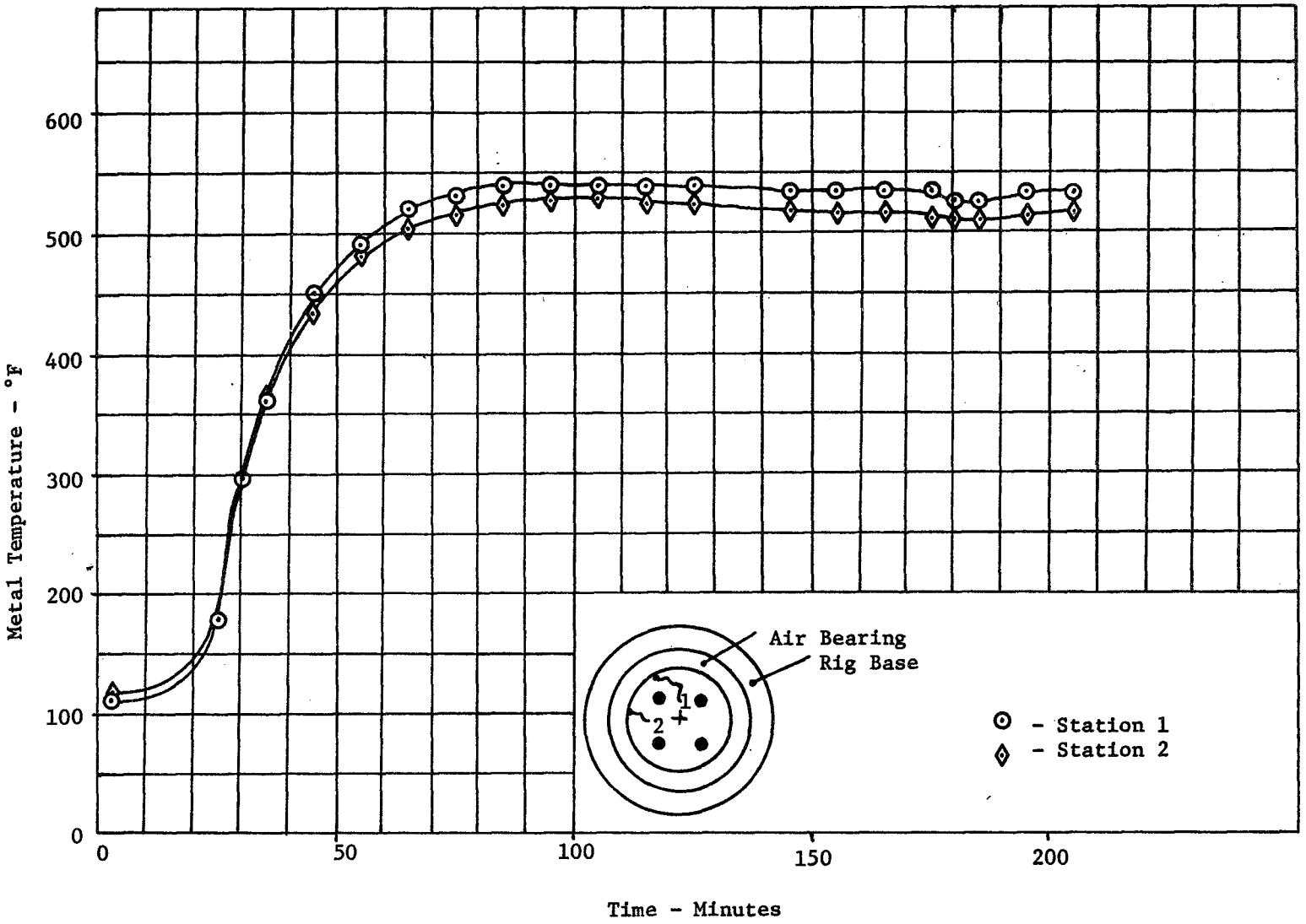

Figure 42. Transient Base Temperature

and bottom air bearing was extremely discouraging, a redesign effort was conducted to isolate the bottom air bearing from the rig. The first design (Figure 43) was discarded because it was pressure loaded against the rig bed, and the possibility of distortion still existed.

The second design, which consisted of a duplicate of the top seal (with a stepped face but no plating) supported on a bed of coil springs (See Figure 5), was completed and purchased. This design made the bottom air bearing independent from the rig bed. An assembly was made, and the seals were tested statically, at room temperature. The air bearing disk floated freely at all inlet pressures between 22 and 180 psig. The rig was then heated to 790°F statically, but dirt ingestion again locked up the disk. It was later found that a local high spot existed on the -131 seal face. The high spot was lapped off by hand.

The rig was rebuilt and heated to 750°F at 150 - 155 psig inlet pressure. After disk freedom was determined manually, the disk speed was brought to 300 rpm and held for approximately one hour. Over a period of approximately one-quarter hour, speed was increased to 950 rpm. Over the final three-quarter hours of running, four rubs occurred, all on the unplated bottom bearing, with recovery after each rub. No rubs occurred on the -131 test seal.

Inspection showed that the bottom air bearing had lost axial clearance on a washer under a bolt head at the same circumferential location as the rub. Air leakage rates recorded during this test are shown below.

First -131 Seal Hot Dynamic Test			
Seal Inlet			
Pressure (PSIG)	Temp. (°F)	Disk (RPM)	System Total Airflow (SCFM)
153	735	300	535
153	740	850	530
153	740	350	540

Parasitic and overboard leakages were not recorded, but judgement would estimate this quantity to be approximately 10 to 30 percent of the total measured flow rate.

The above test was stopped because of excessive pressure drop in the line air filter, not because of the bottom air bearing rubs. Inspection of the filter showed excessive carbon buildup. At this point, the decision was made to install a hydrogen-fired hot-air system because of the

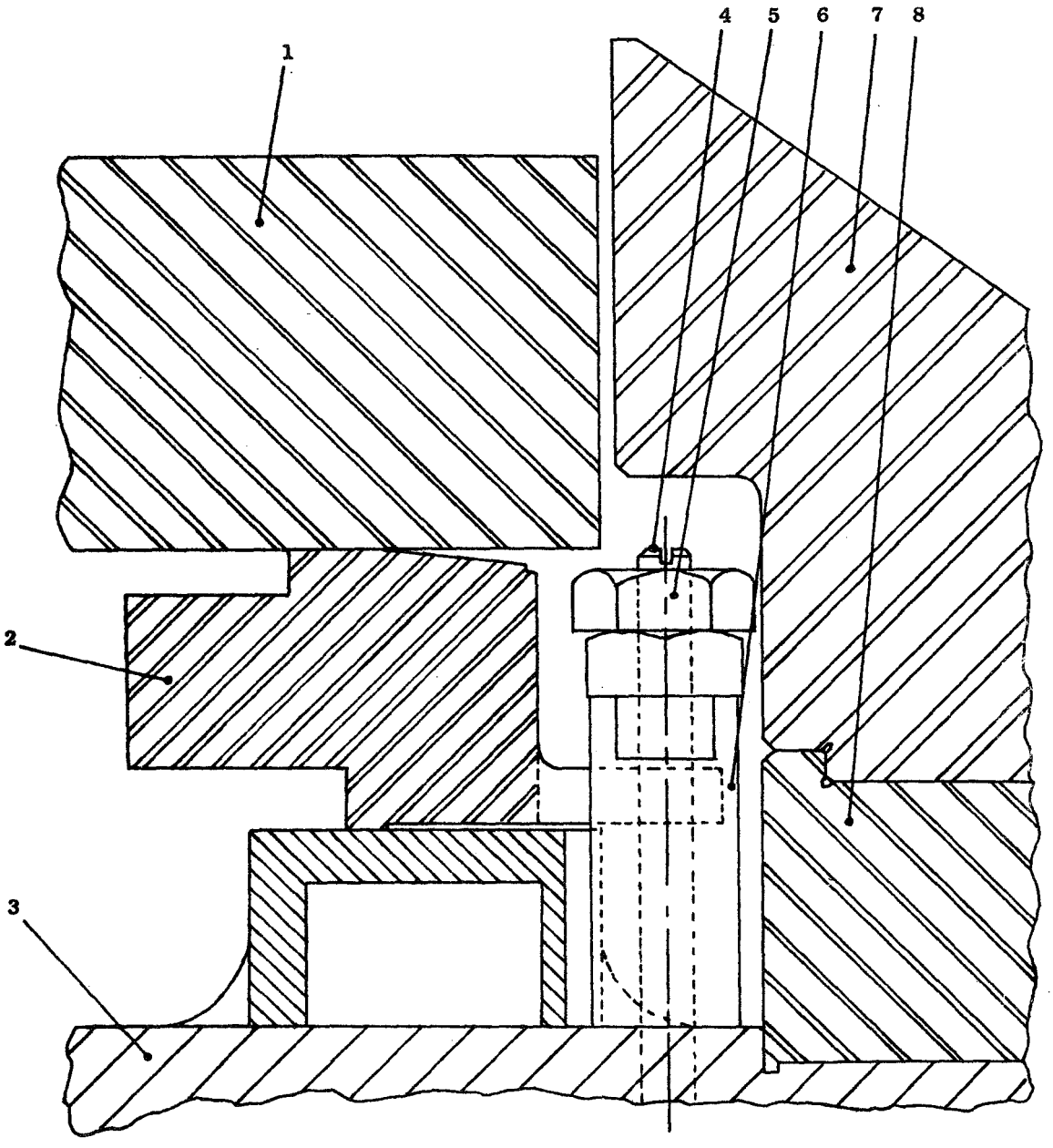

1	Disk	5	Jam Nuts
2	Press. Bal. Air Brg.	6	Cam
3	Bottom Housing	7	Seal Guide
4	Stud	8	Spacer IV

Figure 43. Bottom Air-Bearing Modification

dirt problem with the existing system. The hydrogen system was installed, and several buildups were made in an attempt to conduct hot dynamic testing; however, metal pickup on the unplated face of the bottom air bearing as inlet temperatures were increased caused disk hangup.

The bottom air-bearing face was flame sprayed with titanium-aluminum oxide plating (See Figure 44), a step was ground on the face plating, reassembly was done, and three hot tests were completed as shown.

Second -131 Seal Hot Dynamic Test							
Date	Time	P (PSIG)	T (°F)	N (RPM)	W_a (PPS)	Total Time	Cum. Time
3/5	1200	133	560	1162	---		
	1247	137	596	3000	---		
	1336	142	626	6200	---		
	1344	142	626	6200	---		
	1350	142	626	0	---	1:50	1:50
3/7	2135	155	660	0	0.806		
	2200	165	751	2600	0.945		
	2221	170	712	5700	0.664		
	2255	168	722	5800	0.665		
	2330	170	721	5720	0.668		
	0000	168	719	5750	0.672		
	0024	---	---	0	---	2:49	4:39
3/11	1030	168	680	0	1.104		
	1055	168	730	1800	0.852		
	1145	170	741	4500	0.777		
	1154	---	---	5900	---		
	1155	---	---	0	---	1:25	6:04

One hour and fifty minutes of running time were accumulated on the first test. Maximum conditions were 6200 rpm (630 ft/sec), 142-psig air inlet pressure at 626°F. The test was stopped because the air leakage rate was relatively high, and the desired air temperature of 750°F could not be reached. Inspection after test showed no evidence of seal touchdown. The excessive air leakage rates were caused by excessive step height (0.0015 in.) on the bottom air bearing and galling on the piston rings.

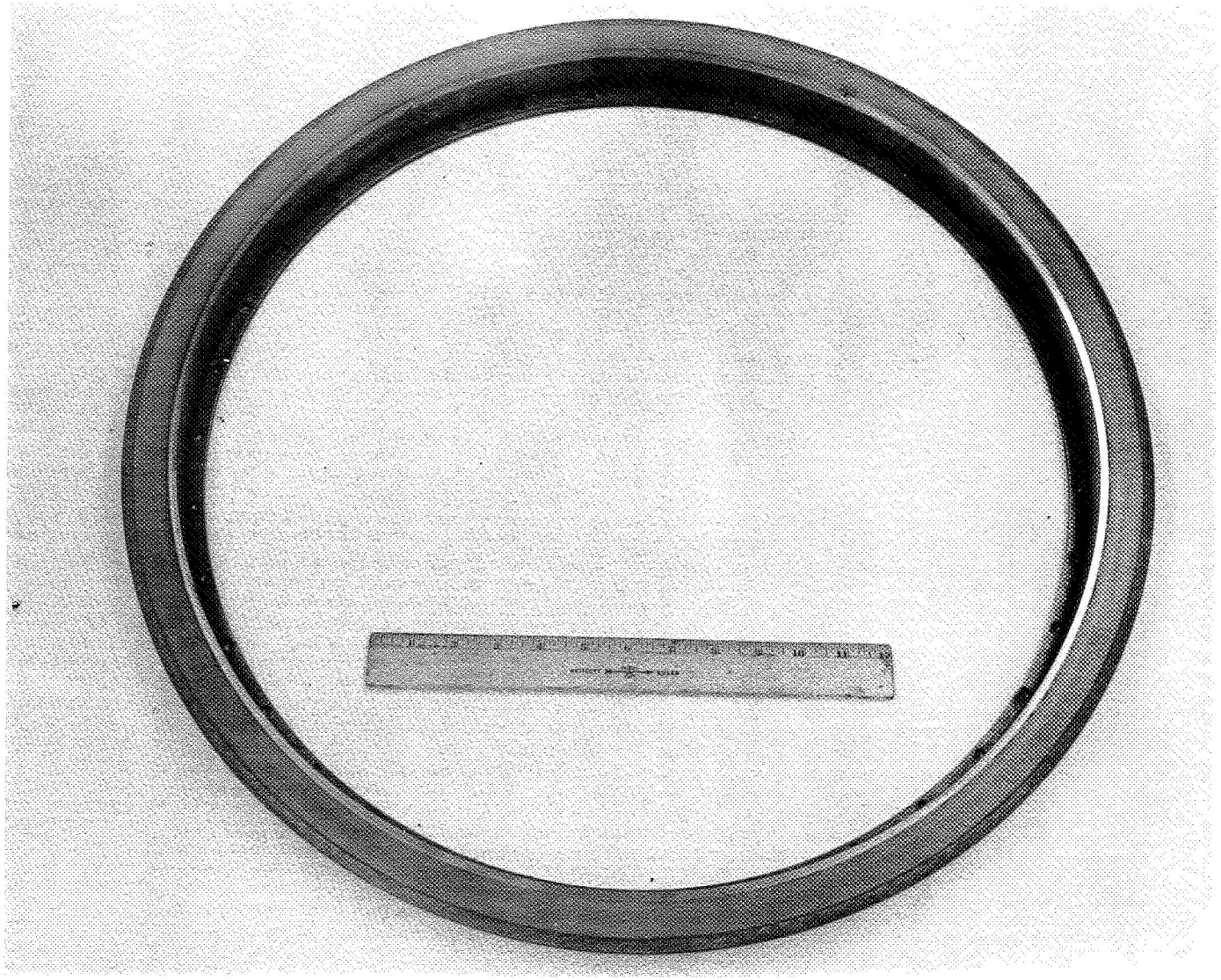

Figure 44. Bottom -131 Seal with Titanium-Aluminum Oxide Spray Plating

The step on the air-bearing face was hand lapped to a 0.0006/0.0009-inch height, the piston rings were reworked by hand, and the rig was reassembled for test.

The duration of the second run of the second test was two hours, fourty-nine minutes. Maximum conditions were 5900 rpm and 170-psig air inlet temperature at 760°F. Total system air leakage rate at this condition was 0.665 lb/sec. The test was stopped to change over to a higher pressure source on the air turbine drive, since speed was limited to 5900 rpm with the existing system. Inspection after test showed all seal and air-bearing parts to be in excellent condition.

Duration of the third hot test in the second test series was one hour, twenty-five minutes. Maximum test conditions were 5900 rpm, with 170-psig air inlet pressure at 746°F. While operating at maximum conditions, the top shaft ball bearing failed, allowing the air-bearing disk to orbit, causing a rub on the top test seal. In addition, the center shaft labyrinth seals (Items 6 and 7, Figure 4) were destroyed, and the disk shaft (Item 4, Figure 4) was damaged.

The above three tests, comprising six hours and four minutes of running time, demonstrate the operational characteristics of the design at 760°F, 170 psig, and 6200 rpm maximum conditions. Replacement of the facility ball bearing, rebuild, and further testing was stopped to conserve funds, since the design principle had been successfully proven. This stepped, hydrostatic design was selected and approved by the NASA Project Manager for the construction of the Flight-Weight Seal Design.

SECTION VI

TASK IV - FLIGHT-WEIGHT DESIGN AND TEST

A. Design

This phase of the program provided for design, manufacture, and test of a total seal assembly in a step-hydrostatic design concept similar to the -131 seal (refer to paragraph 4B) but with a separable race and weight reduced to a magnitude acceptable for a flight engine. This decision was based on the test experience gained from the -131 and -333 seals. The actual measured weight of the finished parts shown in Figure 7 is as follows:

Item No.	Description	Weight (Pounds)	Weight (Lbs/In. Circumference)
2	Seal race pilot	5.02	0.0708
3	Hydrostatic seal	7.10	0.1002
4	Piston ring	0.70	0.0099
5	Seal housing	7.65	0.1079
9	Seal race	10.62	0.1498
	TOTALS	31.09	0.4386

The total weight of the hydrostatic seal and piston ring is approximately two and one half times less than similar parts for the -131 seal. The -131 hydrostatic seal and piston ring alone weighed 19.45 pounds.

Basic mechanical design considerations were as follows:

1. Hydrostatic Seal (Figure 7, Item 3)

   a. Pressure Deflections

The axial and radial location of the center of gravity of the seal section was placed so that the sum of all radial and axial moments taken about this center was zero. Figure 45 shows the force diagram and other data pertinent to the following procedure for calculating moments.

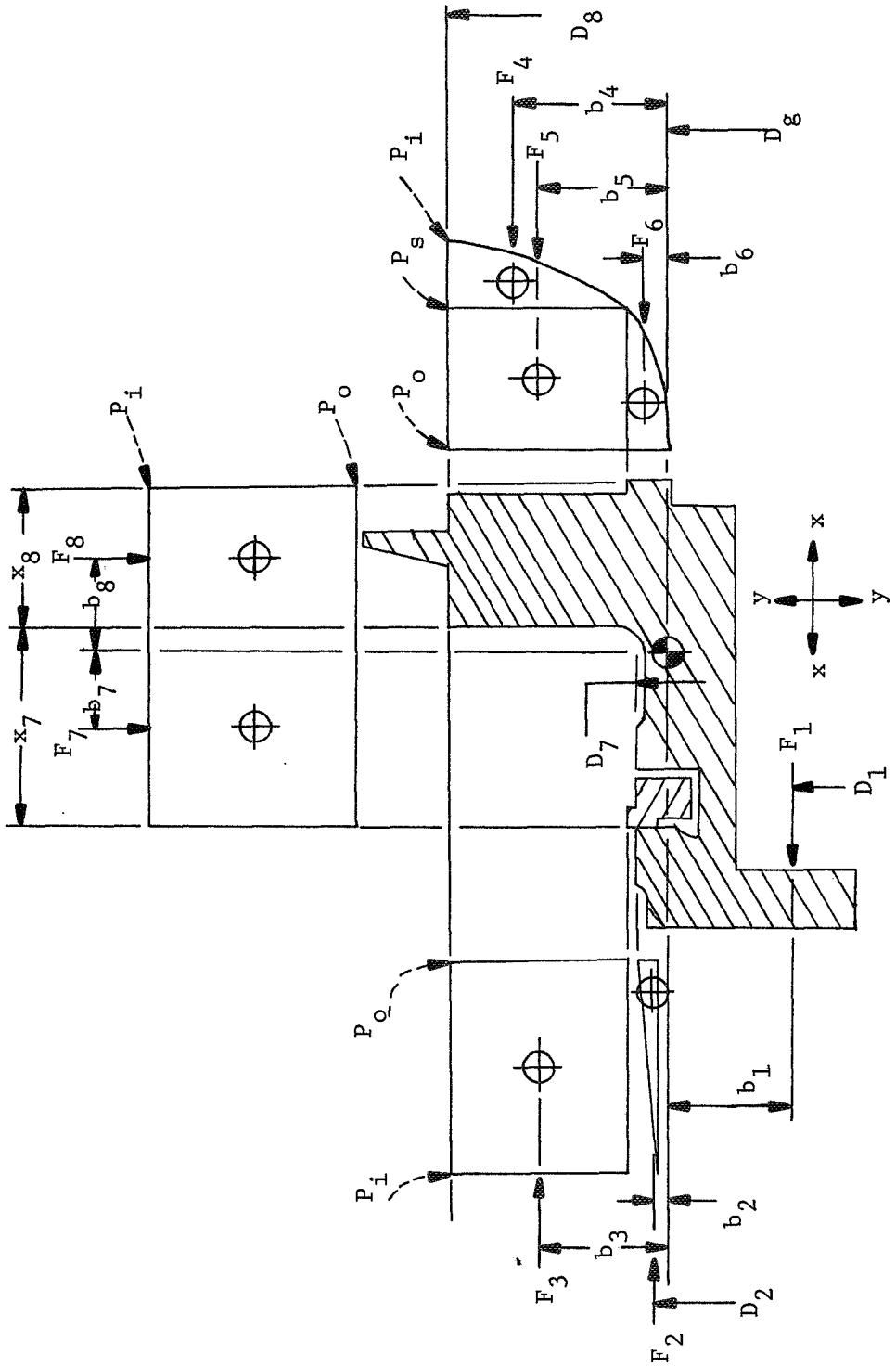

Figure 45. Hydrostatic Seal Pressure Forces

The location of the center of gravity (CG) of the seal structure in the x-x and y-y planes was calculated by subdividing the cross section into incremental areas whose values could be easily calculated, then determining the location of the CG of each individual area with respect to an arbitrary plane and finding the composite CG's by the following equations:

$$\bar{x} = \frac{m_1 x_1 + m_2 x_2 + -- m_n N_n}{m_1 + m_2 + -- m_n} \qquad \text{Eq (9)}$$

$$\bar{y} = \frac{m_1 y_1 + m_2 y_2 + -- m_n y_n}{m_1 + m_2 + -- m_n} \qquad \text{Eq (10)}$$

where $\bar{x}$ = location of center of gravity in the x-x plane.

and $\bar{y}$ = location of center of gravity in the y-y plane.

m = incremental area.

x = distance from arbitrary plane to area in x-x direction.

y = distance from arbitrary plane to area in y-y direction.

The actual pressure forces, f, represented by the vectored areas in Figure 45 were then calculated by the following method:

f_1 = spring force (assumed 30 lbs total)

$f_2 = (1 - \lambda_{i-o})(P_i - p_o) A_2$, where A_2 is the interface area between the piston ring and seal.

$f_3 = (P_i - P_o) A_3$, where A_3 is the axial pressure area between the piston ring and seal face OD.

$f_4 = (P_i - P_s)(\lambda_i)(A_4)$, where A_4 is the face area from the seal OD to the seal face step.

$f_5 = (P_s - P_o) A_5$, where $A_5 = A_4$.

$f_6 = (P_s - P_o) \lambda_o A_6$, where A_6 is the face area of the step.

$$f_7 = (P_i - P_o)(\pi D_7 x_7).$$

$$f_8 = (P_i - P_o)(\pi D_8 x_8).$$

λ = compressibility factor (see paragraph 4B).

Forces f_1 through f_8 were then resolved to equivalent forces per inch of circumference at the radial location of the composite C.G., for example:

$$F = \frac{f_n D_n}{D_g^2}, \qquad \text{Eq (11)}$$

where D_2 through D_6 are taken at the center of gravity of the respective pressure areas, $\oplus$, per Figure 45 (D_1, D_7, and D_8 are shown in Figure 45).

The seal section and pressure areas were then designed so that the sum of all pressure moments about the part center of gravity was zero, as follows:

$$\Sigma M = F_1 d_1 + F_2 d_2 + \text{--------} F_8 d_8 = 0 \qquad \text{Eq (12)}$$

The stress and radial strain were then approximated by assuming the mass to be concentrated at the CG of the part and imposing an external pressure as follows:

$$s_h = \frac{\Delta P (x_7 + x_8) D_g}{2m_t} \qquad \text{Eq (13)}$$

$$= 3342 \text{ psi, when } \Delta P = 175 \text{ psi}$$

$$\sigma_R = \frac{S_h D_g}{2E} \qquad \text{Eq (14)}$$

$$= 0.00131 \text{ inch, at } 70°F$$

where: s_h = hoop stress

m_t = total area of seal cross section

σ_R = radial strain

E = Young's Modulus

$= 28.4 \times 10^6$ psi, for 300-series stainless steel at 70°F

b. Air Leakage, Film Thickness, and Servoforces

Laminar flow air leakage rates versus inlet air pressure for the flight-weight seal face are shown on Figure 46. Force versus air film thickness are shown on Figure 47.

These curves were calculated by the same method as described in paragraph 4B for the -131 seal.

c. Thermal Clearance

To determine the clearance allowable between the hydrostatic seal (Figure 7, Item 3) and the piston ring seat on the bore of the seal housing (Item 5), an approximation was first made to determine the effect eccentricity has on hydrostatic air film thickness.

Figure 48 shows the net seal servoforce, ΔF, per inch of seal circumference versus outlet film opening, h_o, for an inlet pressure, P_i, of 184.7 psia and a discharge pressure, P_o, of 14.7 psia. Neglecting the effect of curvature gives the following as the ΔF at the maximum and minimum clearances, which occur 180° apart for an eccentric seal:

$$\Delta F = (P_i - P_o) E_R = \Delta P E_R \qquad \text{Eq (15)}$$

Using this criterion, eccentricity which brings h_o to zero is:

$$E_R = \frac{\Delta F}{\Delta P} = \frac{9.18}{175} = 0.0524 \text{ inch},$$

where: ΔF is from Figure 48, at $h_o = 0$.

using $E_R = \pm 0.012$ in., ΔF is approximately ± 2.1 pounds, and h_o ranges from approximately 0.00045 to 0.00063 inch.

Assuming $\pm$ 0.012-inch radial clearance between the seal and the housing balance diameter, and a mean coefficient of thermal expansion of 10 in./in. °F for 300-series stainless steel, the Δt at which the clearance is reduced to zero is the following:

$$\Delta t = \frac{0.012 \times 2}{10 \times 10^{-6} \times 22.256} = 106°F$$

This Δt is extremely small when weighed in terms of air inlet temperatures in the 1000 to 1200°F range, but seemed to be a reasonable compromise when compared to the increased possibility of a seal rub as eccentricity increases, and when compared to the increased expense involved in the manufacture of a seal held concentric with side-fitting splines or some similar method. The decision was made to hold the clearance at ± 0.012 inch and to attempt controlling thermals to prevent seal interference at the balance diameter.

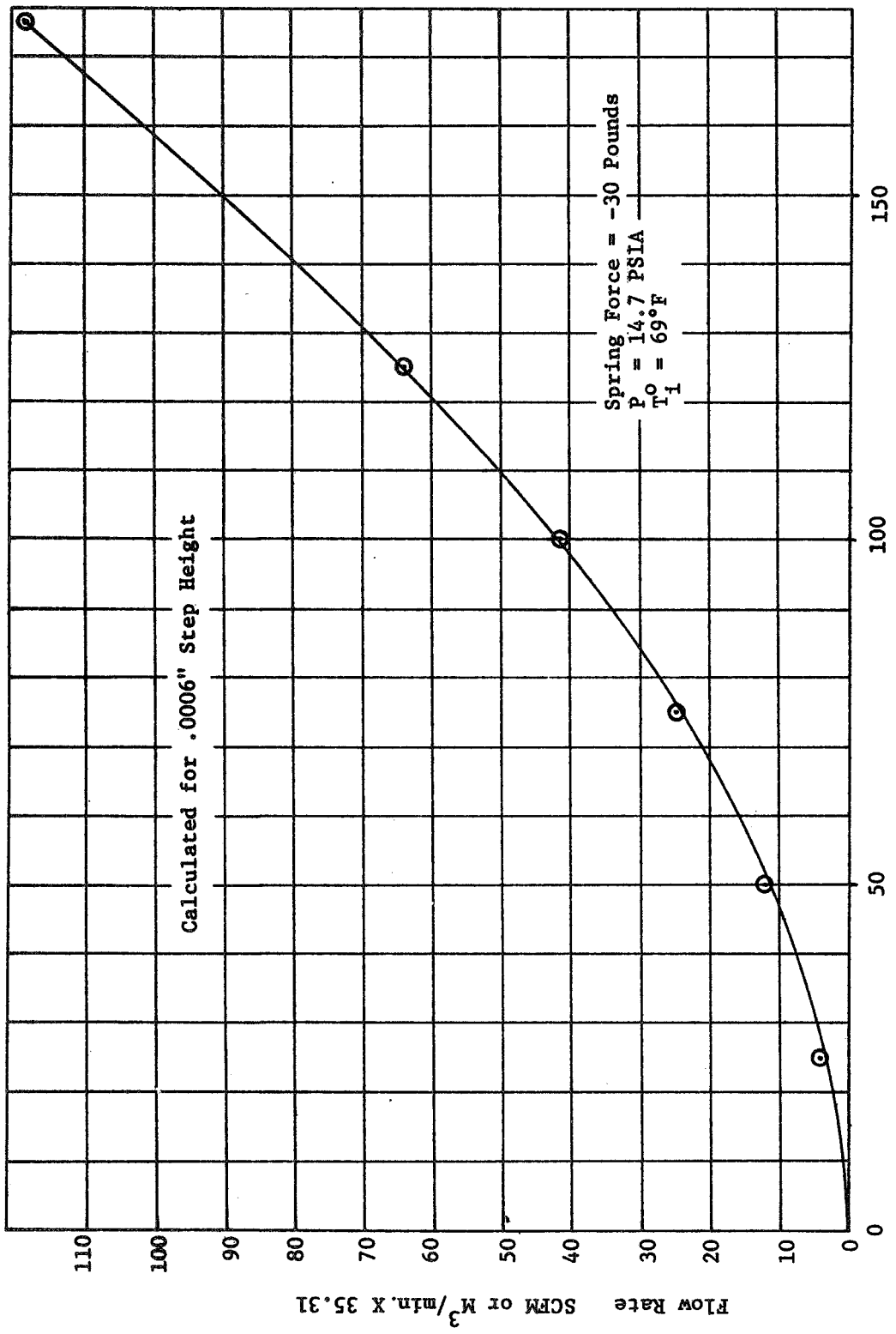

Figure 46. Flight-Weight Seal Air Leakage Rate Vs. Seal ΔP

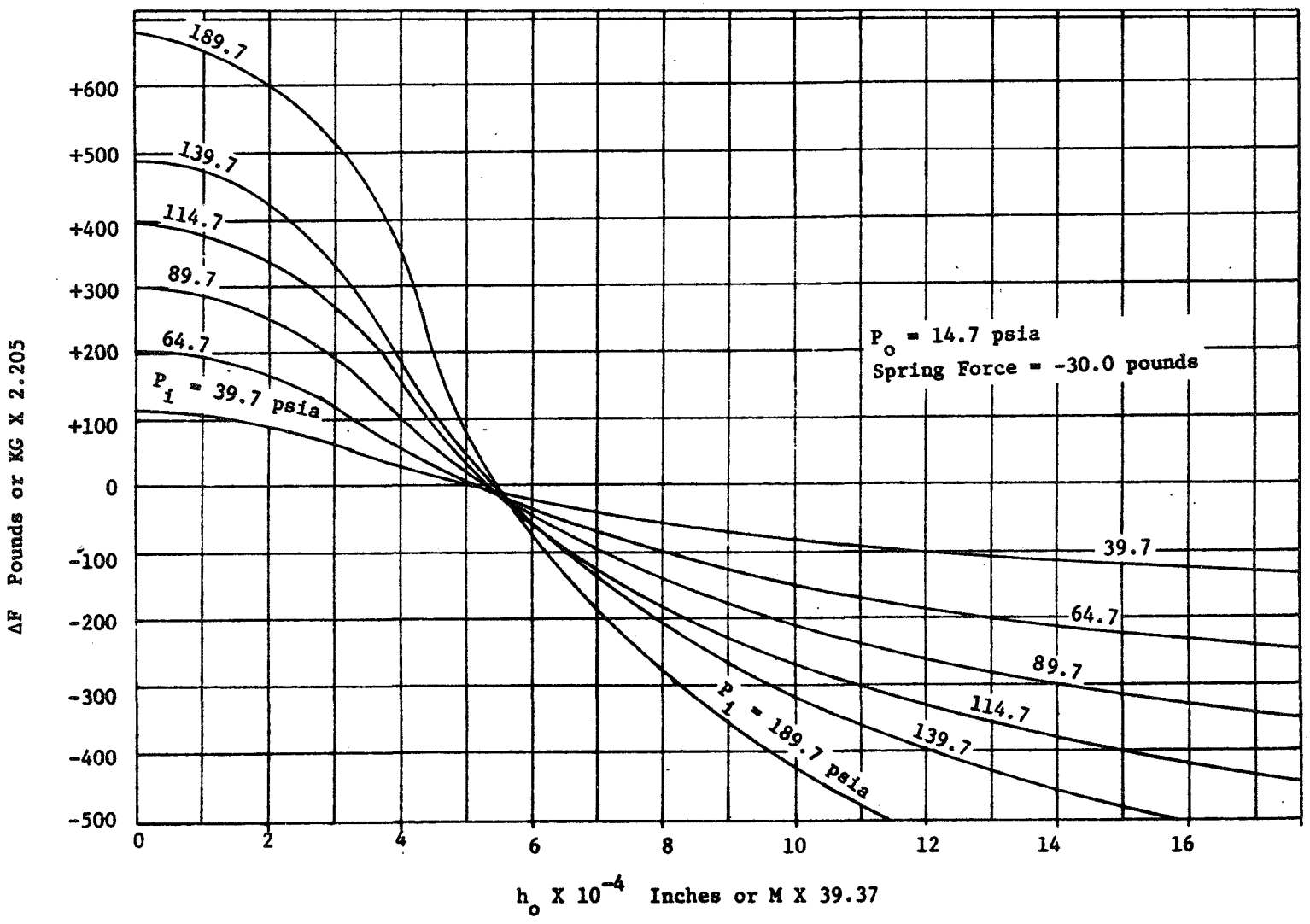

Figure 47. Flight-Weight Seal Servo Forces Vs. Air Film (h_o) Calculated for 0.0006-Inch Step Height

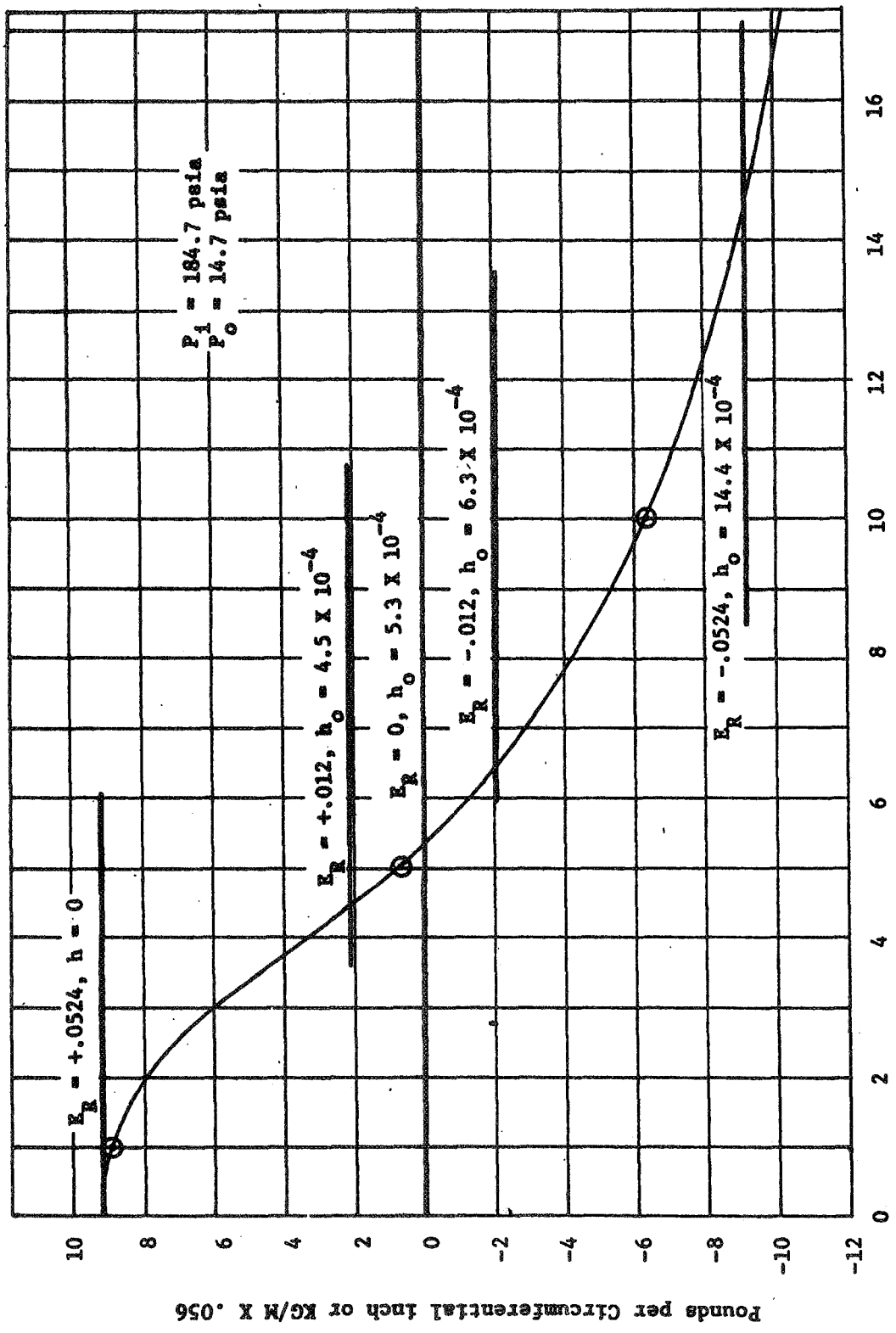

Figure 48. ΔF Vs. Film Thickness Showing Effect of Seal Eccentricity

2. Piston Ring (Figure 7, Item 4)

a. Pressure Balance

Figure 49 shows the pressure balance diagram for the piston ring. The following equations are relevant:

$$J_1 = (P_i - P_o)(y_1 + y_2)$$

$$J_2 = (P_1 - P_o)(y_1)(\lambda)$$

$$J_3 = (P_i - P_o)\, x$$

$$J_4 = (P_i - P_o)(x)(\lambda)$$

The force available to seat the ring in an axial direction, ΔJ_a, is:

$$\Delta J_a = J_1 - J_2$$

$$= [y_2 + (1 - \lambda)\, y_1]\, \Delta P \qquad \text{Eq (16)}$$

The net radial seating force ΔJ_r is:

$$\Delta J_r = J_3 - J_4$$

$$= (1 - \lambda)(\Delta P)\, x \qquad \text{Eq (17)}$$

and,

J = force per unit circumference

P_i = upstream pressure

P_o = downstream pressure

y_1, y_2, and x = areas per unit of circumference

λ = gas compressibility factor (see paragraph 4B)

In order to prevent "hanging" of the piston ring on either the bore or the face, the following criteria must be met:

$$\Delta J_a \geq \Delta J_r\, C_f \qquad \text{Eq (18)}$$

$$\Delta J_r \geq \Delta J_a\, C_f \qquad \text{Eq (19)}$$

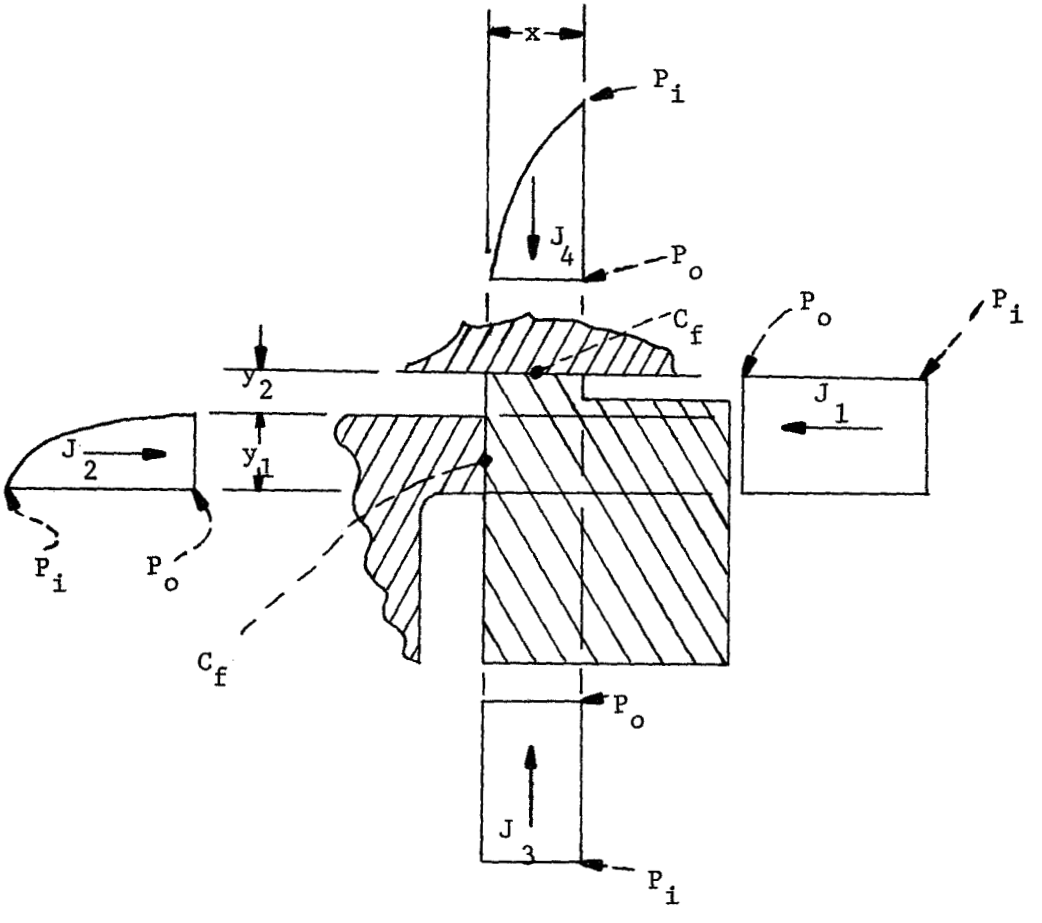

Figure 49. Piston Ring Forces

b. End Gap Clearance

A clearance was provided at the end gap of the piston ring to allow circumferential thermal growth without binding in the bore of the seal housing. The clearance was set at 0.070 initially, but later changed to 0.100, to give approximately the following allowable Δt (assuming the mean coefficient of expansion of 300- series stainless steel to be 10×10^{-6} in./in. °F at 1000°F):

$$\Delta t = \frac{0.100}{10 \times 10^{-6} \quad \pi D_B} = 141°F$$

where, D_B = Bore dia of seal housing = 22.562 in.

3. Race Design (Figure 7, Item 9)

Some of the design considerations for the rotating hydrostatic seal race were as follows:

a. Inertia Force

The pressure balance of the race provides a net axial force to seat the race against the rotating disk (Figure 7, Item 1) at operating pressures. This, of course, is done to prevent gas leakage between the disk and the seal race. It was assumed that the race must remain seated against the disk at all pressure levels above 5 psi, ΔP, to a maximum disk speed of 7460 rpm, when face runout on the disk is $\pm$ 0.002 inch once per revolution. The weight of the seal race was estimated to be 11.67 pounds, and the inertia of the race was calculated as follows:

$$F_I = Mw^2 r_a \qquad \text{Eq (20)}$$

where, $M = \frac{W_T}{g}$ = mass of race

and, W_T = weight

w = angular velocity, radians per unit time

r_a = disk runout, half amplitude

F_I = 35.74 lbs

The pressure seating area (A_p) to provide 35 pounds seating force (F_p) at 5 psi, ΔP, is the following:

$$A_p = \frac{F_p}{\Delta P} = \frac{35}{5} = 7 \text{ in.}^2$$

where $F_p = F_I$

The sealing radius at the interface of the seal race and disk, therefore, must be placed to provide 7 square inches of pressure area, as follows:

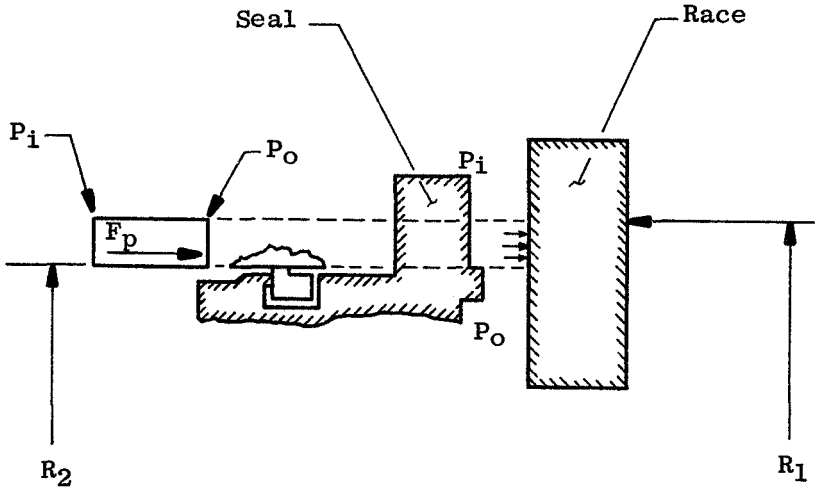

Race Pressure Seating

and, $$R_1 = \sqrt{\frac{A_p}{\pi}} + R_2 \qquad \text{Eq (21)}$$

where, R_1 = location of sealing radius on aft surface of race

R_2 = seal balance piston radius

b. Pressure Moments

The seal race was designed so that the sum of the pressure moments acting on the race is zero.

In Figure 50, F_4, F_5, and F_6 are the same forces as shown on Figure 45. All forces, F, are calculated in the same manner as described earlier for the forces, F, shown on Figure 45; i.e., first calculate actual forces, (f), and then resolve to equivalent forces (Eq 3) at the radial location of the part center of gravity (⊕) shown on Figure 50 as D_g.

The part CG (⊕) is calculated by the same method as described for the seal, using Equations (1) and (2).

Material is removed from one face of the race in order to shift the axial CG of the part to a location which allows the generation of a radial pressure moment, the magnitude and direction of which opposes the net axial moments, and causes the sum of all moments to be equal to zero:

$$\Sigma M_o = \Sigma F_n d_n = 0$$

c. Centrifugal Rotation

The material removal from the aft face of the race, as described in paragraph b above and shown in Figure 50, was done in a manner to prevent centrifugal rotation of the part due to the unsymmetrical section. It was assumed that this would be achieved if the tangential stress across the two sections were equal, as follows:

First, divide the race into sections as follows:

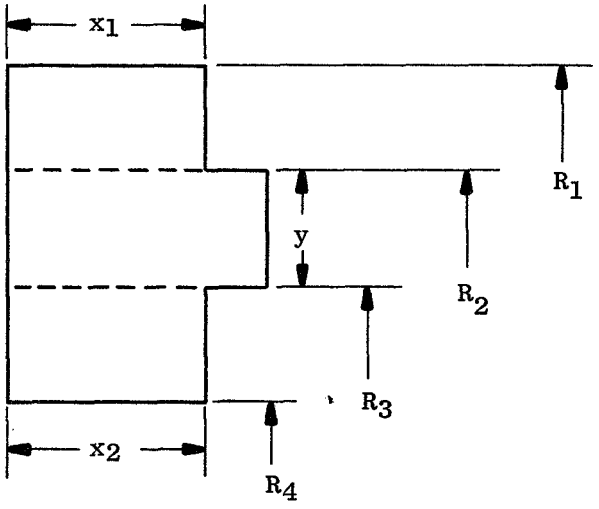

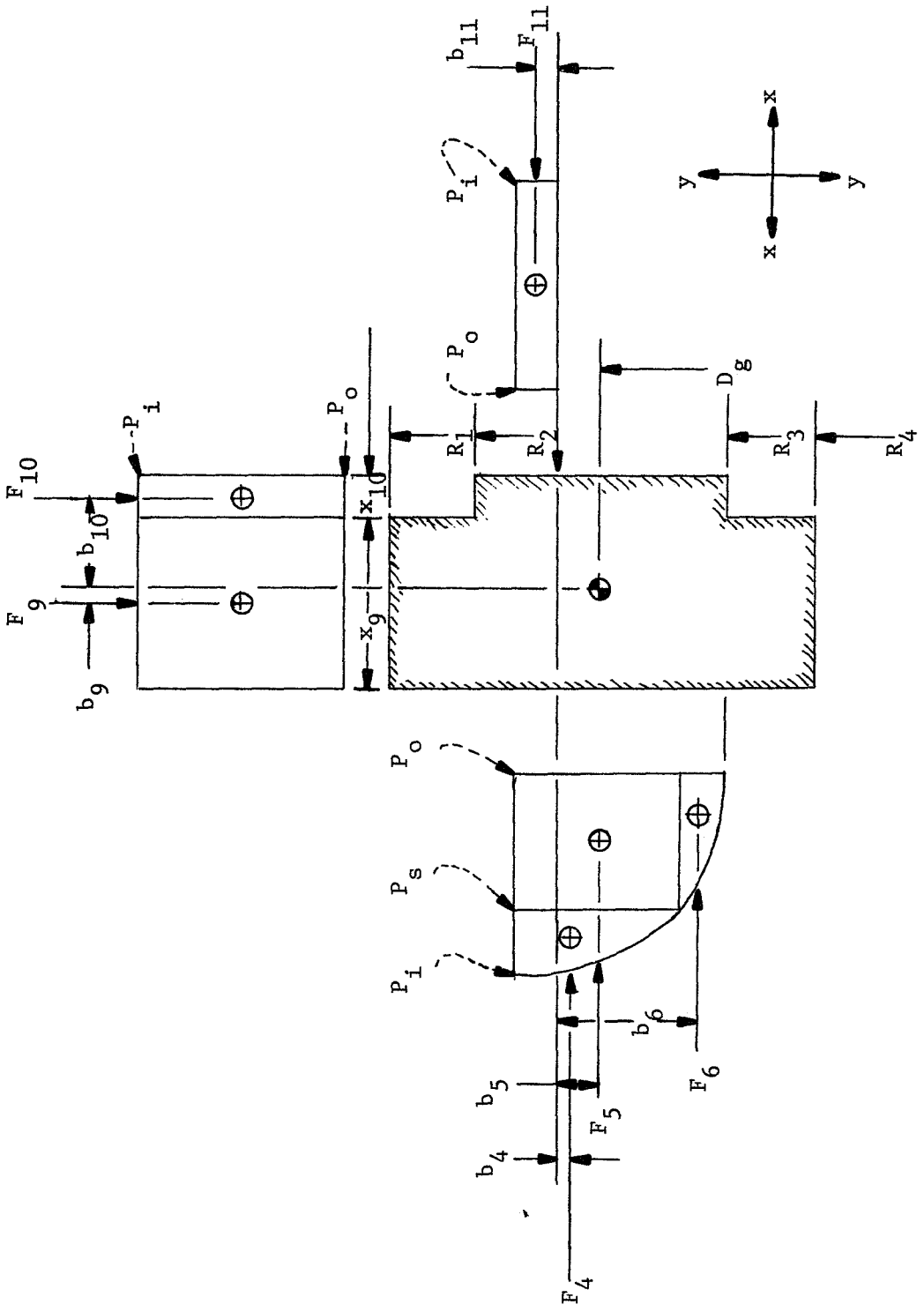

Figure 50. Seal Race Pressure Forces

Neglecting the effect of Poisson's ratio, the center section, since symmetrical, will expand uniformly in a centrifugal field. If the difference in tangential stress from R_2 to R_1, pulling the center section outward, is equal to the stress difference from R_4 to R_3, pulling the center section inward, then the composite section will expand uniformly in a centrifugal field.

The centrifugal stress, s_c, is the following:

$$s_c = \rho G R \qquad \text{Eq (22)}$$

and, $$G = \frac{\omega^2 R}{g} \qquad \text{Eq (23)}$$

and, by substituting Eq (23) into Eq (22):

$$s_c = \frac{\rho \omega^2 R^2}{g} \qquad \text{Eq (24)}$$

where, ρ = weight density

ω = angular velocity

R = radius

g = gravitational constant,

and, $$s_{c1} - s_{c2} = s_{c3} - s_{c4} \qquad \text{Eq (25)}$$

Substituting Eq (24) into Eq (25), and cancelling out the constants ρ, g, and ω, gives the following:

$R_1^2 - R_2^2 = R_3^2 - R_4^2$, and (since y, R_1, and R_4 are known, and $R_3 = R_2 - y$) the values of R_2 and R_3 can be calculated.

d. Spline Pilot Design

Close-fitting face splines were used to pilot the seal race to the disk in order to maintain concentricity of the race while allowing it to grow freely in a radial (or circumferential) direction. The pilot is formed by local splines on the ID of the race (Figure 7, Item 9), which are fitted into slots at the OD of the race pilot (Figure 2, Item 2). The race pilot bottoms out against the disk (Item 1), allowing a small axial clearance between the pilot and the spline faces to prevent distortion.

To prevent rotation of the race section about its CG from the centrifugal load generated by the splines, the spline CG is located directly under the CG of the race, as follows:

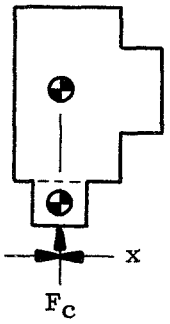

$M_o = F_c x$, and, since $x = 0$, $M = 0$

In order to minimize face distortion from the radial displacement due to the centrifugal weight of the local splines, the mass of the splines was held small, and the radial displacement of the race was calculated.

Radial displacements were determined using the following equations:

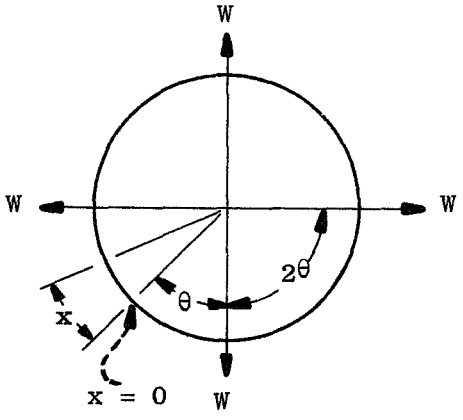

$$\delta_w = \frac{WR^3}{2EI}\left[\frac{1}{2}\left(\frac{\theta}{2}+\frac{SC}{2}\right)-\frac{1}{\theta}\right] \qquad \text{Eq (26)}$$

$$\delta_o = \frac{WR^3}{4EI}\left[\frac{2}{\theta}-\frac{1}{S}-\frac{C}{S^2}\right] \qquad \text{Eq (27)}$$

where, δ_w = outward displacement at $x = \theta$

δ_o = inward displacement at $x = 0$

R = radius

E = Young's Modulus

I = section moment of inertia

S = $\sin \theta$

C = $\cos \theta$

θ = angle in radians

W = applied load

Using splines at four equally-spaced locations and substituting F_c for W in Equations (26) and (27), where:

$$F_c = M\ ^2R,$$

the following displacements were calculated for a rotational velocity of 7460 rpm:

$$\delta_w = + 96 \times 10^{-6} \text{ in.}$$

$$\delta_o = - 85 \times 10^{-6} \text{ in.}$$

$$\delta_w - \delta_o = (96 + 85) \times 10^{-6}$$

$$= 181 \times 10^{-6} \text{ in.}$$

Since this displacement is approximately 10×10^{-6} inch per circumferential inch, or 60 times smaller than the hydrostatic air-film thickness, it was judged to be a safe limit.

4. General Thermal Considerations

This seal design provides for the flow of air past the face in a radially-inward direction. This is preferred to an outward-flow design because it is somewhat more forgiving to thermals generated by shear on the air film, ingestion of dirt particles, and light face rubs. This type of heat generation can cause an increase in operating temperature at the seal and race interfaces, and results in deflections of seal and race in the direction providing a converging flowpath. In this case, the interface servoforce is higher when $h = 0$ than for a flat face, provided the thermal is uniform circumferentially, thereby giving additional margin against a rub.

B. Static Tests of Flight-Weight Design

Inspection, when received, showed the seal face to be grossly out-of-flat. Discussion with the manufacturing source revealed that the parts were flat within drawing tolerances per their inspection prior to shipment; however, they agreed to regrind the seal. The part was hand carried to the manufacturer to review his finishing procedures. The aft face of the seal was flat lapped under its own weight. This face was then set against a grinding fixture which was stiff, properly ground, and indicated. The part was held against the fixture by means of finger clamps which were tightened with the minimum force required to hold the piece for grinding. The piece was reground, removed from the fixture, and inspected. The face taper was 70×10^{-6} inch maximum, and the maximum runout between the sealing face and the aft face was 100×10^{-6} inch. The part was hand carried to General Electric Company, where it was again inspected and found to have developed a 320×10^{-6}-inch taper (average) across a 0.40-inch width on the seal face (high at the OD) and a saddle of approximately 0.004/0.006 inch. The distortion may have been caused by creeping due to grinding stresses.

The part was assembled for test with an average step height of 0.001355 inch, and no additional rework. Film height and static leakage rates were measured and recorded as shown on Figures 51 and 52. Due to the large step height, the leakage was high and rework was done. Compare Figures 46 and 52.

The seal step was hand lapped with a diamond stone to the drawing dimension of 0.0006 inch, and the dual-flight-weight assembly (Figure 7) was made. When pressurized, the disk (Item 1) tilted, causing the seal (Item 3) to bottom out against the tail section of the seal housing (Item 5). The cause for the tilt was traced to loose fitting pilots which allowed a cumulative stackup of eccentricities between the top and bottom seal balance piston diameters of 0.042 inch, imposing a pressure moment on the disk. The rig was rebuilt after setting up an indicator base in the rig bed and indicating and shimming the pilots to obtain concentricity at the balance diameters.

Another build was made but free rotation of the disk was not obtained. The cause was traced to the top flight-weight seal. At two equally-spaced circumferential locations, no seal face leakage could be detected. Measurements of the seal face at these locations showed the OD of the face to be within 0.0001 inch of the plane of the step at the ID, implying additional face distortion from stress-creep. The top and bottom seals were then sent out for titanium-aluminum oxide face plating and regrind. On the subsequent buildup, disk rotation was obtained by hand but drag was evident. Inspection showed slight scoring on the face of the top seal race (Figure 7, Item 9). Cleanup of the race was done by hand, reassembly was made, and binding again occurred.

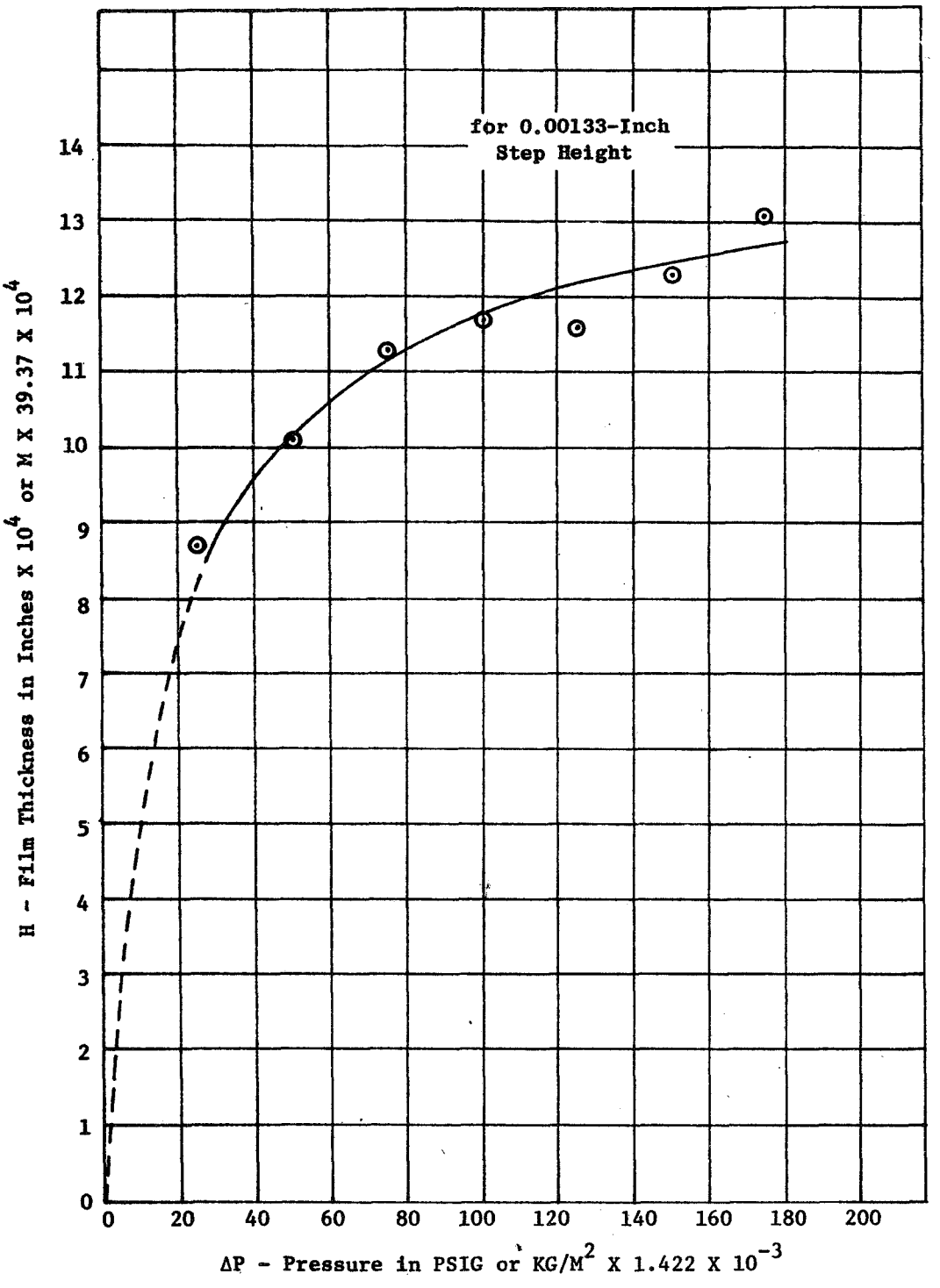

Figure 51. Film Thickness of Flight-Weight Seal Vs. Seal ΔP

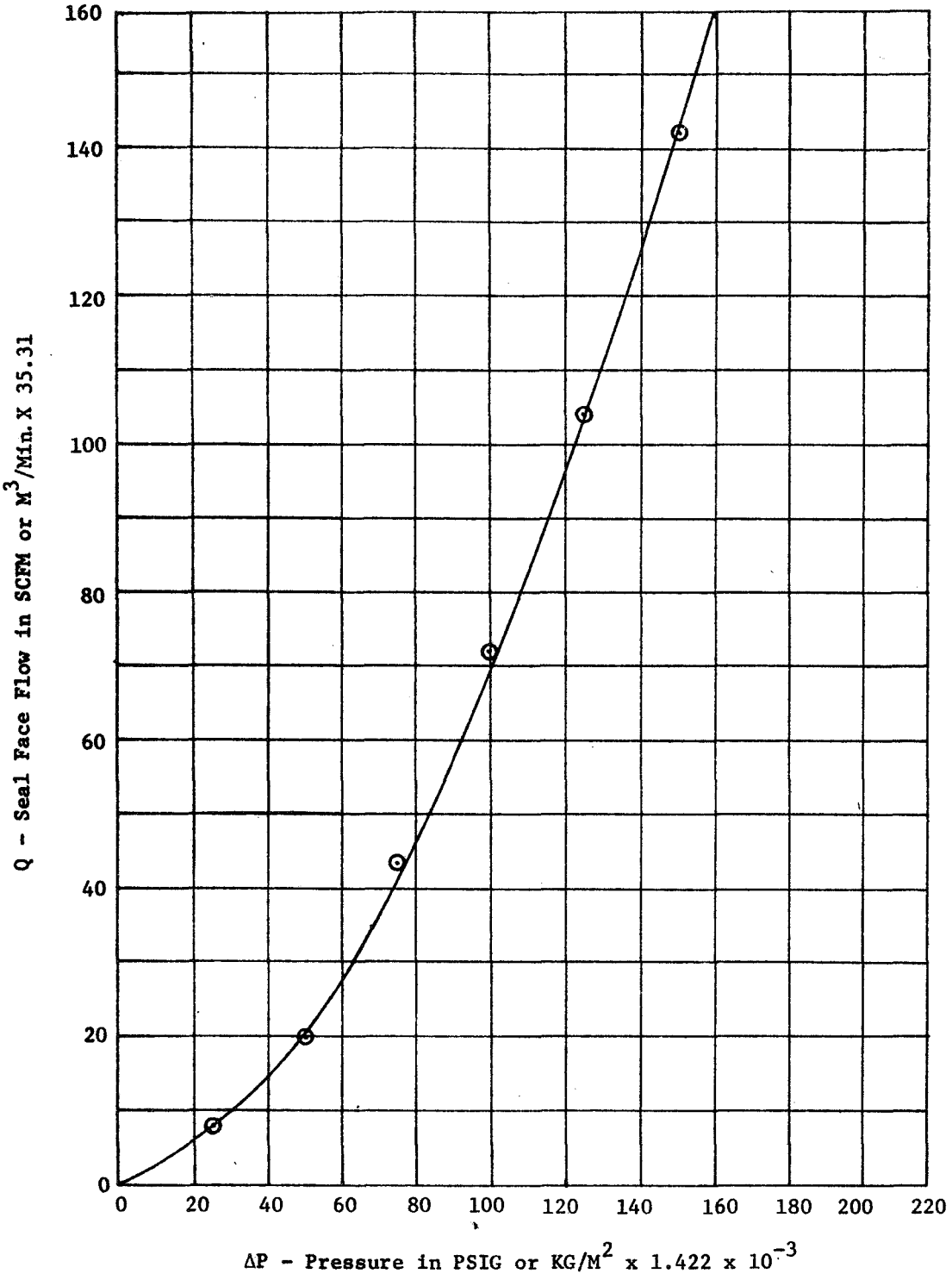

Figure 52. Face Leakage Vs. Inlet Pressure for Flight-Weight Seal, 0.00133-Inch Step Height

Before teardown, it was decided to heat the inlet air to check out the hydrogen burning system. The maximum air inlet temperature attainable was 750°F. This problem was traced to a restriction in the hydrogen control valve, and a larger valve was ordered.

Inspection after teardown showed evidence of light rubbing between the OD of the top seal face and seal race. The possibility of a pressure roll on the top seal and/or race was considered. To check the pressure roll on the race, the assembly direction of the disk was reversed, placing the flight-weight race against the bottom seal and the flat disk surface against the top seal. When pressurized, very little face leakage could be detected from the top seal face, and indicators were set up to check for pressure roll on the top seal. Results showed a slight tilt in a converging direction which would tend to increase face leakage, and not to restrict leakage as observed. Air leakage on the bottom seal during this test was high. The conclusion was reached that the problem was not with the race. The rig was disassembled and the seals were inspected. A diverging (high at OD) face taper of 0.0008 inch was found on the upper seal and a converging 0.011-inch taper on the bottom seal. These parts had been stress relieved in the manufacturing process prior to final machining, but not after finish machining or surface plating. In addition, the surface opposite the sealing face on the bottom seal showed a "phonograph" pattern from a turning operation, while the same surface on the top seal showed a grinding pattern. This evidence showed the possibility that the previous heating to 750°F had relieved residual plating and/or machining stresses; however, it was not reasonable to believe that stress levels from plating and/or machining would be great enough to distort the bottom seal by 0.011 inch.

At this point, a decision was made to stress relieve the seals in the temperature range required for test; ie., above 1000°F. The seals were then soaked at 1100°F in air for 24 hours. This resulted in gross distortion of the bottom seal, including a saddle in the order of 0.025 inch and some loss of Metco 110 plating. In comparison, very little change occurred on the top seal. Since past experience had shown that operation could be obtained with a face saddle of 0.005 inch, it was decided to assemble the bottom seal with its 0.025-inch saddle and check for liftoff. Two builds were made, but results were negative.

An attempt was then made to straighten the bottom seal by over-bending and stress relieving. This resulted in a saddle of 0.075 inch. The seal was then used as a buffer to check the hydrogen burning system, after installing the larger hydrogen control valve, and then discarded.

A new bottom seal was ordered, and the original top seal was returned to the vendor to strip the plating, replate, and regrind. The vendor was instructed to slow heat the seals in air to 1000-1050°F, hold for one hour, and slow cool after plating but before grinding the stepped face. Instructions were also given for the vendor to use the same machining process on all major transverse faces.

In the interim, the AISI 4140 disk (Figure 4, Item 8) was shipped by NASA to a plating source for application of flame-spray plating to the top and bottom sealing surfaces. The disk was returned after plating and subsequently ground. As received from the vendor, the plate thickness on one surface was approximately 0.004 inch and 0.012 inch on the opposite surface. In order to clean up the thinly-plated surface, some of the plating was removed to base metal (see Figure 53). The heavily-plated surface presented no problem (see Figure 54). Visual examination of the plating after grinding suggested a high degree of localized porosity. Judging from visual inspection of grinding results, particularly at the sharp OD edges where chipping of plating would be expected as a result of grinding, the bond strength appeared to be good.

The new bottom seal and reworked top seal were finished and received by 26 September 1969. Three builds were then made. The first two builds were made using the newly-plated disk and the third was made with the flight-weight, wafer-type seal race and A286 disk. Hydrostatic support was achieved on all three builds; however, metal pickup occurred while rotating the disk at very low rpm after the third build.

The pickup was from the flight-weight seal race wafer, which was not plated and was found to be out of flat. The wafer was flat lapped under load while assembled on the air bearing disk, and the rig was reassembled, pressurized to 170-180 psig, and run at approximately 100 rpm for 15 minutes with no difficulties.

A static leakage test was conducted with results as shown on Figure 55. Leakage shown on this curve is total system leakage. This includes the top and bottom seals and piston rings, plus leakage through four ring flanges and approximately sixty-five pipe connections between the flow-measuring section and the test rig. The sudden change in slope on the curve at inlet pressures above 140 psig represents increased joint leakage, particularly the flanges, as detected by physical observations.

C. Room Temperature Dynamic Tests, Flight-Weight Seal

Two room temperature dynamic tests were conducted as shown below:

Test No.	Seal Inlet		RPM	Velocity* (Ft/Sec)	Time (Hours)
	Pressure (PSIG)	Temp. (°F)			
1	175	RT	0 to 2000	0 to 197	0.25
1	175	RT	2000 to 2890	197 to 285	0.91
2	175	RT	0 to 2000	0 to 197	0.05
2	175	RT	2000 to 4000	197 to 394	0.35
2	175	RT	4000 to 4086	394 to 403	2.05

*At seal balance piston diameter

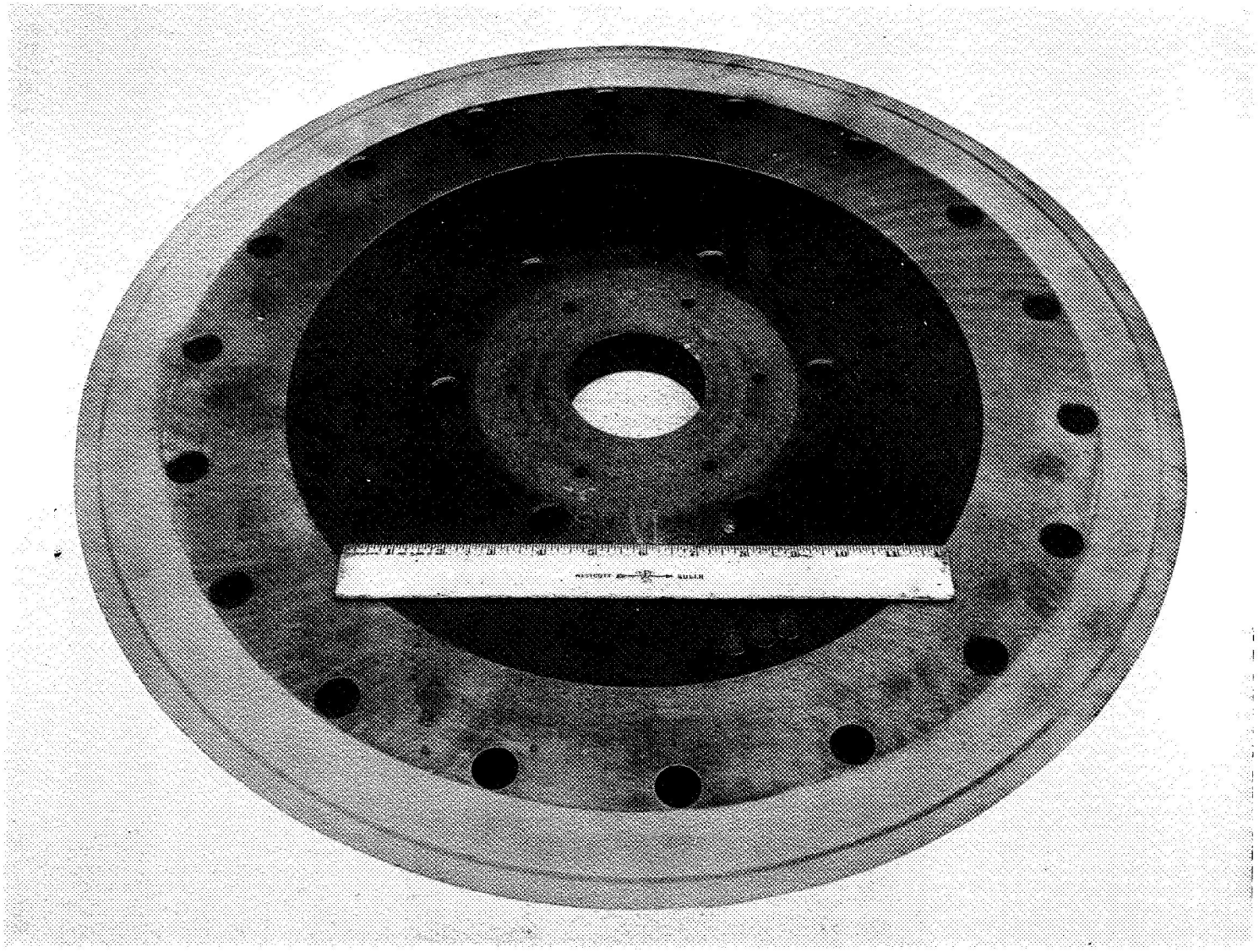

Figure 53. 4140 Disk, Bottom, with Flame-Sprayed Plating

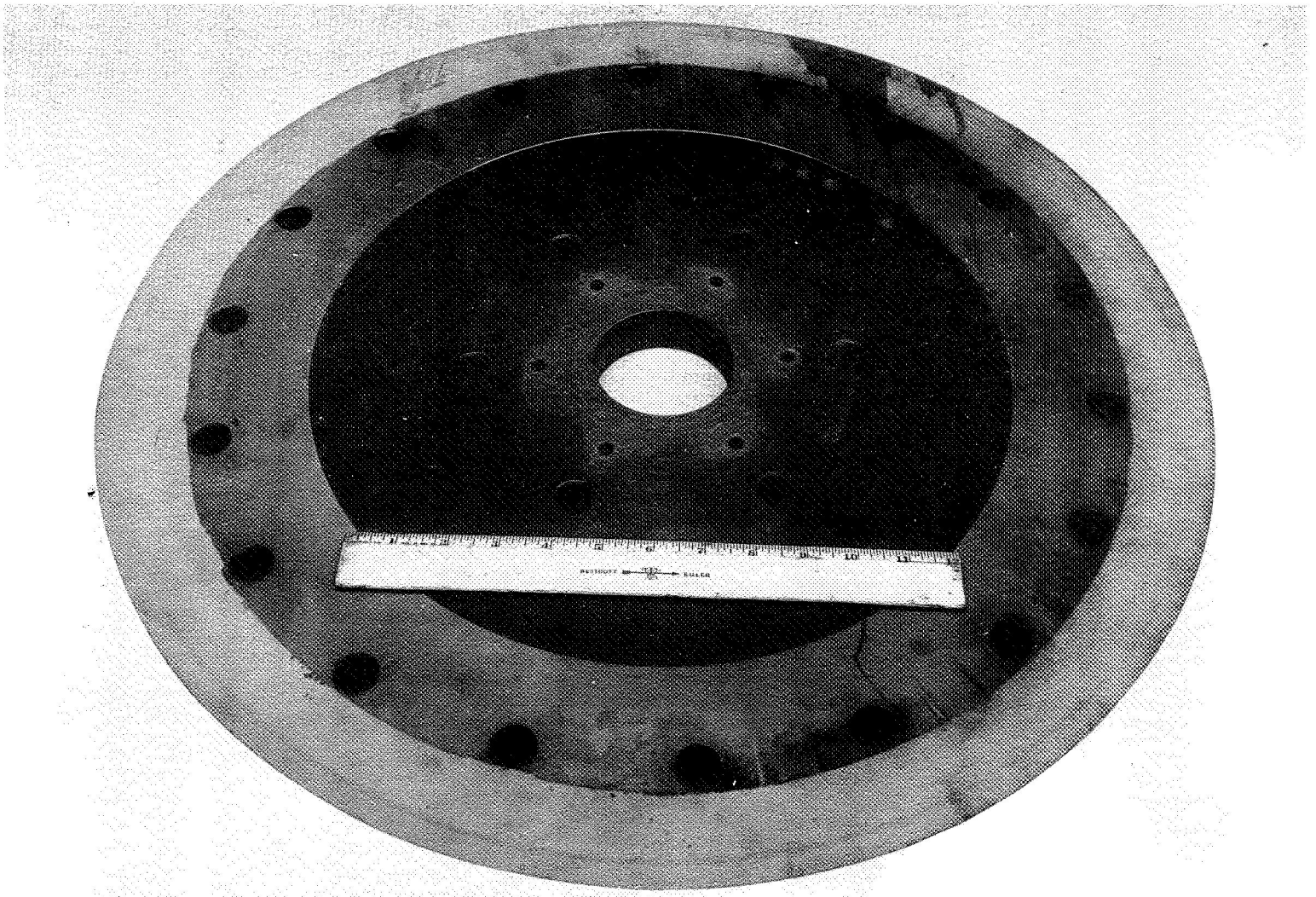

Figure 54. 4140 Disk, Top, with Flame-Sprayed Plating

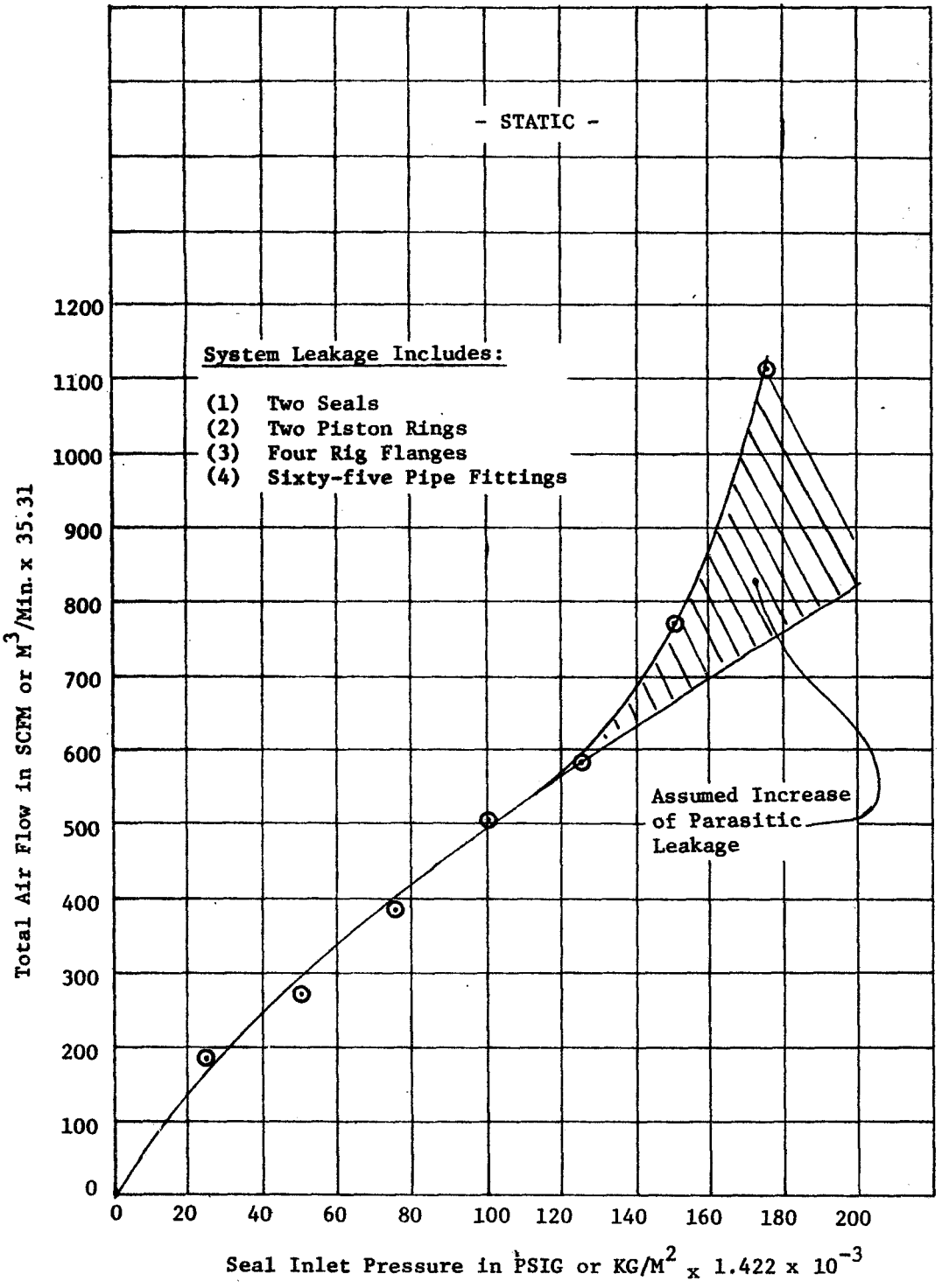

Figure 55. Flight-Weight Seal and System Leakage Vs. ΔP

All testing was done with an inlet pressure of 175 psig. Duration of the first test was 1.16 hours, with a maximum disk speed of 2890 rpm. Coast-down time at the end of the test was in excess of 20 minutes. Total duration of the second test was 2.45 hours with 2.05 hours at a disk rpm between 4000 and 4086. Maximum rpm was 4160, equivalent to a surface velocity of 410 feet per second at the balance piston diameter.

No problems were experienced during the first test, or during powered operation of the second test; however, light rubs occurred on the top and bottom seals during shutdown after the second test. After cutting off the air supply to the drive turbine, the disk floated freely for approximately five minutes. When air was supplied to the turbine to retard disk rotation, the light rubs occurred. The cause for the rub was determined to be loss of clearance between the labyrinth tip on the OD of the flight-weight seal (Figure 7, Item 3) and the seal guide (Item 13). The loss of clearance was due to worn and loose pilot fits between Items 10, 11, 13, 14, and 15. There was no detectable difference between static and dynamic leakage rates at 175 psig inlet pressure during either test. Inspection after test showed burnish marks on both seal faces, but no damage. Some light strictions appearing on the face of the wafered seal race were burnished with a nearly dry lapping ring to remove any possible high ridges.

D. Hot Dynamic Tests

In order to reduce parasitic leakage experienced in the previous cold test, rework was done to the seal secondaries and all pipe fittings and flanges. The secondary balance piston diameters were polished to reduce piston ring friction, and the transverse sealing faces of the piston ring grooves in the seal bodies were hand stoned. To preclude the seal binding due to loss in clearance between the labyrinth tooth and the rig adapter, as experienced in the last test, shim stock was installed between the assembly bolts and bolt holes at six circumferential locations. Using the six tight-fitted bolts, eccentricity between the top and bottom seal balance diameters was reduced from ± 0.021 inch to ± 0.004 inch. The rig was reassembled and pressure checked. Wherever possible, leakage through flanges and pipe connectors was eliminated. Static leakage rates were then measured and recorded (see Figure 56). The total air leakage rate through the two seals and piston rings was 335 scfm at 175 psig inlet pressure.

During lightoff of the hydrogen-burning system, in preparation for hot testing, an extremely high pressure transient was developed, blowing out all the gaskets (wire) at the rig flanges. Inspection showed severe damage to the top seal, seal housing, and rig adapter (Figure 7, Items 3, 5, and 10). Damage to other test pieces was minor, requiring hand lapping only. The balance diameter on Item 5 was severly out of round, and the flanges at the sealing face between Items 5 and 10 were bowed between bolt holes and badly sprung. Items 5 and 10 were reworked by machining.

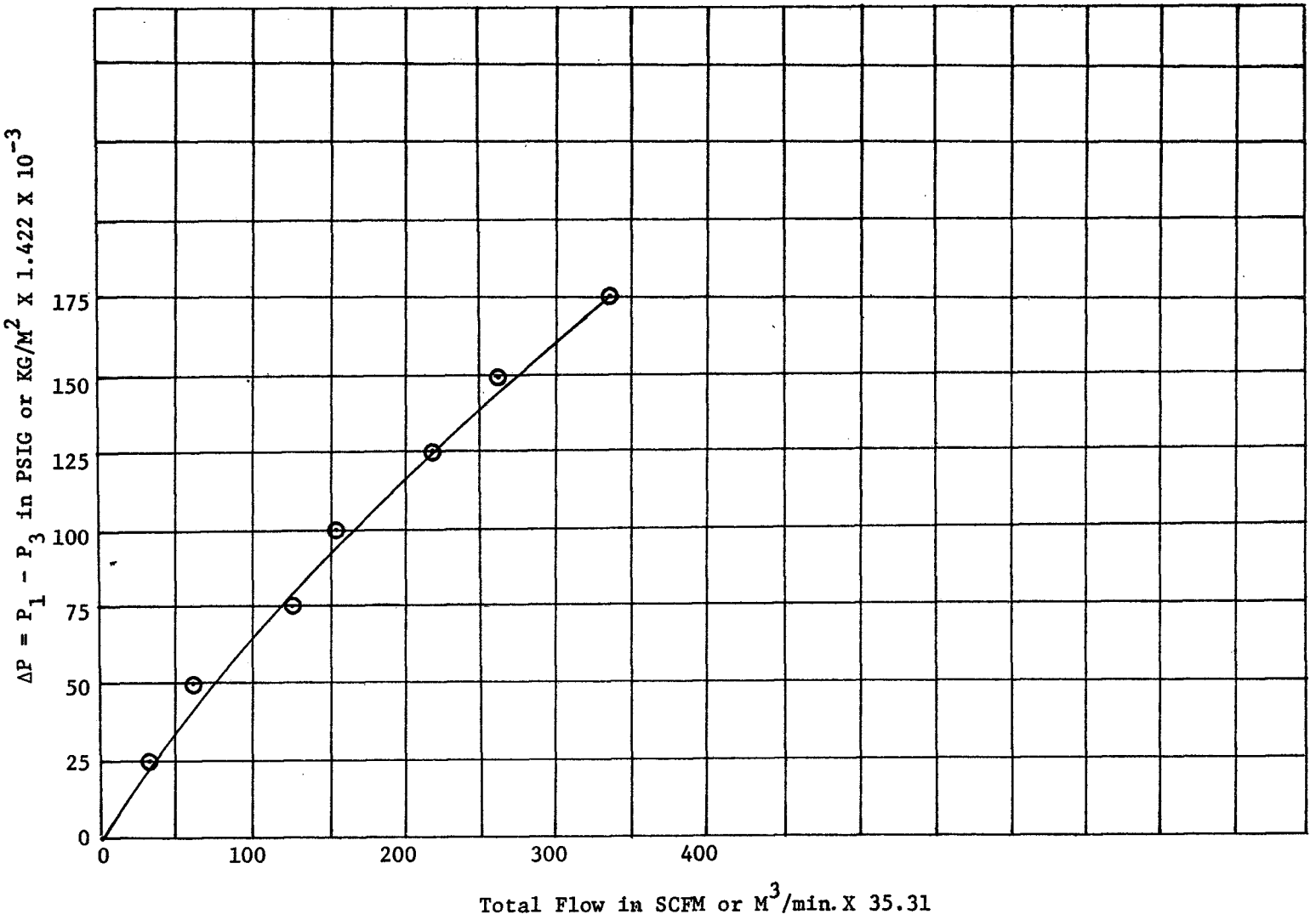

Figure 56. Measured Flow for Two Flight-Weight Seal Vs. Supply Pressure for 0.0006-Inch Step Height

Rework of Item 3 was also done but required removal of substantial material from the seal face so that proper pressure balance of the seal section was doubtful. Two new seals were manufactured, one of each (Items 3 and 20).

The rig was reassembled, using a new seal above the disk and the original seal below the disk. The disk floated freely in the pressure range of 55-175 psig at room temperature. The air heater was then fired, and inlet temperature reached 800°F in six minutes, and 950°F approximately twenty-five minutes later. Approximately forty minutes later, with air temperature at 965°F, air pressure suddenly dropped from 140 to 30 psig, and temperature dropped to 525°F.

Inspection after teardown showed that the 300-series stainless steel coil springs (Figure 7, Item 16) had yielded under the static weight of the disk (Item 1) at temperature. This allowed the disk to drop down approximately 0.20 inch and caused the piston ring (Item 4) in the top seal to slide out of the balance piston diameter in Item 5. It had also been observed that while air temperature was increasing (before the springs yielded), so were seal leakage rates. Since volume flow rate should decrease with increasing air inlet temperature if seal face geometry is constant, a geometric change was implied. Measurement of seal face contours showed that both seals had developed a converging taper (high at the ID) of the following magnitude (see Figure 2, Lines 1 and 2):

Item	Taper Milli-Radians
New Top Seal	1.1
Original Bottom Seal	5.3

The distorted seal face geometry, particularly of the bottom seal, accounts for the increased seal leakage rate with temperature increase.

New Inconel X coil springs (Figure 7, Item 16) were procured, and the rig was reassembled with the new springs and a new bottom seal to replace the original distorted part. Air inlet temperature was brought up to approximately 820°F. The air leakage rate again increased with temperature increase, with the high flow rate limiting any further increase in air temperature. The rig was disassembled, and the seal faces were again measured. No change in face taper could be detected on the top seal. The bottom seal, however, had developed a 14.8-milli-radian taper (see Figure 57, Line 3) high at the ID. The high air leakage rate was attributed to this cause. Since both the original and the new bottom seals now had distorted faces, but the original bottom seal taper was less than the taper on the new seal (5.3 and 14.8 milli-radians, respectively), it was decided to rebuild and attempt a run with the original seal.

Line 1 - New Top Seal after Heating to 960°F and 820°F

Line 2 - Original Bottom Seal After Heating to 960°F

Line 3 - New Bottom Seal after Heating to 820°F

Line 4 - New Top Seal after Heating to 1010°F

Line 5 - Original Bottom Seal after Heating to 1010°F

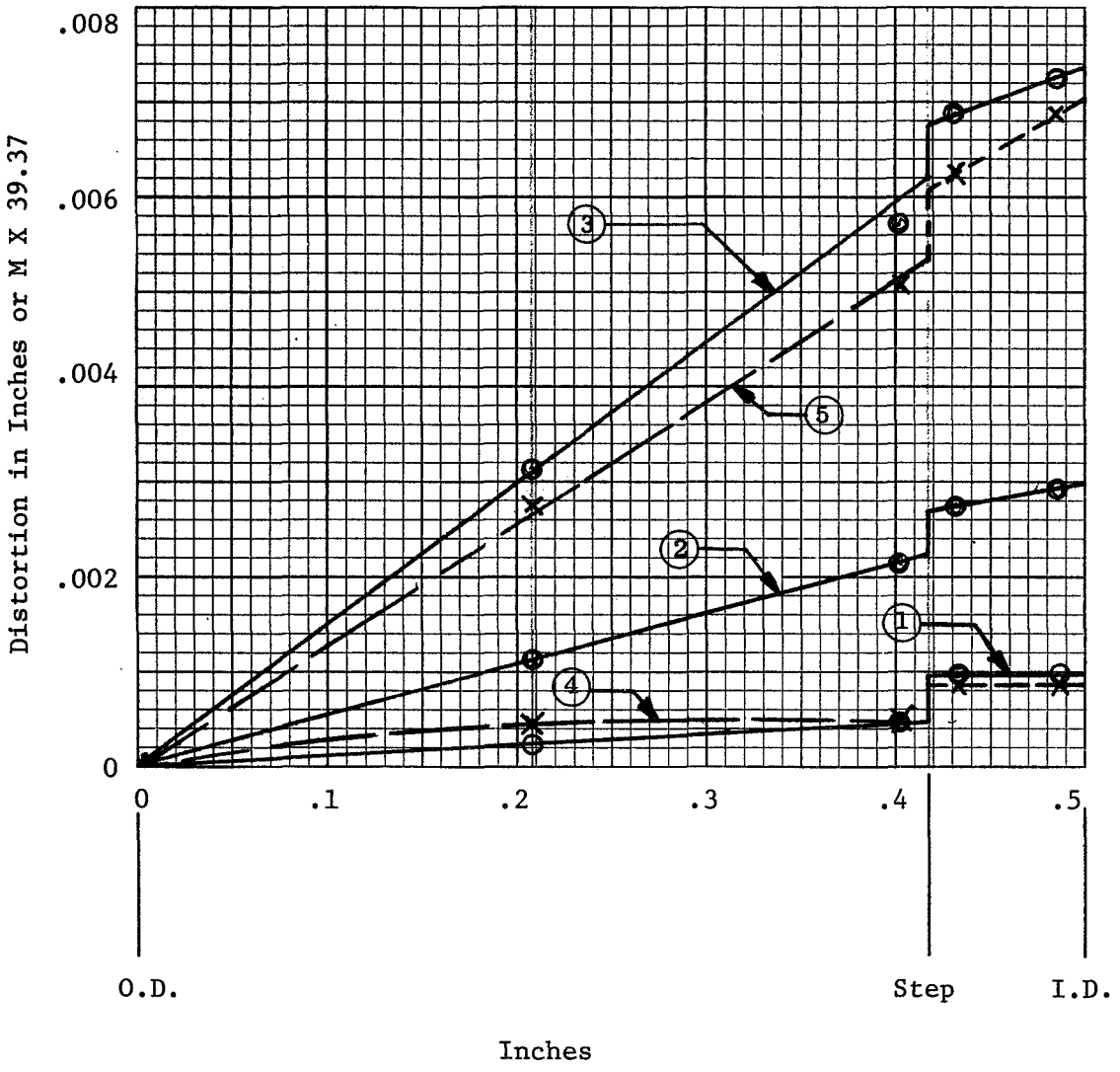

Figure 57. Thermal Distortion of Flight-Weight Seals

To compensate for the expected increase in leakage rate due to the converging seal face taper on the bottom seal, the hydrogen flow control orifice area was increased. The rig was rebuilt and system static leakage rate was measured. The results are shown on Figure 58. Total leakage rate, at 158 psig inlet pressure and room temperature for two seals and piston rings, was 833 scfm. Flow rate was off scale on the flow-measuring equipment at higher pressures.

The following hot dynamic test was then conducted:

Flight-Weight Seal Hot Dynamic Test			
Inlet Press. (PSIG)	Inlet Temp. (°F)	Disk (RPM)	Time (Minutes)
70	RT/710	0	2
100	710/806	0	20
145	806/864	0	8
160	864/1010	0	35
168	1010	0/1820	10

After reaching 1000°F air inlet temperature, the disk speed was brought up to approximately 1400 rpm. At this point, disk drag increased and speed dropped to approximately 600 rpm. Additional airflow was supplied to the air turbine drive; disk drag apparently decreased; and, speed was brought up to 1820 rpm. After a short time at this speed (estimated at approximately one minute), disk drag again increased, gradually dropping rpm. Turbine air supply was increased with no apparent effect, and the rig was secured.

Examination of parts showed the following:

a) Three rubs of varying relative magnitude appeared on the top seal face (see Figure 59 and Figure 60, Areas 1, 4, and 5). The lightest and heaviest rubs (Areas 4 and 1, respectively) were accompanied by loss of plating overspray on the face below and contiguous to the inside radius of the face step. Plating was missing at the same radial location in Areas 2 and 3.

b) Face contour of the top seal was measured at four equally-spaced circumferential locations (not at rub areas), and no change was detectable (see Figure 57, Line 4).

c) A uniform 360° rub appeared on the face of the wafer-type floating seal race (see Figures 61 and 62).

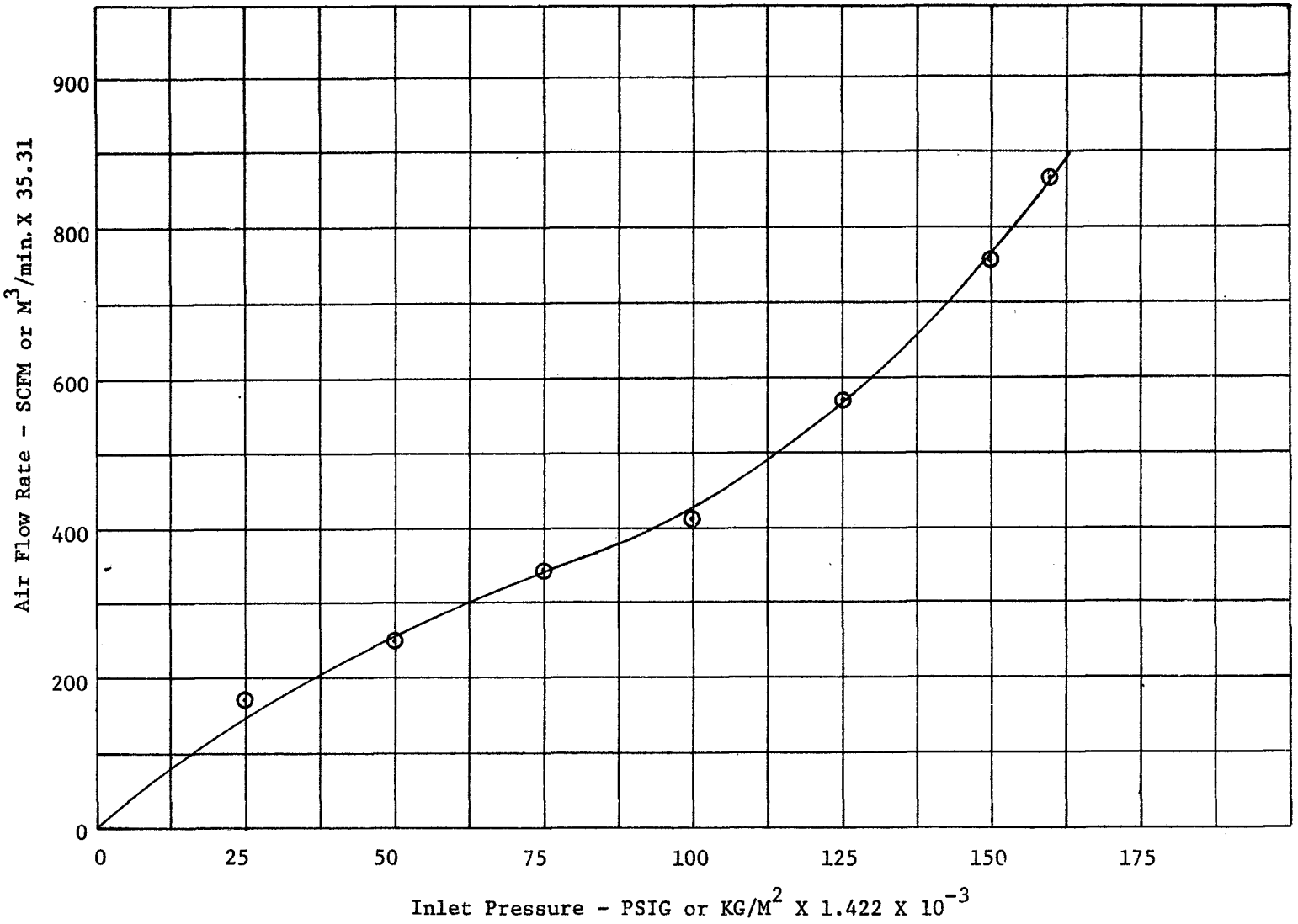

Figure 58. Flight-Weight Seal Assembly Static Leakage at Room Temperature, Two Seals and Two Piston Rings

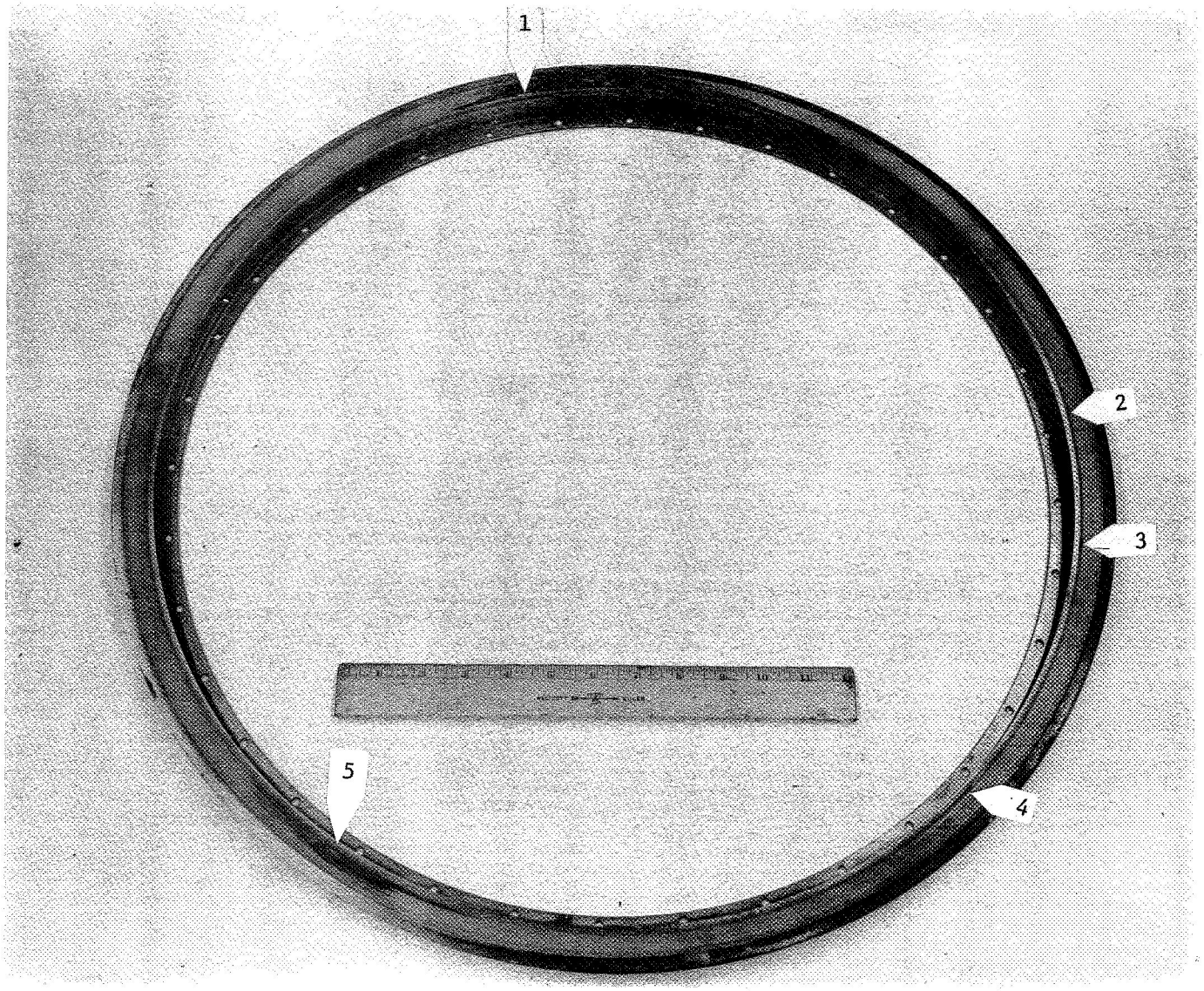

Figure 59. Flight-Weight Top Seal After Hot Dynamic Test

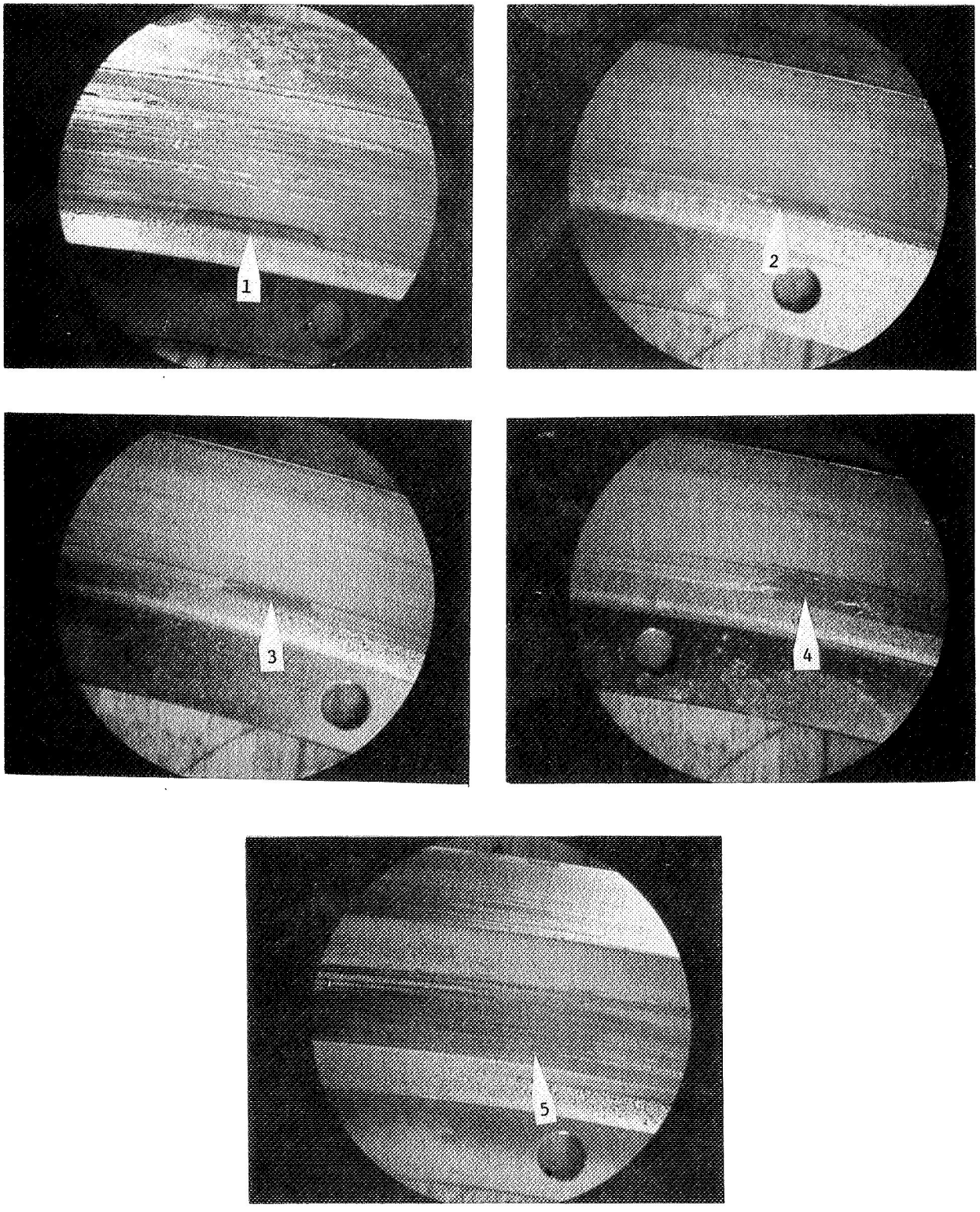

Figure 60. Flight-Weight Top Seal After Hot Dynamic Test Plating Flaked Off

Figure 61. Flight-Weight Seal Race Showing Rubbed Area After Hot Dynamic Test (C70030635)

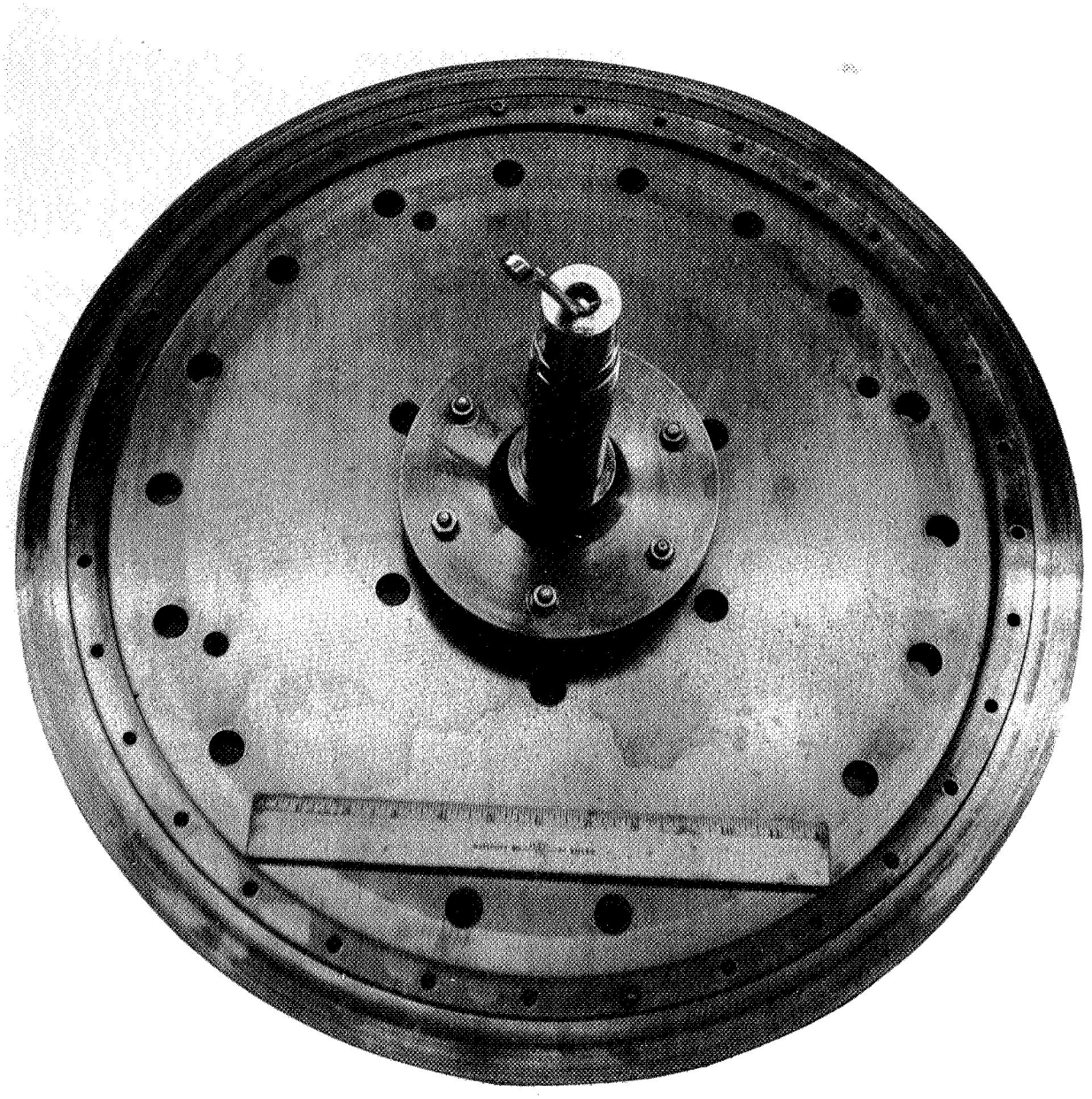

Figure 62. Flight-Weight Seal Race and Disk (Top) After Hot Dynamic Test (C70030630)

d) The convergence of the taper on the bottom seal face had increased from 5.3 to 12.8 milli-radians (Figure 57, Line 5).

e) No rubs occurred on the bottom seal (see Figure 63).

f) No rubbing occurred on the bottom surface of the air bearing disk (see Figure 64).

Several theories, including bending under disk weight and machining and/or plating stress relief, were pursued in an effort to determine the cause of the distortion to the bottom seals. The calculated stress due to bending moment from the disk weight was approximately 500 psi, which is not in the order of magnitude to cause permanent deformation. Distortion, due to machining stress relief and/or plating stress relief, was a possibility, based on past experience; however, all three seals tested were processed and heat treated in identical manners, including stress relief after plating, but only the two bottom seals became severely distorted.

The above fact pointed to the possibility of a thermal interference between the bottom seal (Figure 7, Item 20) and the balance piston diameter (Figure 7, Item 14). This appeared reasonably possible because of the extremely rapid air temperature response (room temperature to 710°F in 1-2 minutes) with the hydrogen-burning system, the large mass and heat sink of Item 14, and small mass and poor heat sink of the seal (Item 20).

In order to evaluate the probability of distortion due to thermal interference, the steady state temperatures of the balance diameter were calculated and are included in Appendix I.

The steady state temperature of the flight-weight seal (Figure 7, Item 20) is estimated using measured air temperatures from test as follows:

	Air Temperature, °F				
Lapsed Time (Minutes)	Seal Upstream			Seal Downstream	Δt
	No. 1	No. 2	Avg.		
2	710	555	633	386	247
22	806	648	727	540	187
30	864	795	830	792	38
65	1000	904	952	918	34
75	1010	939	975	932	43

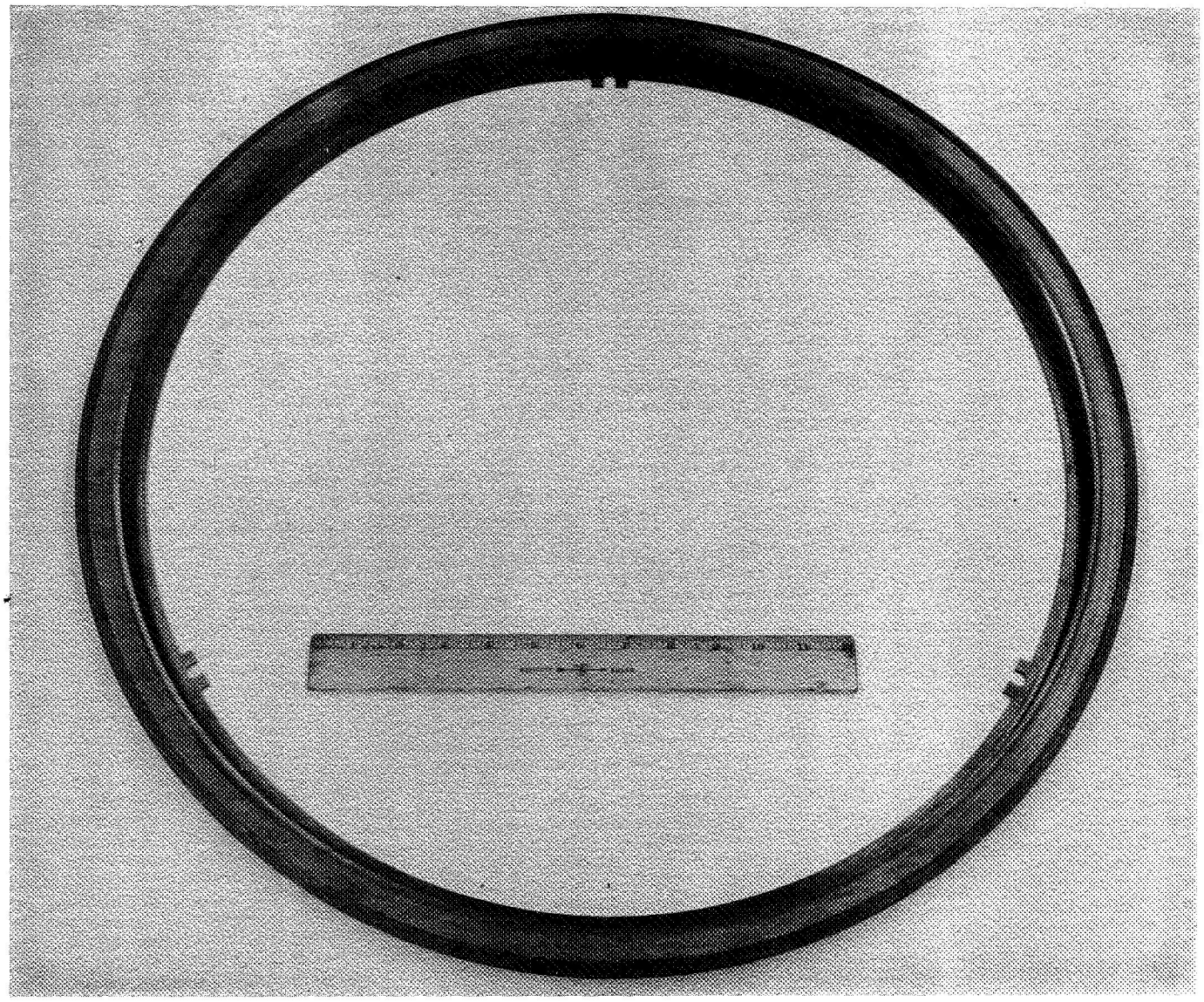

Figure 63. Flight-Weight Bottom Seal After Hot Dynamic Test (C70030638)

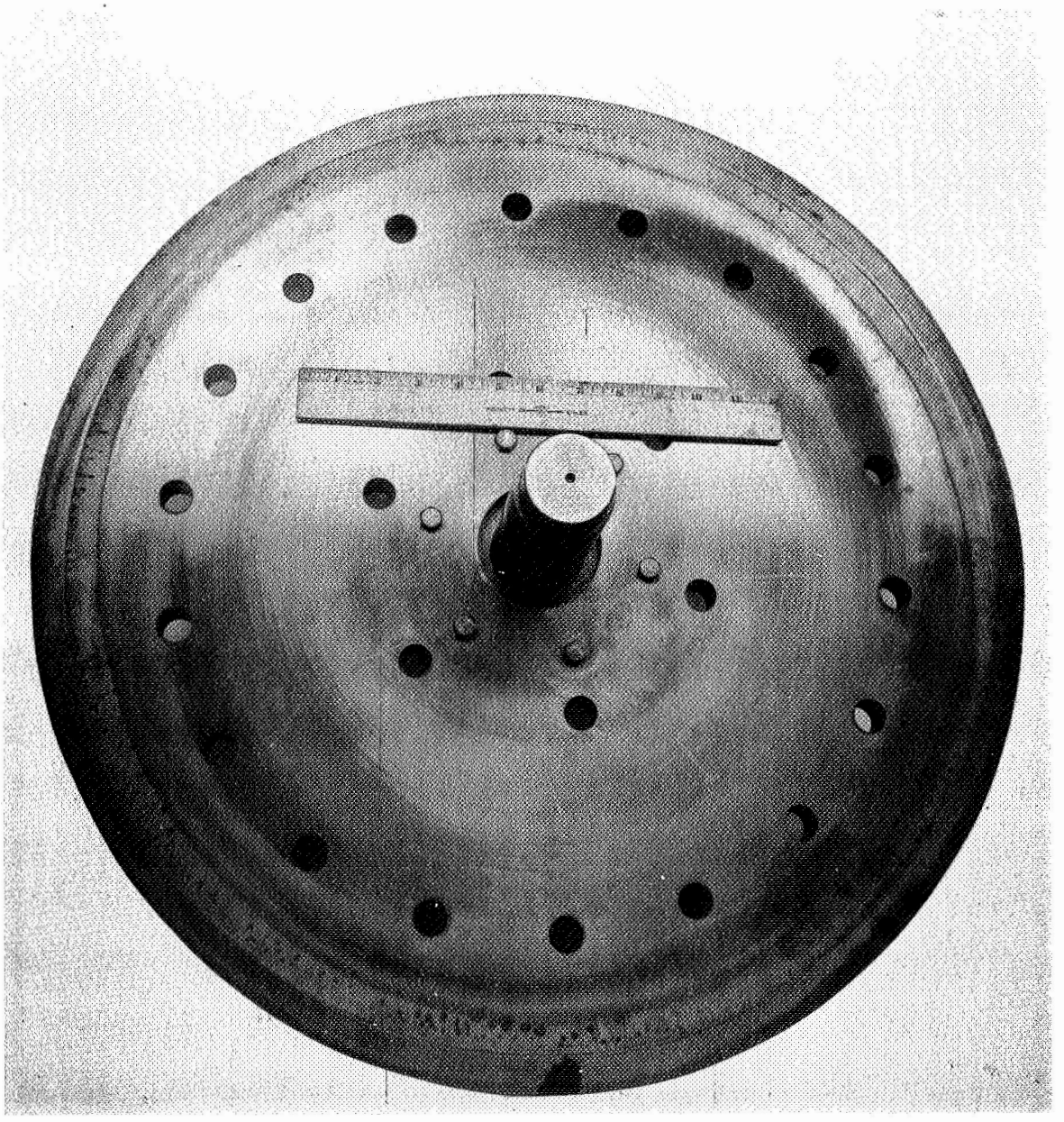

Figure 64. Flight-Weight Disk Bottom After Hot Dynamic Test

With air inlet temperature at 1000°F (average), the Δt from upstream to downstream is approximately 40°F. Since the seal has no heat sink except the surrounding air (with the possible exception of the disk), the seal temperature will be between upstream and downstream temperature. If the average temperature is used, the seal temperature will be:

$$t_s = 1000 - \frac{40}{2} = 980°F$$

Estimate the thermal growth of the seal and adapter:

Using the results of steady state temperatures from Case 2, assume the mean temperature of the adapter is the average of t_2 and t_7:

$$t_A = \frac{t_2 + t_7}{2} = \frac{801 + 588}{2} = 694.5°F$$

Calculate the expansion of the mean radius of the adapter, assuming the mass is concentrated at the mean diameter at which point $t = t_A$:

$$e_A = \alpha D_M (t_A - T_o)$$

$$= 9.0 \times 10^{-6} \frac{\text{inch}}{\text{inch °F}} \times \frac{22.564 + 31.23}{2} \text{ inch } (694.5 - 70)°F$$

$$= 0.1510 \text{ inch}$$

Calculate the expansion of the flight-weight seal using the estimated temperature of 980°F:

$$e_s = 9.4 \times 10^{-6} \times 22.564 \ (980 - 70)$$

$$= 0.1950 \text{ inch}$$

Since the initial clearance between the seal and balance diameter was 0.022 inch (diametral), the steady state clearance with inlet temperature at 1000°F is as follows:

$$C = 0.022 + e_A - e_s$$

$$= 0.022 + 0.151 - 0.195$$

$$= -0.022 \text{ inch (interference)}$$

This result, of course, is only an extimate which will change with changing parameters such as h_8, as shown in Appendix I.

The above calculations are for steady state only. Results would be much worse during transients. Comparing the seal weight of 7.1 pounds

to the adapter weight of 95 pounds, it can be seen that the heating rate of the seal will be at least 13.4 times the heating rate of the adapter. In addition, the adapter has a small heat source in comparison to its overall weight and a large heat sink, whereas the seal has a comparatively small heat sink and a heat source covering nearly its entire outside surfaces. It is, therefore, accurate to assume that the interference between the seal and adapter is worse during a transient increase in temperature than during a steady state condition.

The above results were corroborated by closer inspection of the bottom seals, revealing the following:

a. The diameter of the seal at the piston ring groove had yielded 0.023 inch undersize on both bottom flight-weight seals.

b. The balance diameter on the rig adapter had hard axial score marks at the regularly spaced grinding peaks, 360° around the circumference (see Figure 65, "Bottom Seal"). With the marks about the entire circumference, loss of clearance is indicated (not face drag), since face drag would pivot the seal about the rotation lock pin (Figure 7, Item 19) and cause a touch at one point only.

There was also evidence of thermal interference between the top seal and the balance diameter. Figure 65, "Top Seal," shows the same pattern as described above for the bottom seal balance diameter, except that the marking does not penetrate as deeply into the metal surface. The strength of this evidence suffers somewhat, because the top seal was not locked against rotation in the hot dynamic test and, therefore, could have been marked about the entire circumference as a result of seal rotation. The marks, however, run in an axial direction, not circumferentially, as would be caused by seal rotation. No evidence could be found to suggest rotation of the seal. The evidence strongly supports the probability of thermal interference at the time the rubs occurred, because piston ring friction alone probably could not restrain the seal from rotating from torque generated during a rub. Thermal interference could.

Additional evidence to support the possibility of thermal interference on the top seal is the small clearance between the seal and the balance diameter. Clearance after test ranged from 0.013 to 0.024 inch, diametrally. A cold clearance of 0.013 inch would allow a ΔT of approximately 64°F. This temperature variation would be possible due to small adjustments in hydrogen control pressure or changes in seal leakage rates, both of which occurred during operation. Inspection also showed a rub mark encompassing approximately 80° circumferentially on the ID of the "Seal Guide" (Figure 7, Item 13). The mark was opposite the top labyrinth tooth on the OD of the disk (Figure 7, Item 1), implying a rub between the tooth and the guide. Diametral cold clearance in this area is 0.061 inch. The disk-shaft, ball-bearing-outer-race clearance to the rig was

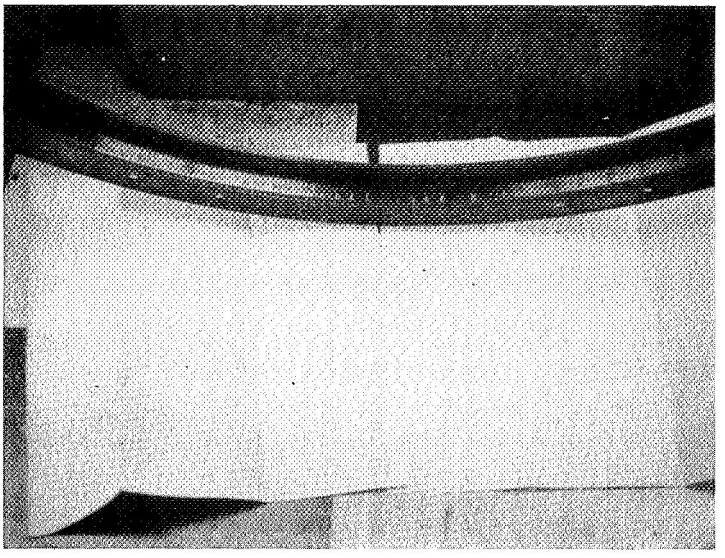

Top Seal

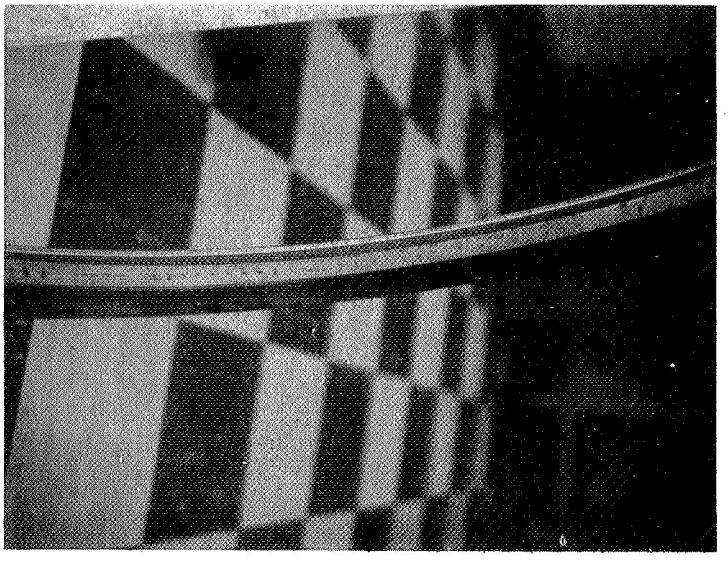

Bottom Seal

Figure 65. Flight-Weight Seal Balance Diameters After Hot Test

0.012 inch, to allow the disk to rotate on its mass center. The tooth clearance could then be 0.049 inch, less eccentricities from loose fitting pilots and thermals.

It is conceivable that a rub-induced moment or vibration on the disk, or small particles of loosened metal injested in the hydrostatic air film, may have contributed to or caused the seal rub.

The following is concluded:

a. Deformation of the bottom seal was caused by thermal interference between the seal and balance diameter.

b. Deformation of the bottom seal was a main contributor to the increasing system air leakage rate with temperature increase.

c. The rub on the top seal may have been caused by any one or a combination of the following:

    1. Thermally-induced interference between the seal and the balance diameter

    2. Interference between the rotating disk and the "seal guide" rig adapter

    3. Ingestion of loosened plating into the hydrostatic air film at the seal face

SECTION VII

CONCLUSIONS

Conclusions concerning the use of hydrostatic/hydrodynamic-type compressor end seals must be made within the framework of their application in gas turbines, when compared with the conventional design practice of labyrinth seal usage. The hydrostatic step design was able to meet the program goal of 20 to 1 reduction in seal leakage, when compared to a labyrinth seal design; however, on the other points, such as reliability, a negative conclusion is evident. Further development work will be necessary before this type of seal approaches the reliability of labyrinth-type seals, since the failure mode (when face geometry is altered by rubs or thermal warping) is disastrous. On the other hand, the operation of this seal at 600 ft/sec 1000°F and 170 psi is encouraging enough to warrent further consideration. The biggest problems in seal operation were encountered in thermal distortion of the test rig, distortion of the parts themselves due to improperly-relieved stresses, and the problem of instantaneous rubbing at high speeds. The analytical basis for hydrostatic steps is well known, and calculations based on isothermal laminar assumptions were able to predict film thickness and flow rates except when these conditions were not present. When film thicknesses less than 0.001 inch existed, laminar flow was present. At film thicknesses over 0.001 inch, flow could be calculated if sonic velocity with a suitable nozzel coefficient was assumed.

Some of the separate conclusions from this program are listed below:

1. The stepped, hydrostatic seal (-131 or Flight-Weight design) has less flow for a given film thickness than the inherently-compensated type (the -333 seal), because of the added parasitic leakage feature of inherent compensation.

2. A hard facing of one or both parts is required to prevent damage during instantaneous high-speed rubs. Hot or cold dynamic operation with uncoated metal was not achieved. It was established that chrome carbide and titanium and aluminum oxide coatings worked successfully.

3. Operation of the step-type design was demonstrated at 750°F, 600 ft/sec, and 170 psi. Failures of the seal were due to causes such as thermal distortion of the rig, removal of plating, and failure of support equipment.

4. The temperature, speed, and pressure level can be extended beyond these limits if a suitable plating material can be found.

5. The hydrostatic step face has the required film stiffness to follow the one per rev shaft runout normally experienced at 22 inches of diameter and appears stable at all operating conditions.

6. The CD847985 NASA-design, hydrodynamic, Raleigh step seal shows promise, since it is a balanced design and has a much less disastrous failure mode than the stepped type.

The following recommendations are made:

1. Further work should be done on the stepped-type device as a high-speed air thrust bearing.

2. Construction of a balanced, hydrodynamic seal (similar to the CD847985) should be investigated using carbon material for use up to 1000°F.

3. Concentricity for the seal body should be provided by means of radial splines, similar to those used on the balanced runner, instead of a diametral fit. This will improve the tolerance of concentricity.

4. Care should be taken that the seal body is thermally isolated from the rest of the equipment.

APPENDIX I

STEADY STATE TEMPERATURE GRADIENTS FOR THE SEAL AND HOUSING

Following is a 1:1 scale cross section of the rig adapter (Figure 7, Item 14):

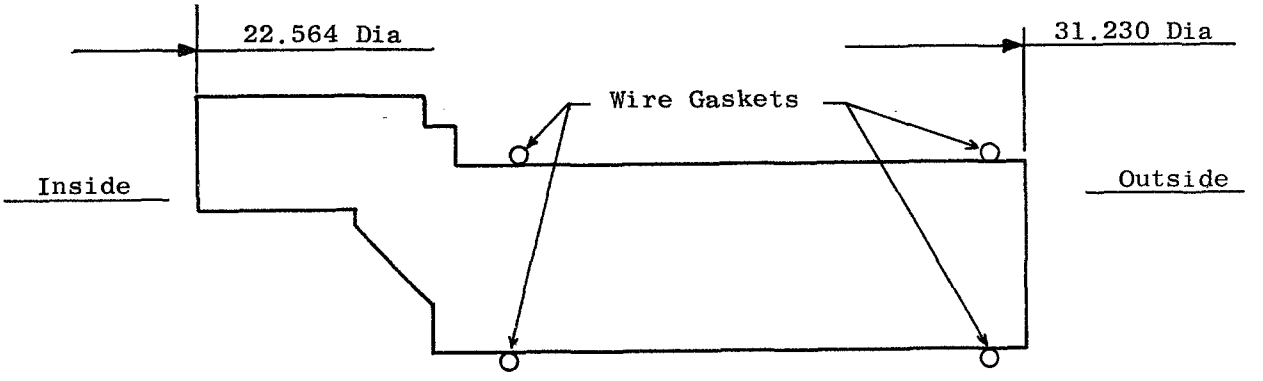

The cross section was projected as follows, to simplify calculations of heat flow area:

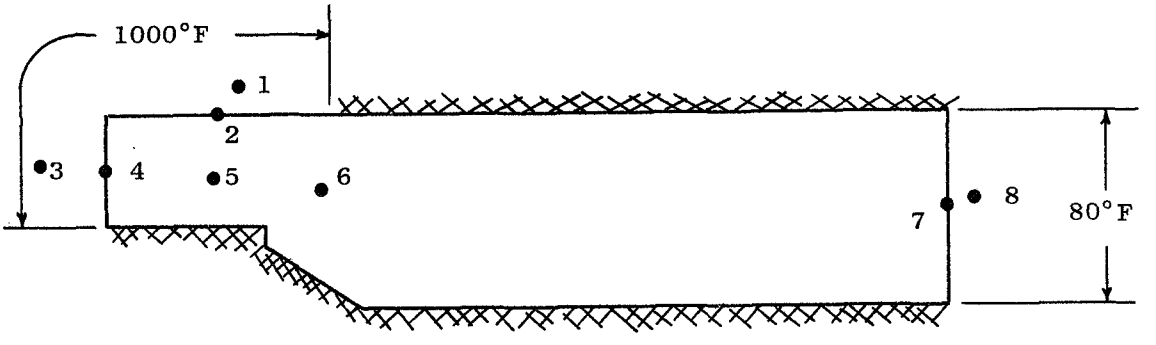

Assumptions:

$t_1 = 1000°F = t_3$

$t_8 = 80°F$

No heat transfer at cross-hatched areas, since an air gap of approximately 0.020 inch exists at these areas, and the mating adapters are subjected to the same Δt, inside to outside.

Following are the equations of heat flow:

$$Q_{1-2} = H_1 a_1 (t_1 - t_2) = \frac{1}{r_1} (t_1 - t_2)$$

$$Q_{2-5} = \frac{K a_{2-5}}{l_{2-5}} (t_2 - t_5) = \frac{1}{r_2} (t_2 - t_5)$$

$$Q_{3-4} = H_3 a_3 (t_3 - t_4) = \frac{1}{r_3} (t_3 - t_4)$$

$$Q_{4-5} = \frac{K a_{4-5}}{l_{4-5}} (t_4 - t_5) = \frac{1}{r_4} (t_4 - t_5)$$

$$Q_{5-6} = \frac{K a_{5-6}}{l_{5-6}} (t_5 - t_6) = \frac{1}{r_5} (t_5 - t_6)$$

$$Q_{6-7} = \frac{K a_{6-7}}{l_{6-7}} (t_6 - t_7) = \frac{1}{r_6} (t_6 - t_7)$$

$$Q_{7-8} = H_8 a_{7-8} (t_7 - t_8) = \frac{1}{r_7} (t_7 - t_8)$$

Assume for Case 1:

$$H_1 - H_3 = 20 \frac{\text{Btu}}{\text{hr ft}^2 \text{ °F}}$$

$$H_8 = 5 \frac{\text{Btu}}{\text{hr ft}^2 \text{ °F}}$$

$$K = 9.6 \frac{\text{Btu}}{\text{hr ft}^2 \text{ °F/ft}} \quad ; \quad \text{(300-series Stainless Steel)}$$

Circuit Analogy:

$t_k = t_3 = 1000°F$

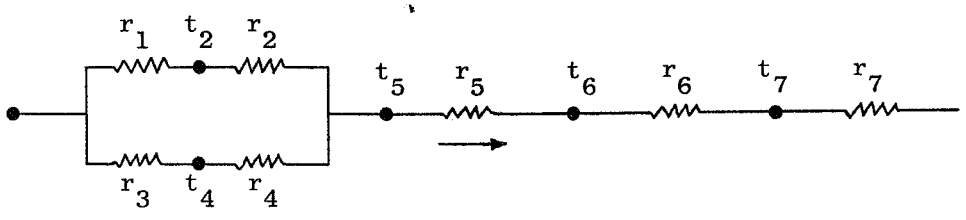

Heat flow areas:

$$a_1 = \frac{\pi}{4} \frac{(D_o^2 - D_i^2)}{144} = \frac{\pi}{4} \frac{\overline{(24.885^2 - 22.564^2)}}{144} = 0.589 \text{ ft}^2$$

$$a_{2-5} = A_1 = 0.589 \text{ ft}^2$$

$$a_3 = \frac{\pi}{144} d_3 w_3 = \frac{\pi}{144} (22.564) (0.6) = 0.2954 \text{ ft}^2$$

$$a_{4-5} = \frac{\pi}{144} d_{4-5} w_{4-5} = \frac{\pi}{144} (23.764) (0.6) = 0.3115 \text{ ft}^2$$

$$a_{5-6} = \frac{\pi}{144} d_{5-6} w_{5-6} = \frac{\pi}{144} (24.160) (0.7) = 0.3695 \text{ ft}^2$$

$$a_{6-7} = \frac{a_7 - a_6}{\ln \frac{a7}{a6}} = \frac{\pi(d_7 - d_6) w}{\ln \frac{d_7}{d_6}} = \frac{\pi}{144} \frac{(31.23 - 24.86) (1.0)}{\ln \frac{31.23}{24.86}} = 0.608 \text{ ft}^2$$

$$a_{7-8} = \frac{\pi}{144} (d_7) W_7 = \frac{\pi}{144} (31.23) (1.0) = 0.683 \text{ ft}^2$$

Length of heat flowpaths:

$$l_{2-5} = \frac{0.3}{12} = 0.025 \text{ ft}$$

$$l_{4-5} = \frac{0.6}{12} = 0.050 \text{ ft}$$

$$l_{5-6} = \frac{0.55}{12} = 0.0458 \text{ ft}$$

$$l_{6-7} = \frac{3.2}{12} = 0.267 \text{ ft}$$

Resistances:

$$r_1 = \frac{1}{(20)\ (0.589)} = 0.0849\ \frac{\text{hr}\ ^\circ\text{F}}{\text{Btu}}$$

$$r_2 = \frac{0.025}{(9.6)\ (0.589)} = 0.00443\ \frac{\text{hr}\ ^\circ\text{F}}{\text{Btu}}$$

$$r_3 = \frac{1}{(20)\ (0.2954)} = 0.1693\ \frac{\text{hr}\ ^\circ\text{F}}{\text{Btu}}$$

$$r_4 = \frac{0.05}{(9.6)\ (0.3115)} = 0.01673\ \frac{\text{hr}\ ^\circ\text{F}}{\text{Btu}}$$

$$r_5 = \frac{0.0458}{(9.6)\ (0.3695)} = 0.01292\ \frac{\text{hr}\ ^\circ\text{F}}{\text{Btu}}$$

$$r_6 = \frac{0.267}{(9.6)\ (0.608)} = 0.0458\ \frac{\text{hr}\ ^\circ\text{F}}{\text{Btu}}$$

$$r_7 = \frac{1}{(5)\ (0.683)} = 0.293\ \frac{\text{hr}\ ^\circ\text{F}}{\text{Btu}}$$

Total resistance:

$$r_T = \frac{(r_1 + r_2)\ (r_3 + r_4)}{(r_1 + r_2 + r_3 + r_4)} + r_5 + r_6 + r_7$$

$$= 0.41212\ \frac{\text{hr}\ ^\circ\text{F}}{\text{Btu}}$$

Total heat flow rate:

$$Q_T = \frac{\Delta t_T}{r_T} = \frac{t_1 - t_8}{r_T}$$

$$= \frac{(1000 - 80)}{0.41212} = 2234\ \text{btu/hr}$$

Temperature difference between nodes:

$$\Delta t = Qr$$

$$\Delta t_{1-5} = (2234)\ (0.0604) = 134.9°F$$

$$\Delta t_{5-6} = (2234)\ (0.01292) = 28.83°F$$

$$\Delta t_{6-7} = (2234)\ (0.0458) = 102.20°F$$

$$\Delta t_{7-8} = (2234)\ (0.293) = 654.0°F$$

$$Q_{1-5} + Q_{3-5} = 2234 \text{ Btu/hr}$$

$$r_{1-5} = r_1 + r_2 = 0.08933 \ \frac{\text{hr } °F}{\text{Btu}}$$

$$r_{3-5} = r_3 + r_4 = 0.18603 \ \frac{\text{hr } °F}{\text{Btu}}$$

$$Q_{1-5} = \frac{\Delta t_{1-5}}{r_{1-5}} = \frac{1000 - 865}{0.08933} = 1512 \text{ Btu/hr}$$

$$Q_{3-5} = \frac{\Delta t_{3-5}}{r_{3-5}} = \frac{1000 - 865}{0.18603} = 725 \text{ Btu/hr}$$

$$\Delta t_{1-2} = Q_{1-2}\ r_1 = 1512\ (0.0849) = 128.3°F$$

$$\Delta t_{2-5} = Q_{2-5}\ r_2 = 1512\ (0.00443) = 6.7°F$$

$$\Delta t_{3-4} = Q_{3-4}\ r_3 = 725\ (0.1693) = 122.8°F$$

$$\Delta t_{4-5} = Q_{4-5}\ r_4 = 725\ (0.01673) = 12.2°F$$

Case 2, $h_8 = 10$ Btu/hr ft^2 °F:

$$r_7 = 0.1465 \ \frac{\text{hr } °F}{\text{Btu}}$$

$$r_T = 0.26562 \ \frac{\text{hr } °F}{\text{Btu}}$$

$$Q_T = \frac{920}{0.26562} = 3462 \text{ Btu/hr}$$

$$\Delta t_{1-5} = (3462)\ (0.0604) = 209.3°F$$

$$\Delta t_{5-6} = (3462)\ (0.01292) = 44.8°F$$

$$\Delta t_{6-7} = (3462)\ (0.0458) = 158.7°F$$

$$\Delta t_{7-8} = (3462)\ (0.1465) = 507.5°F$$

$$Q_{1-5} = \frac{209.3}{0.08933} = 2341 \text{ Btu/hr}$$

$$Q_{3-5} = \frac{209.3}{0.18603} = 1121 \text{ Btu/hr}$$

$$\Delta t_{1-2} = (2341)\ (0.0849) = 198.9°F$$

$$\Delta t_{2-5} = (2341)\ (0.00443) = 10.4°F$$

$$\Delta t_{3-4} = (1121)\ (0.1693) = 190.4°F$$

Summary of rig adapter steady state temperature:

	Case 1 $h_8 = 5$ (°F)	Case 2 $h_8 = 10$ (°F)
t8	80	80
t7	734	588
t6	836	746
t5	865	791
t4	877	810
t3	1000	1000
t2	872	801
t1	1000	1000

APPENDIX II

SYMBOLS

a	Heat transfer area, ft^2
b	Moment arm, inches
A	Pressure area, $in.^2$
A_i	Face area along inlet flowpath, $in.^2$
A_o	Face area along outlet flowpath, $in.^2$
A_p	Pressure seating area, $in.^2$
A_s	Balance piston seating area, $in.^2$
c	Clearance, in.
C	Cosine θ
C_f	Coefficient of friction
CG	Center of gravity
d	Diameter, ft
D	Diameter, in.
D_B	Balance piston diameter (bore of seal housing), in.
D_g	Diameter at CG
D_i	Mean diameter of inlet flowpath, in.
D_M	Mean diameter of seal face, in.
D_o	Mean diameter of outlet flowpath, in.
e_A	Thermal expansion of adapter, in.
e_R	Thermal expansion of seal, in.
E	Young's Modulus, $pounds/in.^2$
E_R	Radial eccentricity, in.
f	Actual gas pressure forces, pounds
F	Equivalent gas pressure forces at CG
F_c	Centrifugal force, pounds
F_I	Inertia force, pounds
F_p	Pressure seating force, pounds
F_s	Pressure force to seat seal, pounds
F_u	Pressure force to unseat seal, pounds

ΔF	Net force, pounds
g	Acceleration due to gravity, in./sec^2
G	Ratio of centripetal force to per unit weight, dimensionless
h	Distance separating parallel plates
h_i	Film thickness at inlet to seal, in.
h_o	Film thickness at seal exit, in.
Δh	Step dimension on seal face, in.
H	Film heat transfer coefficient, Btu/hr ft^2 °F
I	Moment of inertia, in.^{4}
J	Pressure force, pounds/circumferential inch
k	Air film stiffness, pounds/in.
l	Length of heat flowpath, ft
L	Length of air flowpath, in.
L_i	Length of inlet air flowpath, in.
L_o	Length of outlet air flowpath, in.
m	Incremental area of cross section, in.^{2}
m_t	Total cross-sectional area, in.^{2}
M	Mass, pound sec^2/in.
M_o	Moment, inch-pound
ΣM_o	Sum of moments, inch-pounds
P	Standard atmosphere, pounds/in.^{2}
P_h	Hydrostatic pressure, pounds/in.^{2}
P_i	Pressure at inlet to seal face, pounds/in.^{2}, absolute
P_o	Pressure at exit of seal face, pounds/in.^{2}, absolute
P_s	Pressure at inlet to face step, pounds/in.^{2}, absolute
ΔP	Pressure difference, pounds/in.^{2}
ΔP_M	Manometer gauge readings, in.
q	Standard volume airflow rate
q_i	Standard volume airflow rate at inlet, in.^{3}/sec
q_o	Standard volume airflow rate at exit, in.^{3}/sec
Q	Heat flow rate, Btu/hr

r	Resistance to heat flow, hr °F/Btu
r_a	Face runout, 1/2 amplitude, in.
R	Radius, in.
s_c	Centrifugal inertial stress, pounds/in.^{2}
s_h	Hoop stress, pounds/in.^{2}
S	Sine θ
t	Temperature, °F
T	Absolute temperature, °R
T_i	Absolute temperature at seal inlet, °R
u	Absolute viscosity
u_i	Absolute viscosity of inlet air, pound sec/in.^{2}
W	Weight, pounds
W_T	Total weight, pounds
x	Distance in x-x plane, in.
x-x	Horizontal plane
$\bar{X}$	Composite CG in x-x plane
y	Distance in y-y plane, in.
y-y	Vertical plane
$\bar{Y}$	Composite CG in y-y plane
α	Mean coefficient of thermal expansion, in.in.°F
δ_w	Outward displacement, in.
δ_o	Inward displacement, in.
θ	Angle, radians
λ	Gas compressibility factor
ρ	Weight density, pounds/in.^{2}
σ_R	Radial strain, in.
ω	Angular velocity, radians/sec

DISTRIBUTION LIST

Addressee		Copies
1. NASA Headquarters Washington, D.C. 20546		
Attn.	N.F. Rekos (RAP)	1
	A.J. Evans (RAD)	1
	J. Maltz (RRM)	1
2. NASA-Lewis Research Center 21000 Brookpark Road Cleveland, Ohio 44135		
Attn.	A. Ginsburg, MS 5-3	1
	E.E. Bisson, MS 5-3	1
	R.L. Johnson, MS 23-2	1
	W.R. Loomis, MS 23-2	1
	L.P. Ludwig, MS 23-2	1
	M.A. Swikert, MS 23-2	1
	D.P. Townsend, MS 6-1	5
	C.H. Voit, MS 5-3	1
	M.J. Hartman, MS 5-9	1
	L. Schopen MS 77-3	1
	Report Control Office, MS 5-5	1
	Library, MS 60-3	1
	Technology Utilization Office, MS 3-19	1
	N.T. Manual, MS 501-3	1
3. NASA-Scientific and Technical Information Facility P.O. Box 33 College Park, Maryland 20740		
Attn:	NASA Representative	6
4. NASA Langley Research Center Langley Station Hampton, Virginia 23365		
Attn:	Mark R. Nichols	1

DISTRIBUTION LIST

Addressee	Copies
5. United States Air Force Wright-Patterson Air Force Base AF Systems Command USAF Wright-Patterson AFB, Ohio 45433	
Attn: AFAPL (APFL), K.L. Berkey and L. Debrohum	1
AFAPL (APTC), C. Simpson	1
APTP, I.J. Gershon	1
SEJDF, S. Prete	1
MANL, R. Adamezak	1
MANE, R. Headrick	1
MAAE, P. House	1
6. FAA Headquarters 800 Independence Avenue, S.W. Washington, D.C. 20553	
Attn: General J.C. Maxwell	1
F.B. Howard	1
7. U.S. Naval Air Material Center Aeronautical Engine Laboratory Philadelphia, Pennsylvania	
Attn: A.L. Lockwood	1
8. U.S. Naval Research Laboratory Washington, D.C.	
Attn: Charles Murphy	1
9. Department of the Navy Bureau of Naval Weapons Washington, D.C.	
Attn: A.D. Nehman, RAAE-3	1
C.C. Singletorry, RAPP-4	1
10. Department of the Navy Bureau of Ships Washington, D.C.	
Attn: Harry King, Code 634A	1
11. U.S. Navy Marine Engineering Laboratory Friction and Wear Division Annapolis, Maryland	
Attn: R.B. Snapp	1

DISTRIBUTION LIST

Addressee	Copies
12. U.S. Navy Underwater Weapons Research and Engineering Section Newport, R.I. 02840 Attn: Technical Library CS12(B566)	1
13. Department of the Army U.S. Army Aviation Material Labs Fort Eustis, Virginia 23604 Attn: John W. White, Chief Propulsion Division	1
14. AVCOM AMSAVEGTT Mart Building 405 South 12th Street St. Louis, Missouri 63100 Attn: E. England	1
15. Aerojet-General Corporation 20545 Center Ridge Road Cleveland, Ohio 44116 Attn: W.L. Snapp	1
16. Avco Corporation Lycoming Division Stratford, Conneticut Attn: R. Cuny	1
17. Baber-Nichols Engineering Co. 6235 West 55th Street Arvada, Colorado 80002 Attn: K.E. Nichols	1
18. Battelle Memorial Institute 505 King Avenue Columbus, Ohio 43203 Attn: C.M. Allen	1
19. Bendix Corporation Fisher Building Detroit, Michigan 48202 Attn: R.H. Isaacs	1

DISTRIBUTION LIST

Addressee	Copies
20. B.F. Goodrich Company Aerospace & Defense Products Div. Troy, Ohio Attn: L.S. Blalkowski	1
21. Boeing Aircraft Company 224 N. Wilkinson Dayton, Ohio 45402 Attn: H.W. Walker	1
W.K. Torson	1
J.D. Raisbeck	1
22. Borg-Warner Corporation Roy C. Ingersoll Research Center Wolf and Algonquin Roads Des Plaines, Illinois 60018	1
23. Carbon Products Division of Union Carbon Corporation 270 Park Avenue New York, New York 10017 Attn: J. Curran	1
24. Cartiseal Corporation 3515 West Touhy Lincolnwood, Illinois Attn: R. Voltik	1
25. Chicago Rawhide Mfg. Co. 1311 Elston Avenue Chicago, Illinois Attn: R. Blair	1
26. Clevite Corporation Cleveland Graphite Bronze Div. 17000 St. Clair Avenue Cleveland, Ohio 44110 Attn: Thomas H. Koenig	1
27. Continential Aviation & Engrg. 12700 Kercheval Detroit, Michigan Attn: A.J. Follman	1

DISTRIBUTION LIST

Addressee	Copies
28. Crane Packing Company 6400 Oakton Street Morton Grove, Illinois 60053 Attn: Harry Tankus	1
29. Douglas-McDonnell Corp. Suite 620 333 W. First Street Dayton, Ohio 45402 Attn: R.G. Donmayer	1
30. Durametallic Corporation Kalamazoo, Michigan Attn: H. Hummer	1
31. Fairchild-Stratos-Western 1800 Rosecrans Ave. Manhatten, California 90266 Attn: Alex D'Angio	
32. Fairchild-Hiller Corporation Republic Aviation Division Farmingdale, Long Island New York 11735 Attn: C. Collis	1
33. Franklin Institute Laboratories 20th & Parkway Philadelphia, Pennsylvania Attn: J.V. Carlson	1
34. Garlock, Inc. Palmyra, New York 14522 Attn: A. Silver	1
35. Garrett Corporation Air Research Mfg. Div. 9851-9951 Scpulvelda Blvd. Los Angeles, California 90009 Attn: A. Silver	1

DISTRIBUTION LIST

Addressee	Copies
36. General Dynamics Corporation 5100 W. 164th Street Cleveland, Ohio 44142 Attn: W. Geudtner, Jr.	1
37. General Electric Company Advanced Engine and Technology Department Cincinnati, Ohio 45215 Attn: L.B. Venable	1
38. General Electric Company Electro-Mechanical Eng. Unit Bldg. 55-263 1 River Road Schenectady, New York Attn: E.R. Booser	1
39. General Electric Company Research and Development P.O. Box 8 Schenectady, New York 12301 Attn: G.R. Fox	1
40. General Motors Corporation Allison Division Speedway Indianapolis, Indiana 46206 Attn: E.M. Deckman	1
41. Hughes Aircraft Company Centinela Ave. & Teale St. Culver City, California 90230	1
42. Huyck Metals Company P.O. Box 30 45 Woodmont Road Milford, Connecticut Attn: J.I. Fisher	1

DISTRIBUTION LIST

Addressee	Copies
43. I.I.T. Research Foundation 10 West 35th Street Chicago, Illinois 60616 Attn: Dr. Strohmeier	1
44. Industrial Tectonics Box 401 Hicksville, New York 11801 Attn: J. Cherubin	1
45. Koppers Company, Inc. Metal Products Division Piston Ring and Seal Department Baltimore, Maryland Attn: F.C. Kuchler E. Taschenburg	1 1
46. Lockheed Aircraft Company 118 W. First St. Room 1400 Dayton, Ohio 45402 Attn: L. Kelly	1
47. Martin Marietta Corp. Parkview Plaza Office Bldg. 1700 Needmore Road, P.O. Box 14153 Dayton, Ohio 45414 Attn: Z.G. Horvath	1
48. Mechanical Technology, Inc. 968 Albany-Shaker Road Latham, New York Attn: Donald F. Wilcock	1
49. Metal Bellows Corporation 20977 Knapp Street Chatsworth, California Attn: Sal Artino	1
50. Midwest Research Institute 426 Volker Blvd. Kansas City, Missouri Attn: V. Hopkins	1

DISTRIBUTION LIST

Addressee	Copies
51. Morganite, Inc. 33-02 48th Avenue Long Island City, New York Attn: S.A. Rokaw	1
52. North American Rockwell Corp. 5100 West 164th Street Cleveland, Ohio 44142 Attn: George Bremer	1
53. Northrop Corporation 1730 K Street N.W. Suite 903-5 Washington, D.C. Attn: S.W. Fowler, Jr.	1
54. Pesco Products Division Borg-Warner Corporation 24700 N. Miles Bedford, Ohio	1
55. Pressure Technology Corp. of Am. 453 Amboy Avenue Woodbridge, New Jersey Attn: A. Dobrowsky	1
56. North American Rockwell Corp. Rocketdyne Division 6633 Canoga Avenue Canoga Park, California Attn: M. Butner	1
57. Sealol Inc. P.O. Box 2158 Providence, Rhode Island Attn: Justus Stevens	1
58. SKF Industries, Inc. 1100 First Avenue King of Prussia, Penn. Attn: L.B. Sibley	1
59. Southwest Research Institute 8500 Culebra Road San Antonio, Texas 78206 Attn: P.M. Ku	1

DISTRIBUTION LIST

Addressee	Copies
60. Stanford Research Institute Menlo Park, California Attn: R.C. Fey	1
61. Stein Seal Company 20th St. & Indiana Avenue Philadelphia, Pennsylvania Attn: Dr. P.C. Stein	1
62. United States Graphite Co. 1621 Holland Sagnaw, Michigan Attn: F.F. Ruhl	1
63. Westinghouse Electric Corp. 55 Public Square Cleveland, Ohio 44113 Attn: Lynn Powers	1
64. Wright Aeronautical Division Curtiss-Wright Corporation Main & Passaic Streets Wood-Ridge, New Jersey 07075 Attn: SD Brinsfield	1
65. The University of Tennessee Dept. of Mechanical & Aerospace Eng. Knoxville, Tennessee	1
Attn: Professor W.K. Stair	1